ENHANCEMENT OF FAST PYROLYSIS OIL FUEL PROPERTIES THROUGH CO-PYROLYSIS AND IMPROVED ANALYSIS

By

© Anke Krutof B.Sc. M.Sc.

A thesis submitted to the School of Graduate Studies
in partial fulfilment of the requirements of the degree of

Doctor of Philosophy

Process Engineering
Faculty of Engineering and Applied Sciences
Memorial University of Newfoundland

October 2019

St. John's, Newfoundland and Labrador
Canada

Supervisory Committee:
Prof. Dr. Kelly Hawboldt (Supervisor)
Prof. Dr. Mike Katz
Prof. Dr. Faisal Khan

Abstract

Fast pyrolysis is a thermochemical process converting biomass into fast pyrolysis bio-oil (FPBO, 50-75 wt%), non-condensable gases (13-16 wt%), and biochar (12-20 wt%) at 450-550 °C in an inert atmosphere with short residence times and high heating rates. FPBO is a complex organic mixture of lignocellulose degradation products with high water (20-30 wt%) and oxygen content (35-40 wt%) causing chemical instability and corrosion to storage tanks and burners. In this work, the improvement of FPBO quality was investigated through co-pyrolysis of forestry residues with waste mussel shells and through improved understanding of phase behaviour and composition of forestry based FPBO using an advanced distillation curve analysis. Co-pyrolysis with waste mussel shells was studied by: (1) direct contact with the forestry residues in the reactor and (2) contacting only the hot vapours with the mussel shells at the reactor exit. The impact of temperature, residence time, mussel shell loading, and type of contact (operational mode) on the FPBO and biochar were studied. There was a reduction in FPBO oxygen and acid content through dehydration and decarboxylation with mussel shell addition and an increase in biochar pH and functionality (O- and N-containing functional groups) for soil amendment and adsorption applications, respectively. The FPBO phase behaviour was studied using an advanced distillation method and a model developed to simulate the distillation curves of the whole FPBO. The 17 surrogates used in the model to represent the range of functional groups and boiling points of FPBO components

showed a good fit of simulated and experimental distillation curves and some bulk properties. GC analysis of the vacuum distillate fractions concluded six distillable steps as a basis for chemical separation procedures.

Keywords: Fast pyrolysis bio-oil, softwood, mussel shell, co-pyrolysis, advanced distillation curve, thermodynamic model

Acknowledgements

This research would not have been possible without the financial support of BioFuelNet Canada, the National Science and Engineering Research Council of Canada (NSERC), the Centre for Forest Science and Innovation (CFSI, NL Provincial Government), the Newfoundland Aquaculture Industry Association (NAIA), and the Memorial University of Newfoundland's (MUN) School of Graduate Studies and Faculty of Engineering and Applied Science in St. John's, Canada.

I would like to express my sincere gratitude towards my supervisors Prof. Dr. Kelly Hawboldt and the late Prof. Dr. Marco Satyro for their suggestion of the research question and their valuable advice, guidance, and mentoring. Prof. Satyro leaves behind a legacy, I hope to carry on with his work. He will be dearly missed.

Moreover, I want to extend my appreciation to the other members of the BioFuelNet research group; especially toward Prof. Dr. Stephanie MacQuarrie, Prof. Dr. Robert Helleur, Dr. Shofiur Rahman, Dr. Hanieh Bamdad, Dr. Tobias Brueckner, and Dr. Sadegh Papari for their direct collaboration.

Thank you to my supervisory committee members Prof. Dr. Mike Katz and Prof. Dr. Faisal Khan for their guidance and to my friends and family for their emotional support.

For their technical support, I would like to thank the National Institute of Standards and Technology, in particular Dr. Thomas Bruno, Dr. Tara Lovestead and Megan Harris, the MUN technical service, the MUN chemistry department and CREAIT staff, and Prof. Dr. Leonard Lye.

Last but not least, I want to recognize the work term and other students that have contributed to this research project: Parsa Abdi, Erin Butler, Sam Byrne, Sonja Hanna-Quinn, Noubahar Hasnain, Annabell Heintz, Brittany Lockyer, Mareike Serra, Matthew Sheaves, Brittany Traverse, and Joachim Urbanek.

Table of contents

List of abbreviations

Abbreviation	Description
2FI	2-factor interaction
AAEM	Alkali and alkaline earth metals
ADC	Advanced distillation curve
AIC	Akaike information criterion
ANOVA	Analysis of variance
ASTM	American Society of Testing and Materials
BDT	Bone dry tonnes
BET	Brunauer, Emmett and Teller (surface area analysis technique)
BP	Boiling point
BTX	Mixtures of benzene, toluene, and the three xylene isomers
CFP	Catalytic fast pyrolysis
C/H/N(O)	Elemental analysis for carbon, hydrogen, nitrogen, and oxygen (by difference)
df	Degrees of freedom
DoE	Design of experiment
DVF	Distillate volume fraction
EFB	Empty fruit bunch
EoS	Equation of state
ESP	Electro static precipitator
FAO	Food and Agriculture Organization
FCC	Fast catalytic cracking
FID	Flame ionization detector
FPBO	Fast pyrolysis bio-oil
FTIR	Fourier transform infrared spectrometry
GC-MS	Gas chromatography-mass spectrometry
GHG	Greenhouse gases
HDO	Hydrodeoxygenation
HHV	Higher heating value
HPLC	High performance liquid chromatography
HR	High resolution
HW	Hardwood
HYD	Hydrogenation
IBP/T	Initial boiling point/temperature
LC	Liquid chromatography
LCA	Life cycle analysis

List of abbreviations (continued)

Abbreviation	Description
LHV	Lower heating value
MePh	Methoxyphenol
MS	Mussel shell
MSW	Municipal solid waste
MW	Molecular weight
NCG	Non-condensable pyrolysis gases
NF	Newfoundland
NIST	National Institute of Standards and Technology
NMR	Nuclear magnetic resonance
PAHs	Polyaromatic hydrocarbons
PP	Polypropylene
RM	Red mud
RRSB	Rosin-Rammler-Sperling-Bennet particle size distribution
RSM	Response surface methodology
SEM	Scanning electron microscope
SS	Shrimp shell
SW	Softwood
TAN	Total acid number
TBP	True boiling point
TGA	Thermogravimetric analysis
TGRP	Tail gas recycling pyrolysis
UNIQUAC	Universal quasi-chemical activity coefficients
V-ADC	Vacuum advanced distillation curve
VGO	Vacuum gas oil
VLE	Vapour-liquid equilibrium

List of figures

List of tables

Chapter 1 Introduction and overview

In 2018, CO_2 emissions increased by 0.5% in industrial countries after a 5-year decline, despite efforts to mitigate greenhouse gas emissions [1]. Global CO_2 emissions increased by 2.4% in 2017 [1]. To mitigate the global temperature increase caused by climate change, reduction of greenhouse gas (GHG) emissions caused by human activity, the main cause of climate change, is crucial [2]. The primary source of GHGs, such as CO_2 and methane is the burning of fossil fuels [2–4]. Of all know sustainable energy sources biomass is the world's largest, most widely available, and the only source that can be converted into liquid fuels and chemicals [5]. First generation biofuels produced from energy or food crops have received criticism in the past resulting in a shift to second generation or advanced biofuels produced from biomass that does not compete with food production, such as waste from food and agricultural processing, wood residues, and municipal solid waste (MSW) [5,6]. To meet sustainability requirements biomass in non-food applications should ideally be limited to high-value applications and those with the highest GHG/CO_2 mitigation potential. Energetic uses such as combustion are at the very bottom/end of life cycle of biogenic products; energy should come from other renewable resources (wind, solar, or hydro) wherever possible [7]. However, biomass for energy use in rural sparsely populated areas, and biofuels for (e.g. shipping or air transportation), where there are no other renewable alternatives, are feasible [7]. In fact, the growth of the bioeconomy increases revitalization of rural areas [7]. Local waste biomass is a preferable feedstock for the bioeconomy considering existing infrastructure, local product use or small distance to market depending on the product value, and reducing CO_2 emission during decomposition in landfills [8]. If sustainability requirements are met, biofuels sourced from biomass could reduce the impacts of fuel use

on climate change [3]. In Canada, forestry and fisheries resources are especially abundant and are considered as the basis for a bioeconomy [9].

Fast pyrolysis bio-oil (FPBO) derived from forestry residues (bark, shavings, chips, and sawdust) could reduce fossil fuel consumption, increase energy security, and enhance waste management [5]. Fast pyrolysis is characterized by moderate temperatures (450-500 °C) in an inert atmosphere, short vapour residence times, and high heating rates [10]. The vapours are condensed to produce the primary product, a liquid bio-oil (50-75 wt% of the dry biomass) as outlined in Figure 1-1. The FPBO consists of over 300 main and 700 minor organic components [11–13] chemically different from petroleum oils containing little to no hydrocarbons [14]. Two other products: Non-condensable gas (NCG, 13-16 wt%), and biochar (12-20 wt%) are produced [10]. The NCG can be combusted to supply process heat or used in turbines, engines, or boilers [10,15]. The biochar is a valuable fuel as well and is being investigated for value-added applications, as a soil amendment, catalyst, or an activated carbon-like adsorbent [16–18].

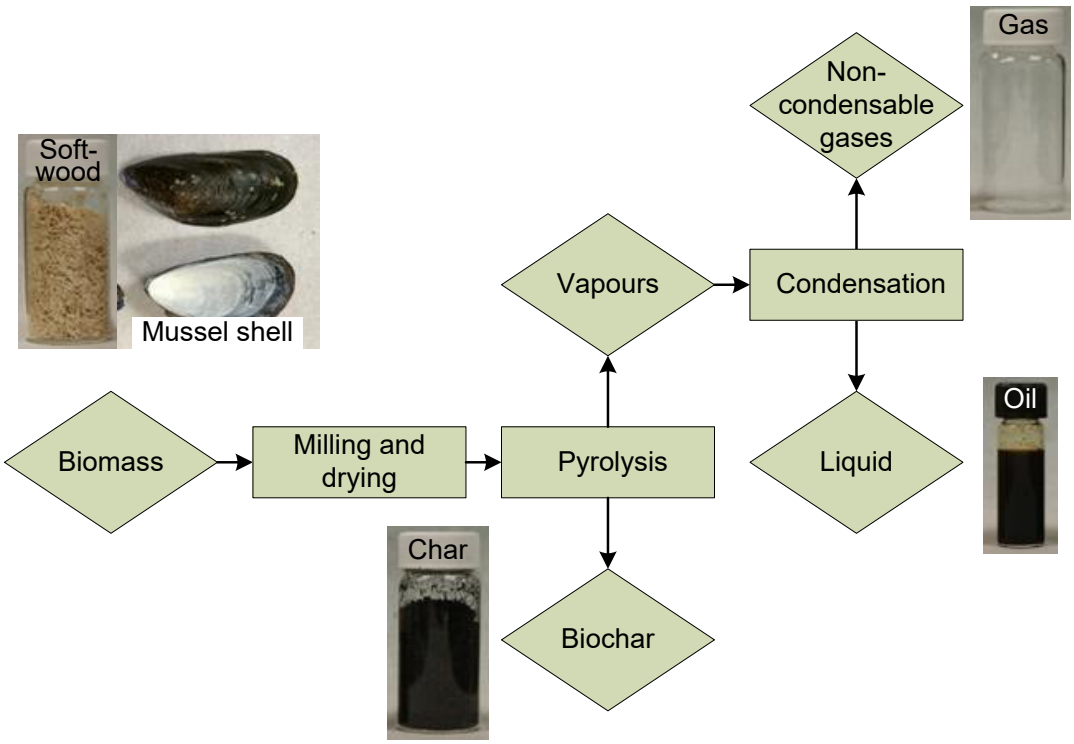

Figure 1-1: Pyrolysis process flow chart

The yield and composition of the three products depend on feedstock type and moisture content, pretreatment methods, processing conditions, reactor type, and condensation system [13,19]. The FPBO's usability in fuel applications is limited due to high water and oxygen content of 15-30 wt% and 35-40 wt%, respectively [19]. The high water and oxygen contents lead to poor flammability and lower heating values (LHV 13-18 MJ/kg) compared to fossil fuels (40-50 MJ/kg) [14,20]. FPBO has similar viscosities to No. 4 fuel oil and can be corrosive due to formic, acetic, etc. acids limiting its use to stainless steel systems [21,22]. The composition change over time or "ageing" impacts fuel quality [14,23].

The lack of data on the thermal and compositional properties of FPBO limits the ability to predict phase and reaction behaviour, which limits reactor and condenser system design and operation optimization. FPBO contains approximately 20-30 wt% water, 40-50 wt% components which can be detected by gas chromatography (65-85 area % of which are identifiable), 15 wt% non-volatile compounds detectable by liquid chromatography and 15 wt% high-molecular-weight components (residue or pyrolytic lignin) which cannot be identified by chromatography analysis [13,24]. Analysis of chemical composition is completed by GC/MS or GC/FID in most labs due to the low cost and wide availability of these applications compared to others. Other analytical techniques include GCxGC (comprehensive two-dimensional gas chromatography), LC (liquid chromatography), HRMS (high resolutions mass spectrometry), NMR (nuclear magnetic resonance), and FTIR (Fourier transform infrared spectroscopy). Even though GC is the most widely used application, it has drawbacks limiting the identification of detected components such as insufficient chromatographic resolution, peak coelution, unavailability of mass spectra of some components, difficulties with quantification due to lack of analytical standards, no characterization of non-volatiles (sugars and lignin oligomers) [13,25,26]. Additionally, quantification is time-consuming, as calibration with different concentrations of each individual compound and a known mass of internal standard (e.g. fluoranthene) is required [11,13]. Thus, compositional GC data is mostly recorded as area %, not wt%.

Further, there is a lack of data on the impact of adding other waste streams to improve FPBO fuel quality. The purpose of this dissertation is to improve the understanding of and ability to predict the properties of whole FPBO and its fractions and thereby methodologically enhance oil quality.

1.1 Objectives

The overall objective of this work is to enhance the fuel properties of woody biomass generated FPBO by obtaining a better understanding of the bio-oil properties (e.g. phase behaviour and composition) and combining other waste streams with the forestry residues. This objective was achieved in steps (Figure 1-2): Co-pyrolysis of softwood and mussel shell waste products (*Section 1.1.1*) and the creation of a thermodynamic model to predict FPBO volatility (*Section 1.1.2*).

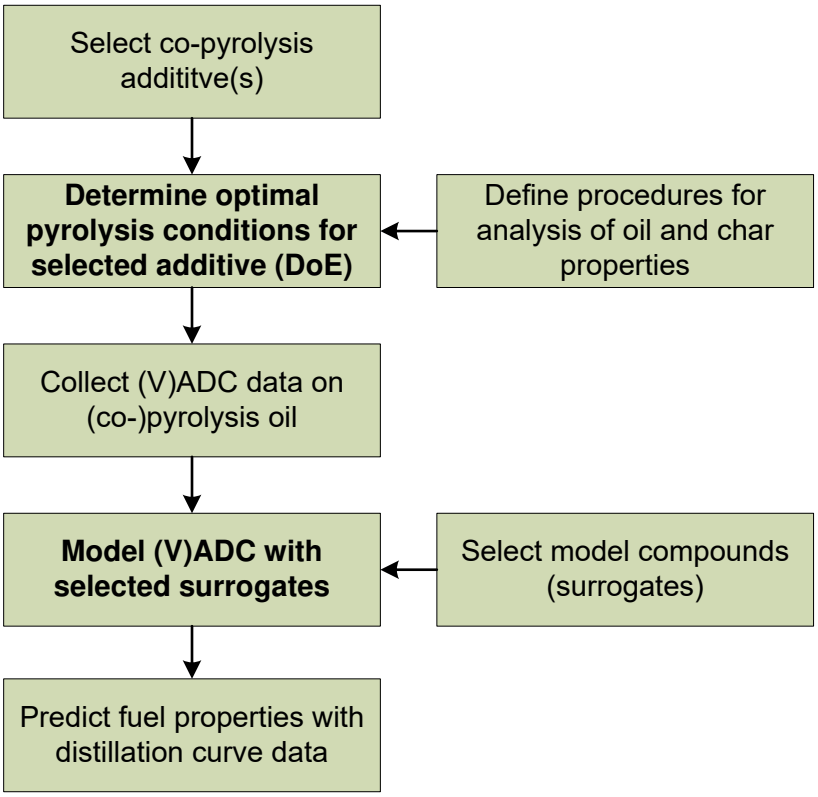

Figure 1-2: Thesis approach and objectives

1.1.1 Co-pyrolysis

Enhancing the quality of FPBO has been identified as one of the necessities to expand the possible applications from heating to transport fuels [10]. However, enhancement or refinement through catalytic upgrading or hydroprocessing of crude FPBO can be problematic due to the high cost of commercial catalysts, catalyst poisoning by carbon deposits and water, limited catalyst regeneration, and low yield [6]. Another possible, less costly and more sustainable option, is to co-pyrolyse the forestry residues with other residue streams that could improve oil and/or char properties. By utilizing processing waste from other industries, cost of disposal in landfills or to the ocean and the associated environmental impact are mitigated. Red mud (RM) and the fisheries by-products, mussel (MS) and shrimp shell (SS), were investigated as co-pyrolysis additive in preliminary experiments (*Chapter 3*). These feedstocks were chosen due to availability, the potential for oil/char enhancement, and represent a disposal issue for the respective industries. Based on preliminary study results (*Appendix B*), MS was selected as the most promising additive for further experiments. An optimally designed experiment (DoE, response surface methodology [RSM]) was carried out comparing both designs: co-pyrolysis (*in-situ*) and vapour treatment (*ex-situ*). The factors studied included reaction temperature, nitrogen flow, operational mode (*in-* or *ex-situ*), and MS additive loading. Produced oils were analyzed to determine FPBO quality, physical, chemical, and thermal properties, and applicability for fuel use (*Chapter 4*). The biochar was analyzed for adsorbent qualities (*Chapter 5*).

1.1.2 Thermodynamic modelling

In parallel with the co-processing study, FPBO derived from sawmill residues (soft-wood shavings) was analyzed to determine thermodynamic properties and subsequently develop a thermodynamic model (*Chapter 6*). Attempts have been made to model the vapour-liquid equilibrium (VLE) of pyrolysis oil surrogate mixtures and model compounds [27–29]. However, comprehensive models of pyrolysis oil thermodynamic properties could not be found in the literature. Our goal was to model FPBO volatility by measuring advanced distillation curve (ADC) data of whole FPBO. A model based on a surrogate mixture and the UNIQUAC phase behaviour equation was developed in VMGSim™. This model was then improved through the input of the ADC data. The objective of the model is to predict fuel properties such as enthalpy (heating value, heat capacity, flash point), flow properties (viscosity, density), and average molecular weight with the VMGSim™ model and compare it to experimental data.

1.2 Co-authorship statement

The principal author of this thesis (Anke Krutof), under supervision and after correspondence and detailed feedback with the supervisor and co-author (Dr. Kelly Hawboldt), performed all the experimental work, analyzed and discussed the data, prepared all drafts of manuscripts, submitted the drafts for publication, and replied to the comments of the reviewers and editors for all materials in this thesis. The data presented in Chapter 3 is the author's contribution to the referenced publication; parts of this publication by other authors were not added to the dissertation because they do not meet the scope of this work. The co-authors, Dr. Hanieh Bamdad and Dr. Stephanie MacQuarrie, assisted with the Discussion and Conclusions of Chapter 5 due to their biochar expertise.

1.3 Bibliography

[1] Chestney N, Fenton S (Editor). Carbon emissions from rich nations set to rise in 2018-IEA. CNBC 2018. https://www.cnbc.com/2018/12/04/reuters-america-carbon-emissions-from-rich-nations-set-to-rise-in-2018-iea.html?utm_campaign=IEA newsletters&utm_source=SendGrid&utm_medium=Email (accessed December 20, 2018).

[2] Lee H. The IPCC's scientific assessments of Climate Change. COP22 United Nations Clim Chang Conf 2016:18–9.

[3] BioFuelNet. Annual report 2016. Montreal, Quebec, Canada: 2016.

[4] COP22. The COP22, the COP of Action. Marrakech, Morocco: 2016.

[5] Abnisa F, Wan Daud WMA. A review on co-pyrolysis of biomass: An optional technique to obtain a high-grade pyrolysis oil. Energy Convers Manag 2014;87:71–85. doi:10.1016/j.enconman.2014.07.007.

[6] Butler E, Devlin G, Meier D, McDonnell K. A review of recent laboratory research and commercial developments in fast pyrolysis and upgrading. Renew Sustain Energy Rev 2011;15:4171–86. doi:10.1016/j.rser.2011.07.035.

[7] Priefer C, Jörissen J, Frör O. Pathways to Shape the Bioeconomy. Resources 2017;6:10. doi:10.3390/resources6010010.

[8] Hawboldt KA, MacQuarrie S, Papari S, Bamdad H, Krutof A. Biomass residues to bioproducts – challenges and opportunities in rural regions. Manuscript Submitted for Publication 2019.

[9] Natural Resources Canada. Forest Fact Book 2018–2019 2018.

[10] Bridgwater A V. Review of fast pyrolysis of biomass and product upgrading. Biomass and Bioenergy 2012;38:68–94. doi:10.1016/j.biombioe.2011.01.048.

[11] Branca C, Giudicianni P, Di Blasi C. GC/MS characterization of liquids generated from low-temperature pyrolysis of wood. Ind Eng Chem Res 2003;42:3190–202. doi:10.1021/ie030066d.

[12] Zhang L, Liu R, Yin R, Mei Y. Upgrading of bio-oil from biomass fast pyrolysis in China : A review. Renew Sustain Energy Rev 2013;24:66–72. doi:10.1016/j.rser.2013.03.027.

[13] Staš M, Kubička D, Chudoba J, Pospíšil M. Overview of analytical methods used for chemical characterization of pyrolysis bio-oil. Energy and Fuels 2014;28:385–402. doi:10.1021/ef402047y.

[14] Elliott DC, Oasmaa A, Preto F, Meier D, Bridgwater A V. Results of the IEA Round Robin on Viscosity and Stability of Fast Pyrolysis Bio-Oils. Energy &

Fuels 2012;26:3769–76. doi:10.1021/ef300384t.

[15] Demirbaş A. Biomass resource facilities and biomass conversion processing for fuels and chemicals. Energy Convers Manag 2001;42:1357–78. doi:10.1016/S0196-8904(00)00137-0.

[16] Bamdad H, Hawboldt K, MacQuarrie S. A review on common adsorbents for acid gases removal: Focus on biochar. Renew Sustain Energy Rev 2018;81:1705–20. doi:10.1016/j.rser.2017.05.261.

[17] Butler L, Altdorff D, Young E, Galagedara L, Hawboldt K, Helleur R, et al. Organic Waste in Newfoundland: A Review of Available Agriculture, Fishery, Forestry and Municipal Waste Literature. St. John's, NL: 2017.

[18] Bamdad H, Hawboldt K. Comparative study between physicochemical characterization of biochar and metal organic frameworks (MOFs) as gas adsorbents. Can J Chem Eng 2016;94:2114–20. doi:10.1002/cjce.22595.

[19] Oasmaa A, van de Beld B, Saari P, Elliott DC, Solantausta Y. Norms, Standards, and Legislation for Fast Pyrolysis Bio-oils from Lignocellulosic Biomass. Energy & Fuels 2015;29:2471–84. doi:10.1021/acs.energyfuels.5b00026.

[20] Oasmaa A, Elliott DC, Müller S. Quality Control in Fast Pyrolysis Bio-Oil Production and Use. Environ Prog Sustain Energy 2009;28:404–409. doi:10.1002/ep.

[21] Chiaramonti D, Bonini M, Fratini E, Tondi G, Gartner K, Bridgwater A V., et al. Development of emulsions from biomass pyrolysis liquid and diesel and their use in engines - Part 1: Emulsion production. Biomass and Bioenergy 2003;25:85–99. doi:10.1016/S0961-9534(02)00183-6.

[22] Chiaramonti D, Bonini M, Fratini E, Tondi G, Gartner K, Bridgwater A V., et al. Development of emulsions from biomass pyrolysis liquid and diesel and their use in engines - Part 2: Tests in diesel engines. Biomass and Bioenergy 2003;25:101–11. doi:10.1016/S0961-9534(02)00184-8.

[23] Alsbou E, Helleur R. Accelerated aging of bio-oil from fast pyrolysis of hardwood. Energy & Fuels 2014;28:3224–35. doi:10.1021/ef500399n.

[24] Alsbou E, Helleur R. Whole sample analysis of bio-oils and thermal cracking fractions by Py-GC/MS and TLC-FID. J Anal Appl Pyrolysis 2013;101:222–31. doi:10.1016/j.jaap.2013.01.003.

[25] Alsbou E. Pyrolysis Bio-oil as a Renewable Fuel and Source of Chemicals: Its Production, Characterization and Stability. Memorial University of Newfoundland, 2014.

[26] Kanaujia PK, Sharma YK, Agrawal UC, Garg MO. Analytical approaches to characterizing pyrolysis oil from biomass. TrAC - Trends Anal Chem 2013;42:125–36. doi:10.1016/j.trac.2012.09.009.

[27] Hallett WLH, Clark NA. A model for the evaporation of biomass pyrolysis oil droplets. Fuel 2006;85:532–44. doi:10.1016/j.fuel.2005.08.006.

[28] Zhang L, Kong SC. Multicomponent vaporization modelling of bio-oil and its mixtures with other fuels. Fuel 2012;95:471–80. doi:10.1016/j.fuel.2011.12.009.

[29] Ille Y, Kröhl F, Velez A, Funke A, Pereda S, Schaber K, et al. Activity of water in pyrolysis oil—Experiments and modelling. J Anal Appl Pyrolysis 2018;135:260–70. doi:10.1016/j.jaap.2018.08.027.

Chapter 2 Literature review

A modified version of the chapter has been published; A. Krutof, K. A. Hawboldt. Upgrading of biomass sourced pyrolysis oil review: Focus on co-pyrolysis and vapour upgrading during pyrolysis. Biomass Conversion and Biorefinery. July 6, 2018. 8:775-787.

Abstract

Fast pyrolysis bio-oil (FPBO) from lignocellulosic feedstocks has been successfully used as a fuel for boilers in heating applications. However, the oil quality limits application as a transport fuel due in part to the high oxygen, and resulting acid content of the pyrolysis oil which complicates storage, handling, and use in traditional petroleum-based systems. Reduction of the acid or oxygen content can be accomplished via a number of refinery approaches from catalytic upgrading of the liquid post production to co-pyrolysis. While past reviews have focused on catalytic upgrading of the post-production oil, this work compares studies in post-production catalytic processes, *in-situ* and *ex-situ* pyrolysis vapour upgrading, and co-pyrolysis. The review includes studies of "natural" additives/catalysts, sourced from waste biomass, as the co-pyrolysis material or catalyst. Additive/catalysts sourced from waste biomass is potentially a more sustainable approach than commercial catalysts. In general, upgrading the liquid post-pyrolysis can improve quality, however the overall oil yield decreases and cost increases due to the additional upgrading step. Co-pyrolysis and/or *in-* and *ex-situ* vapour upgrading during pyrolysis potentially enhance FPBO quality while recovering high-value chemicals.

Keywords: Pyrolysis bio-oil, oil upgrading, co-pyrolysis, catalytic fast pyrolysis

2.1 Introduction

Enhancing the quality of bio-oil produced from the fast pyrolysis of biomass would be necessary to expand into transportation and higher end fuel markets [1]. However, enhancement through catalytic upgrading (e.g. hydroprocessing) during or post-pyrolysis can be costly due to the high cost of commercial catalysts and additional processing steps, catalyst poisoning by carbon deposits and water, limited catalyst regeneration, and reduced yield [2]. The potentially less costly and more sustainable option is to co-pyrolyse the biomass with residue streams from other industries that could improve oil and/or char properties. By utilizing these processing wastes, costs due to disposal in landfills or to the ocean and the associated environmental impact are mitigated. Ideally, a co-pyrolysis additive (derived from waste) would improve oil as well as char properties (as part of char by-product), and therefore, eliminate the need for disposal.

This paper will focus on the upgrading of fast pyrolysis oil from woody (lignocellulosic) biomass, particularly forestry residues. Fast pyrolysis is characterized by temperatures in the range of 450-600 °C, short vapour residence times (seconds), and rapid heating and quenching rates [3,4]. Oil (at a yield of 50-75 wt%), char (12-20 wt%), and non-condensable gases (NCG) (13-16 wt%) are produced during fast pyrolysis [1,5–7]. The short vapour residence times reduce secondary reactions and increase the liquid yield. The main compounds in the gaseous product are CO_2, CO, methane and other light hydrocarbons, and H_2 [8,9]. The char consists of elemental carbon, oxygen, hydro-

gen, and nitrogen (< 1 wt%), minerals, and other inorganics [10–12]. The liquid product, referred to as fast pyrolysis bio-oil (FPBO), is a mixture of organics chemically different from hydrocarbon-based oils [13].

Biomass-derived FPBO is a feasible alternative to petroleum-based heating oils requiring minimal modifications to the combustion systems and resulting in lower overall CO_2 emissions depending on the source of the biomass [13]. Fast pyrolysis is an economically feasible way to convert biomass into liquid fuels compared to the gasification and biochemical conversion, which is the most expensive. The price for pyrolysis oil production ranges from US$ 2.00 to US$ 5.50 per gallon gasoline equivalent [14]. Yang et al. investigated FPBO as the fuel for a combined heat and power plant with an energy efficiency of 42.5% in a techno-economic study [15]. Additionally, lignocellulosic biomass does not contain sulphur, and therefore, no additional energy is required for sulphur removal [16]. Locally sourced waste biomass is used to produce FPBO fuel. This offers further advantages in regions where distance to market, infrastructure, and other challenges make import of fuels into or biomass out of the region costly both economically and environmentally [13, 15-17].

2.1.1 Applications of pyrolysis oil

In addition to fuel, FPBO is a source of platform chemicals [4,18]. FPBO has been tested as a fuel for furnaces and boilers, diesel engines, gas turbines, and Stirling engines for heat and power generation [19,20]. A detailed review of the use as a fuel and the necessary modifications to furnaces and boilers can be found in [18,21]. Blending bio-based oils with petroleum fuels and/or low chain length alcohols (methanol/ethanol)

to improve performance during combustion [19,21–24] has also been studied, and e.g. blends with biodiesel and petroleum diesel have been tested in diesel engines [18]. Additionally, blending with alcohols increases the stability of FPBO [25]. Examples of chemicals extracted from FPBO that have high-value applications include anhydrosugars, which could be used in the pharmaceutical industry, for surfactants, and biodegradable polymers [20]. Industrial products from whole FPBO include BioLime used in SO_x removal, biodegradable slow-release nitrogen fertilizer and alternative wood preservatives, asphalt bio-binder, liquid smoke and wood flavours [18,20,26]. However, the bulk of applications of FPBO is in fuels. A summary of pyrolysis oil production facilities (installed and under construction) and their capacities can be found in [1,6,21,27].

2.2 Feedstocks

2.2.1 Wood and forestry residues

Woody biomass consists of cellulose (35-60 wt%), hemicellulose (15-30 wt%), and lignin (16-31 wt%), organic extractives, and inorganic minerals varying with species [6,25]. The composition of the common Newfoundland (NF) tree species is given in Table 2-1.

Table 2-1: Chemical composition of NF's main tree species [25,28,29]

	Balsam fir [28]	**Spruce** [25]	**Black spruce** [28]	**White spruce** [28]	**Pine** [25]	**Aspen**
Cellulose	54.6	42.7-49.8	56.5	55.6	35-40.8	59.1
Hemicellulose	15.4	20.7-27.3	15.2	16.4	27.1-29	21.2
Lignin	27.7	27.0-28.2	27.3	27.0	28-28.1	18.1
Extractives		0.8-2.5			3-4	

Forest residues include forest harvest residues (tops, branches, and leaves from harvest and thinning operations), residues from the removal of small and low value standing trees for selection or shelterwood partial harvesting systems, and sawmill residues (chips, slabs, sawdust, shavings, and bark). Harvest residues are typically left in the forest to maintain soil quality [30,31], whereas sawmill/pulp and paper residues are used for energy generation, pulp, particle or strand board and pellet production, compost, playground cover, or livestock bedding [30]. Location or quality can limit the use of the residues, and therefore, they are often stockpiled on site, to degenerate slowly [30].

Seventy-five million board feet were produced at Newfoundland and Labrador's (NL) 581 commercial and 994 domestic sawmills, with the 4 large integrated mills accounting for 95% equivalent to 70 million board feet [29]. An inventory in 2009 showed 24,414 bone dry tonnes (BDT) logging residues (in-forest), 7,568 green t/a of sawmill residues (40-50 wt% moisture content for non-kiln-dried residues, 20 wt% moisture kiln dried), and 29,000 BDT pulp and paper residues, landfilled as black bark, were generated in NL [30,32,33]. This results in over 250 kt/a of residues (bark, sawdust, sludge, etc.) per year generated by sawmill and forestry operations in NL [33].

2.2.2 Fisheries by-products

In 2015, the worldwide marine fish capture was 81 Mt (megatons) [34] with another 106 Mt from aquaculture [35]. Canada's total fish production was approximately 823 kt (capture) and 187 kt (aquaculture) in 2015 [34]. In Canada, 23 kt blue mussels worth 34 mil. USD were farmed in 2015 [35]. By-product from fish processing plants is 40-70 wt% of the harvested depending on fish species, product, and processing methods [36,37]. In Atlantic Canada, fish processing plants produce 418 kt/a of waste.[38]. Current methods to use waste streams from the fish industries are not economically attractive and include sanitary landfills and effluent treatment ponds [39,40]. The waste can be potentially transformed into valuable products such as proteins, peptides, amino acids, fish oil, gelatin, dispersants, etc. [38]. The products can be used in biotechnology, medicine, food industry, chemical industry, agri-/aquaculture as nutraceuticals, fuel, for oil spill cleanups, and feed additives, among others [38]. Rural, coastal regions can benefit economically from turning fisheries waste streams into value-added products [38,41].

2.2.2.1 Shrimp shells

Shrimp shells contain proteins, minerals (calcium carbonate), secondary metabolites, including carotenoid pigments, and carbohydrates [38]. Extraction of the valuable carbohydrate biopolymers chitin and chitosan from shells of shrimp, crab, and lobsters is a use of these by-products currently under investigation [38]. For this research, commercially available dried, ground shrimp shells were supplied by Shell-Ex Canada [42].

2.2.2.2 Blue mussel shells

Mussel shells can be used as substitutes for aggregates in construction materials or cement clinker, tiles, lime for plastering, or low-value material for road fill, fertilizer, soil conditioner, liming agent, mulch, aquaculture, animal feed additive, and a reagent for phosphate removal from wastewater or to treat acid-mine drainage waste [38,43,44]. In NL, mussel shells (Figure 2-1) are disposed of in landfills, wasting a valuable by-product and incurring costs [43].

Figure 2-1: Blue mussel shells from NF aquaculture cleaned off organic residue with enzymes (left) and same mussels ground in a ball mill (right)

Organic residues should be removed from the shells before landfilling or in any of the applications listed above by calcinating the shells (heating to high temperatures in air or oxygen, at 500 °C for 15 min) or cleaning the shells using enzymes [45]. The use of enzymes is potentially less expensive from an energy use perspective and avoids crystal structure changes due to heating (conversion from aragonite polymorph with orthorhombic crystal structure to calcite polymorph with trigonal- rhombohedral structure [44,45]). Mussel shells consist of 95-99 wt% calcium carbonate ($CaCO_3$) and 1-5 wt% organic matrix composed of β-chitin fibrils in silk fibroin-like proteins that determine

crystallization structure and counteract calcite brittleness [43]. The calcium carbonate exists in the three stable anhydrous polymorphs: calcite (triclinic), aragonite (orthorhombic), and vaterite (hexagonal). Thermodynamic stability decreases from calcite to vaterite [44–46]. A detailed analysis of the shell's crystal structure can be found in [43,45,46]. The water content of the calcite, aragonite, and vaterite, is 0.0, 0.0, and 0.8 wt%, respectively [47]. Therefore, mussel shells as a co-pyrolysis additive do not increase the moisture content of the pyrolysis oil expect through possible changes in the pyrolysis reactions. At temperatures above 700-900 °C, calcium carbonate forms lime (calcium oxide, CaO) and carbon dioxide [43,44].

$$CaCO_{3\ (s)} \rightleftharpoons CaO_{\ (s)} + CO_{2\ (g)} \qquad (2.1)$$

Calcium oxide has been investigated as a co-pyrolysis additive, successfully improving the pyrolysis oil quality (*Section 2.4.4.1*) [48–52].

2.2.3 Red mud

Red mud is a bauxite mining waste produced at 120 Mt/a with an estimated total of 3 Gt worldwide stored as a slurry in lagoons or sludge in dry-stacking storage sites [53]. Due to high alkalinity, red mud storage sites are safety and environmental hazards [53]. Mineralogically red mud is a highly complex mixture of iron, aluminum, silicon, titanium, and calcium oxides [53]. During fast pyrolysis around 500 °C, red mud (iron III oxides (hematite Fe_2O_3 and goethite) turns to iron II oxides (magnetite Fe_3O_4 and wüstite), iron carbides or iron metals which are known as reducing catalysts for Fischer Tropsch, water gas shift reaction, cracking, and hydrogenation catalysts for carboxylic acids [53–

55]. Several studies have been carried out utilizing red mud as a co-pyrolysis catalyst (*Section 2.4.4.1*) [8,53–56].

2.3 Properties of fast pyrolysis bio-oil

FPBO derived from woody biomass is a multi-compound mixture resulting from the de-polymerization reactions of cellulose, hemicellulose, and lignin [18]. Six factors that influence the composition and properties of the oil are feedstock type, biomass ash content, temperature, biomass particle size and shape, reactor type, and condenser systems [3,25,57]. The FPBO is a complex mixture of over 300 organic components: water, and oxygenated compounds such as organic acids, esters, alcohols, ketones, aldehydes, alkenes, phenols, guaiacols, catechol, syringols, vanillins, furancarboxaldehydes, isoeugenol, pyrenes, sugars, miscellaneous oxygenates and trace inorganics [7,13,58,59]. A detailed review of the reactions involved in the thermal decomposition of cellulose, hemicellulose, and lignin as a function of temperature can be found in [60,61]. FPBO is a microemulsion in which an aqueous solution of polar holocellulose (cellulose and hemicellulose) decomposition products including water form a continuous phase that stabilizes the discontinuous phase of pyrolytic lignin macro-molecules through mechanisms such as hydrogen bonding (Figure 2-2) [62,63]. High water content reduces viscosity and heat of combustion as well as flame temperature, thereby, contributing to lower nitrogen dioxide emissions during combustion. However, if the water content of pyrolysis oil is too high (typically > 35 wt% [3]), phase separation occurs (ASTM D7544).

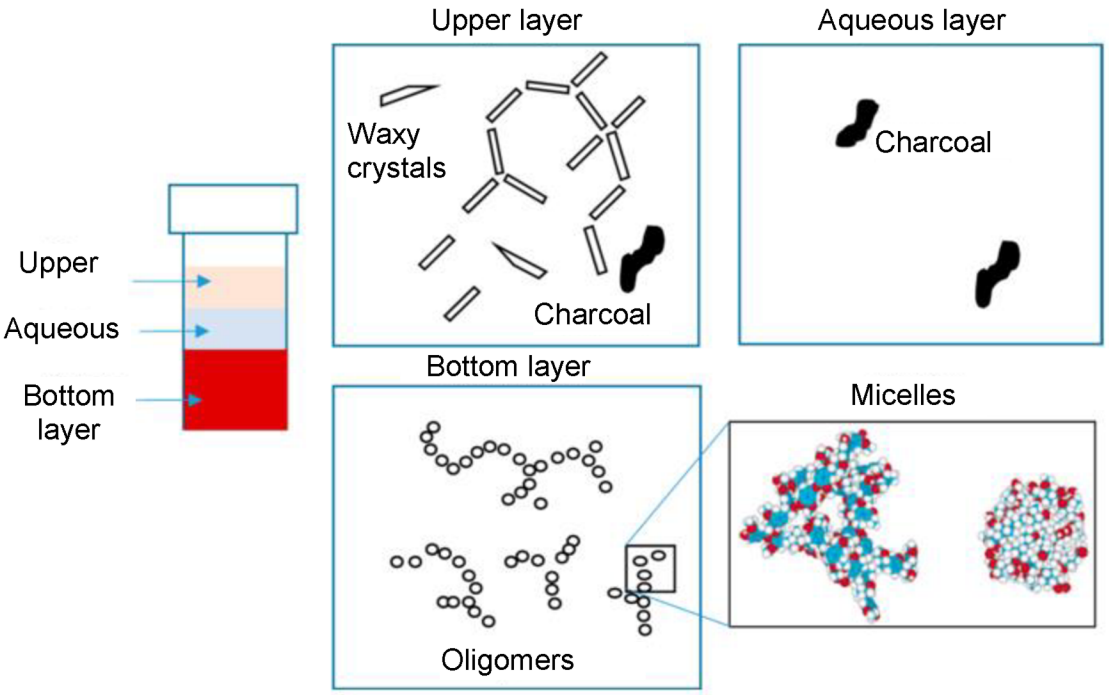

Figure 2-2: Multiple phases of fresh crude pyrolysis liquid from [25,64,65]

In general, FPBO contains 20-30 wt% water, 40-50 wt% components that are detectable by GC (65-85 area% of which are identifiable), 15 wt% non-volatile compounds detectable by LC, and 15 wt% high-molecular weight compounds (residue) that can not be detected with chromatographic techniques [7,66]. The water originates from moisture in the biomass as well as secondary reactions in the pyrolysis vapour phase. Pyrolysis reaction water is due to the cleavage of glucosidic bonds of cellulose and hemicellulose and secondary cracking reactions [3].GC/MS analysis has identified and quantified up to 40 chemical components in the FPBO [5].

The temperature and type of condenser system impact both the FPBO composition and liquid yield. The optimal yield of lignin oligomers, and therefore, of total liquid, occurs between 450-550 °C. Secondary cracking and repolymerization reactions due to long

residence times, temperatures above 550 °C, or when hot vapour filtration is used, reduce the oil yield [25]. The biomass particle size and shape influence the heat and mass transfer during the pyrolysis reaction. Reactions are kinetically controlled for particle sizes below 2 mm [25,57]. Table 2-2 summarizes the required fuel properties of FPBO (ASTM D7544), the properties of a typical FPBO (2012 and 2017 IEA studies) as well as properties of a typical catalytic FPBO [3,67,68].

Table 2-2: Summary of pyrolysis oil standard ASTM D7544, typical and catalytic oil properties [3,67,68]

Property	**Test Method**	**Grade G**	**Grade D**	**Typical FPBO** [3,67–69]	**Catalytic pyrolysis oil** [68]
Gross heat of combustion, MJ/kg, min	D240	15	15	13-18	25-30
Water content, wt%, max	E203	30	30	20-40	30-40
Pyrolysis solids content, wt%, max	D7579	2.5	0.25	0.01-1	
Kinematic viscosity at 40 °C, mm²/s, max	D445*	125	125	15-35	
Density at 20 °C, kg/dm³	D4052	1.1-1.3	1.1-1.3	1.05-1.25	0.95
Oxygen content, wt%				30-60	20-40
Sulfur content, wt%, max	D4294	0.05	0.05	0-0.05	0-0.05
Ash content, wt%, max	D482	0.25	0.15	0.01-0.2	0.2
pH	E70	Report	Report	2-3	5
Flash Point, °C, min **	D93, Procedure B	45	45	40-110	
Pour Point, °C, max	D97	-9	-9	-9 to -36	

*Without filtering, ** now Sustained Combustion Test [70]

There are two grades of FPBO oil, grade G and grade D; grade G is intended for use in industrial burners and not suitable for residential heaters, small commercial boilers, engines or marine applications; grade D is for commercial/industrial burners requiring

lower solids and ash content and suitable in residential heaters, engines, or marine applications modified to handle these types of fuel. The drawbacks of FPBO oil properties, use as fuel, and options to enhance quality have been summarized by Bridgwater [71]. Drawbacks include acidity or low pH, degradation rates, alkali metals, poor distillability, high viscosity, low H:C ratio, material incompatibilities, low miscibility with hydrocarbons, high oxygen content (reactivity, instability), phase separation or inhomogeneity, solids, and water content [62,71]. The energy density of typical FPBO (13-18 MJ/kg) is half that of gasoline/diesel (45 MJ/kg) by volume and one third by mass [68].

Phase separation is one of the challenges associated with FPBO [1,8,72,73]. As indicated above, FPBO is a microemulsion, the breakdown of the emulsion results in instability, and therefore, phase separation [1,8,73]. If the amount of polar component in the liquid is high (water content > 30-35 wt%), liquid-liquid phase separation occurs resulting in a polar top phase of pyroligneous water (often referred to as aqueous phase). This phase contains polar compounds (water, alcohols, and organic acids), light oxygenates, and sugars [74]. The bottom phase, or organic-rich phase, consists of non-polar, lignin-derived compounds [25]. A top phase of an oily extractive rich lignocellulosic, waxy material with a low water content of 3-6 wt% has been observed in some studies [25].

Two different types of phase separation are observed in the FPBO. The separation described above is due to liquid-liquid equilibrium in the liquid product; the second is a result of the vapour-liquid equilibrium during condensation [25]. Phases can be separated into different fractions through condenser design; pyrolysis systems with two or

more condensers produce two or more fractions that can be separately utilized. The heavy fractions, dominated by polar and non-polar high boiling compounds, is collected in the first condenser. The lighter organics are concentrated in the liquid obtained in the second (cooler) condenser. Additionally to water, these lighter compounds include acetic acid, hydroxyacetaldehyde, and acetol [25].

2.4 Upgrading of pyrolysis oil

FPBO is used in stationary engines and boilers [18,19,21] and commercially used for hospital heating [75] but has limited use in transportation unless upgraded [2] due to high oxygen content (30-60 wt%). The reactive oxygen-containing compounds and resulting degradation reactions cause storage instability due to an increase in acidity, viscosity, and water content [69,76–78]. The goal is, therefore, to reduce the oxygen content in the oil during pyrolysis or in subsequent processing of the oil. The FPBO quality can be further improved by cracking high molecular weight compounds [14]. This increases the H/C ratio and results in a decrease of the FPBO oil product yield [52,72]. Ideally, upgrading would yield a stable liquid with 5-10 wt% oxygen to reduce soot formation during combustion compared to no oxygen, with oxygen present as stable low acidity alcohol groups (e.g. non-phenolic alcohols) [72]. Liu et al. suggest the degree of oxygen removal to rate upgrading efficiency (Equation (2.2)).

$$Oxygen\ removal\ degree = \left[1 - \frac{x_{Oxy\ in\ FPBO} \cdot Y_{FPBO}}{x_{Oxy\ in\ biomass}}\right] \qquad (2.2)$$

Where $x_{Oxy\ in\ FPBO}/x_{Oxy\ in\ biomass}$ is the weight percentage of oxygen in FPBO/biomass and Y_{FPBO} is the yield of FPBO in wt% [14].

In a study of the pyrolysis of southern pine, red oak, and sweet gum sawdust in a fixed bed tube furnace reactor under nitrogen or helium, and temperatures between 371 °C and 871 °C there was a decrease in oxygenated compounds in pyrolysis gas and liquid as pyrolysis temperature increased [79]. There was a corresponding increase in gas yield and the CO/CO_2 ratio, while liquid yield decreased and percent of aromatic hydrocarbons in the liquid increased [79].

Processes to improve FPBO can be grouped into catalytic and non-catalytic processes and further subdivided into processes that focus on upgrading of pyrolysis oil post or during pyrolysis. During pyrolysis, the vapours can be upgraded prior to condensation (*ex-situ* vapour upgrading), or the additive/catalyst can be in contact with the biomass during *in-situ* upgrading (most commonly referred to as catalytic fast pyrolysis (CFP)) or co-pyrolysis (combination of different feedstocks) (Figure 2-3).

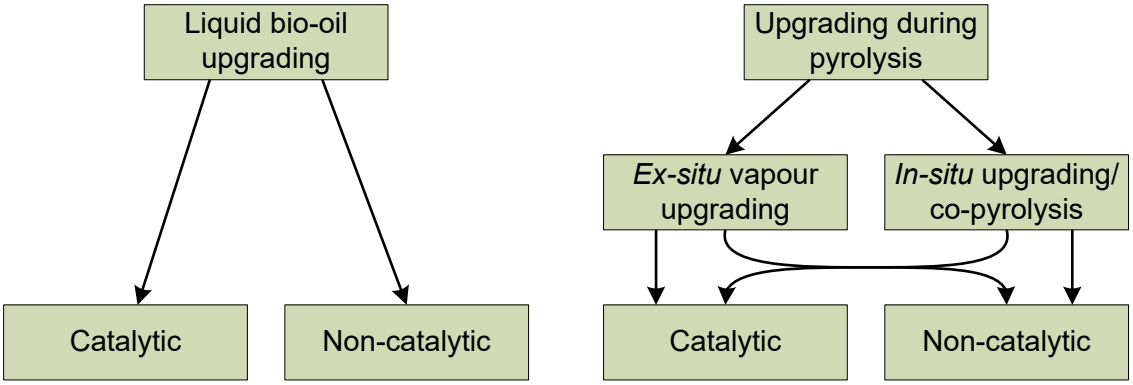

Figure 2-3: Overview of enhancement techniques for fast pyrolysis bio-oil

This review focuses on the last two approaches. Catalysts and/or co-pyrolysis can be used to enhance or upgrade oil quality. The high oxygen (40-50 wt%) content of the feedstock biomass and the need to process aqueous streams or vapours with non-neutral

pH requires processing in multiple steps and severe conditions [80]. The main issues of biomass conversion to fuels or chemicals are poor atom efficiency, product selectivity and catalyst deactivation [80].

The primary advantage of upgrading with a commercial or specially designed catalyst is the control over oil quality [69]. However, these processes can be expensive due to catalyst deactivation by coke/char deposits and water, high operational pressure (or vacuum), and the potential requirement for hydrogen co-feed increasing catalyst, capital, and operational costs [69]. Co-pyrolysis with an additive, particularly, if the additive is another waste/by-product, could decrease costs and increase sustainability of the process [72]. The additive should improve oil, char, and/or gas properties and be non-toxic/inert before or after pyrolysis. Co-pyrolysis or *in-situ* upgrading is typically carried out at the same pyrolysis conditions as pyrolysis of the pure feedstock resulting in little change in equipment or additional cost [69].

2.4.1 Biomass pretreatment and effect of indigenous catalysts

Biomass is dried to reduce the water content, as water in the biomass feed will end up in the FPBO in addition to the water produced during pyrolysis [68]. Other biomass pretreatment methods include size reduction, pelletization, and water and/or acid washing to decrease the ash content of the biomass (alkali and alkaline earth metals (AAEM), silicon, and other inorganics) [25,81]. These inorganics affect the degradation reactions of lignocellulose, catalyze secondary vapour cracking reactions, and therefore, decrease the oil yield and increase the water content and probability of phase separation [25]. Decreasing the AAEM increases the overall liquid yield and oxygen content of the liquid

(on dry basis) while gas (specifically CO_2) and char yield decrease [81]. Washing with acid solutions, such as HCl or HF, is more effective compared to water washing [68]. These processes are especially useful for biomass high in AAEM, such as agriculture residues [68]. Removal of inorganics from biomass inhibits the negative effect of AAEM on storage stability of FPBO and, in *in-situ* catalytic pyrolysis, catalyst deactivation through inorganic deposits is reduced [81]. Suggestions for the treatment of spent washing liquid include biological treatment and subsequent use in irrigation [81]. Stefanidis et al. investigated the effect of inorganics and found that washing at high temperatures (50 °C) with nitric acid removes more than 90 wt% of inorganics from low ash content biomass, 40-70 wt% from medium ash content biomass, and only 22-54 wt% from high ash content biomass due to high Si content from soil contamination in agricultural residues [81]. Compared to acid washing, water washing only removed 17-42 wt% of the inorganics [81]. Stefanidis et al. estimate a decrease in energy efficiency through acid washing by 7-10% [81]. Water washing only removes water-soluble metal salts: K, Cl, S, Na, P, and Si; while acid washing additionally removes cations bound to reactive sites: Mg, Ca, Al, Fe, and Zn [81]. Metals in the biomass increase the homolysis of the pyranose rings to low MW products (CO_2, C=O compounds, furans, and acids) [81]. Dehydration of cellulose through weakened hydrogen bonds and promoted cross-link reactions increases char and water yield when inorganics are present [81]. Inorganics, such as calcium, favour the cracking of lignin structure and oligomers to phenolic monomers [81–83]. Therefore, the char yield increases after demineralization for high lignin feedstock [81,84]. Mullen et al. found that potassium exchanged HZSM-5 catalysts (KZSM-5), with lower acidity compared to HZSM-5, shows

similar results compared to HZSM-5 deactivated by ash (containing large amounts of K) deposits. Both increased the yield of monomeric alkylphenols and 2-methylfuran while decreasing the yield of monoaromatic hydrocarbons [85]. Fermoso et al. compared the influence of de-ashed biomass (through acid washing) with raw biomass containing indigenous catalysts (minerals) and external (HZSM-5) catalysts on the pyrolysis of two herbaceous and two woody biomass species [86]. Both indigenous and external catalyst reduced the oil yield on a water-free basis. However, while HZSM-5 significantly reduced the oxygen content in the produced FPBO through decarbonylation (CO), the deoxygenation route favoured in the presence of indigenous catalysts (decarboxylation) led to increased char yield containing 40% of the chemical energy content of the biomass feed [86]. Dehydration (H_2O) is the main deoxygenation pathway for ash free biomass feed [86].

2.4.2 Liquid bio-oil upgrading

Non-catalytic liquid bio-oil upgrading processes include solvent (low chain length alcohol) addition [25,74,87], antioxidant addition or limited access to oxygen [74], mild hydrogenation [74], esterification (alcohol plus acid catalyst and dehydrating agent), and blends with other fuels such as diesel, bunker C and acetone, biodiesel, waste cooking oil, or glycerol [88,89]. Liquid oil upgrading processes using catalysts, solvents, and hydrogen are summarized in [69] by Abnisa et al. The most common upgrading processes are hydrodeoxygenation (hydrotreating, catalyst: supported hydrogenating metal), (fast

catalytic) cracking (catalyst: zeolite or others), ketonization (catalyst: metal oxides), aldol condensation (catalyst: basic catalyst, solid heterogenous metal oxides, etc.), and esterification (catalyst: solid or liquid acid catalyst, zeolites, metal oxides) [53,68].

Liquid processes such as hydrodeoxygenation (HDO) have the advantage of a better fuel quality due to aromatic hydrocarbon production and less coke production [90]. During HDO oxygen is eliminated as H_2O using hydrogen. Alkenes are produced through hydrogenation-dehydration-hydrogenation. Therefore, bifunctional catalysts with acid and hydrogenation sites are needed [72,90]. Adding an HDO upgrading step to the pyrolysis process reduced the oil yield to 26 wt% compared to 65 wt% mainly due to reduction of oxygen. Although the HDO oil had a higher energy density, the yield lost during HDO outweighs the increase in energy density compared to untreated pyrolysis oil [2,91,92]. Other disadvantages of HDO include high costs for hydrogen, catalysts acquisition and regeneration, and high-pressure equipment [90]. Hydrolytic destruction of the support matrix and leaching of active hydrotreating metals have been identified as issues by Karimi et al. [53]. Ruddy et al. summarized the challenges of liquid and vapour phase HDO upgrading, the most important being the large amounts of high-pressure hydrogen required (62 kg hydrogen per 1000 kg pyrolysis oil) [72]. The high cost and loss of energy yield can be reduced if catalytic fast pyrolysis oil is used as a feed [76,80].

Fast catalytic cracking (FCC) can also be used to upgrade the oil. De Rezende Pinho et al. co-fed 10 and 20 wt% FPBO with vacuum gas oil (VGO) in a demonstration-scale FCC riser reactor with zeolite catalysts (V and Ni on Al_2O_3, Na_2O, and Re_2O_3). Direct

feeding of FPBO in FCC leads to the formation of char, coke, and water resulting in operational issues such as line plugging [93]. The FPBO co-feed increased the aromatics level (particularly phenols) and octane number in the gasoline range products compared to pure VGO feed, as well as the amount of other oxygenated compounds formed (mainly water, CO, and CO_2) [93]. FPBO upgraded via CFP can be more easily hydrodeoxygenated, requiring less hydrogen and lower pressures relative to no pretreatment [93]. The larger scale experiment showed improved product slate due to feed dispersion of FPBO and VGO (separate feed at different temperatures and reactor heights) and differences in catalyst-feed contact compared to lab-scale experiments [93]. Due to these positive effects of scale, upgrading (e.g. HDO) of FPBO is not necessary when co-fed (up to 20 wt% of FPBO) with VGO [93]. However, alkaline metals content of the pyrolysis oil causes destruction of zeolite FCC catalyst, and higher make-up rates would have to be employed to ensure FCC equilibrium catalyst activity [93].

2.4.3 Upgrading during pyrolysis

Due to the disadvantages of liquid upgrading listed above, *in-/ex-situ* vapour or co-pyrolysis upgrading can be an attractive option or first upgrading step. In *ex-situ* vapour upgrading, the hot pyrolysis vapours are passed through a catalyst or additive before condensation. In *in-situ* upgrading and co-pyrolysis, the biomass is mixed with a catalysts/additive and pyrolyzed. In *ex-situ* vapour upgrading the operational conditions (pressure, temperature, and residence time) during pyrolysis and upgrading can be varied, char separation is straightforward, and less additive is required compared to *in-situ*

upgrading or co-pyrolysis [14]. However, the process requires an additional unit operation increasing fixed assets investment and operational cost [14]. *In-situ* upgrading or co-pyrolysis, on the other hand, is a simplified process with immediate contact of the vapours with the catalysts or additive [14]. Reactions in the early stages of pyrolysis are affected with an increase in decomposition of high molecular weight compounds, thereby increasing the chance of secondary reactions and char formation [14]. *In-situ* upgrading or co-pyrolysis allows for better heat integration compared to *ex-situ* vapour upgrading [14]. However, during the short residence time in *in-situ* upgrading (seconds), only the most active components react, limiting the deoxygenation. Other operating conditions (particularly. temperature) are dictated by the pyrolysis process as well and might not be ideal for upgrading reactions [14]. In addition, it is proposed higher additive:biomass ratios are necessary to decrease the effective volume and efficiency depending on pyrolysis conditions, biomass, and additive used [14]. Separation of char and additive is more difficult [14]. Fluidized bed reactors and auger reactors are especially suitable for *in-situ* upgrading or co-pyrolysis due to the good mixing during the pyrolysis process [77,80]. An advantage of auger reactors over fluidized bed reactors is the tolerance for different biomass feed, heat carrier, and catalyst/additive particle sizes and densities [52,80,94].

2.4.3.1 *In-situ* catalytic upgrading

A comprehensive review on catalytic fast pyrolysis (CFP), was carried out by Liu et al. [14]. The most common process is catalytic deoxygenation, a combination of catalytic cracking and/or hydrotreating. CFP improves the FPBO quality by removing oxygen as

CO, CO_2, and H_2O, where decarbonylation (CO) is the least preferred route as it removes a carbon for every oxygen removed resulting in lower overall energy density [68]. The amount of H_2 required for follow up treatment such as HDO is reduced. However, energy/yield is lost in the pretreatment step [14]. This process yields an aromatic hydrocarbon oil produced from biomass directly without the need for additional processing steps such as gasification and Fischer-Tropsch synthesis [14]. Catalysts include soluble inorganics (K, KCl, Na, NaCl, NaOH, Na_2O_3, Na_2SiO_3, Ca, $CaCl_2$, P, H_3PO_4, $(NH_4)_3PO_4$, $MgCl_2$, $FeSO_4$, $FeCl_2$, $CuCl_2$, and $ZnCl_2$), metal oxides, microporous and mesoporous materials, and supported transition metal catalysts [14]. The soluble inorganics reduce the reaction temperature of cellulose decomposition. Common metal oxides include acid (Al_2O_3, SiO_2, SiO_2-Al_2O_3), basic metal oxides (MgO, CaO), and other transition metal oxides (TiO_2, Fe_2O_3, NiO, ZnO, NiO and ZrO_2/TiO_2, Fe_2O_3 and ZrO_2/TiO_2, SiO_2) [14]. Microporous catalysts are zeolite based; the most common are HZSM-5 and ZSM-5 [14]. Zeolites are the most studied CFP catalysts [77,80,86] and the impact of ZSM-5 modified with Ga, Zn, Ni and Co, Fe and Cu, Ni, Ni/Co/Mo/Pt, Ce, Mg/B has been investigated as well as the impact of the zeolite pore size on the oil composition [14,80]. Mesoporous materials include SBA-15, Al-SBA-15, MSU-H_{BEA} and MSU-W_{BEA} [14]. Supported transition metal catalysts for HDO include SiO_2 and Al_2O_3 supported Fe, Cu, Pd, Ni, Pd-Cu, Pt, etc. [14]. Metal oxides, especially bi- and multi-metal with suitable supports (e.g. zeolites), have proven to be the most promising catalyst [14,80]. Catalysts and impacts reviewed by Liu et al. are summarized in *Appendix C* Table A-1 [14].

Serrano et al. highlight zeolites as suitable catalysts for CFP with the possibility to transform biomass to transportation fuels, a sector lacking sustainable renewables [80]. Zeolite catalysts are a nanoporous material with a crystalline framework, uniform microporosity, shape selectivity, and high surface area [80]. Benefits regarding biomass conversion with zeolites are hydrothermal stability, hydrophobicity, tuneable acid-base properties, and high resistance against deactivation by carbon deposits [80]. Zeolites are good catalysts for the production of deoxygenated FPBO because they selectively form aromatic hydrocarbons (with high proportion of alkyl-substituted benzenes and naphthalenes) [80]. The main limitations of zeolites are their deactivation due to carbonaceous deposits and extensive decarbonylation reactions [68]. Five reaction pathways/routes to improve pyrolysis oil quality with zeolites are catalytic cracking/pyrolysis, hydrotreatment (esp. HDO), condensation, isomerization, and dehydration [80]. Zeolites can be tailored to combine several reactions in one processing step (one-pot reactions) by creating hierarchical porosity, changing type (Brønsted or Lewis), ratio, and concentration of active acid sites, addition of basic sites, or incorporation of metal phases to create multifunctional catalysts [80]. Hierarchical porosity is the combination of intrinsic zeolite micropores with secondary porosity in the mesoporous range allowing for more accessibility, less diffusional and steric hindrance (good for bulky biomass particles), and reduced deactivation by carbon residues [80]. Zeolite acid site concentration, strength, and type (Brønsted/Lewis) can be finely controlled, and through the incorporating of Sn and Zr a new type of Lewis acid sites beneficial for sugar conversion is created [80]. Basic sites in cation-exchange zeolites favour multiple positive upgrading reactions,

such as (aldol) condensation reactions, sugar isomerization, and carboxylic acid ketonization [80]. Multifunctional zeolites are created through the incorporation of metals or metallic phases (usually added by impregnation) creating Brønsted acid sites with metallic centers that favour hydrogenation, HDO, and reduction reactions (e.g. Ru/Beta for sugar hydrogenation) [80].

2.4.3.2 *Ex-situ* catalytic upgrading

As noted above, *ex-situ* vapour upgrading can be accomplished with catalysts/additives, hot gas filtration, addition of reactive gases, and tail gas recycling pyrolysis (TGRP).

2.4.3.2.1 Non-catalytic *ex-situ* vapour upgrading

Non-catalytic processes (Table 2-3) such as hot gas filters, made from materials compatible with the acidic nature of the oil, produce a narrower molecular weight distribution in FPBO. However, 10-30 wt% of liquid product yield is lost in hot gas filtration due to cracking reactions and plugging issues of the filters are common [1,18,95]. Other approaches include introducing reactive gases such as H_2, CO_2, CO, CH_4, syngas, or steam to the reactor. The addition of steam has been proposed to increase the oil yield and decrease coke production [14,96]. Zhang et al. used fast pyrolysis on corncob in a fluidized bed reactor and compared N_2, H_2, CO_2, CO, and CH_4 atmospheres. CO gave the lowest oil yield (49.6 wt%), and CH_4 the highest (58.7 wt%) compared to N_2 (57.1 wt%) [14,97]. H_2 and CO created a reducing atmosphere, converting oxygen in the oil to H_2O and CO_2. The higher heating value (HHV) was increased to 24.4 MJ/kg for H_2 and 23.7 MJ/kg for CO compared to N_2 at 17.8 MJ/kg [97]. The strong reducing

CO atmosphere and the slightly oxidative CO_2 atmosphere increased the amount of acids, ketones and monofunctional phenols in the oil and decreased other phenols, sugars, and methoxy-containing compounds compared to the N_2 atmosphere [97]. H_2 suppressed char formation (and, with catalyst, influences composition and yield of liquid product) [97].

In TGRP, the non-condensable gases (NCG) are recycled back to the reactor. Mullen et al. [98] and Elkasabi et al. [99] investigated TGRP of lignocellulosic, pennycress presscake (protein-rich biomass), and horse manure feedstocks (500 °C, 2 kg/h fluidized bed reactor, sand heat carrier). Approximately 50-70% of the NCG was recycled back through the reactor. TGRP improved the quality of the oil recovered in the electrostatic precipitator (ESP), specifically improving thermal stability, HHV, and the reductive atmosphere leading to a reduction in oxygen content and TAN (0.2-4% total acids), but an increase in water [98,99]. The C/O ratios for the lignocellulosic feedstocks were 8.5-9.1 for TGRP compared to 2.1 under N_2 atmosphere. The char yield decreased by 2-3 % from 12 wt% (oak) and 8 wt% (switchgrass) while gas yield increased by 19% (oak) and 7% (switchgrass) from 15 wt% (both) [14,98]. The effect of deoxygenation, and therefore, water content, TAN, and HHV, was reduced for the proteinaceous pennycress presscake [98]. Mullen et al. compared the oil quality of TGRP oils produced via CFP with acid zeolite HZSM-5 catalysts in N_2 atmosphere and proposed the chemical mechanism of deoxygenation to be similar, where the acid-catalyzed process is initiated by protonation of oxygen functional group, followed by dehydration and dehydrogenation

forming olefins [98]. Table 2-3 summarizes selected studies in non-catalytic vapour upgrading.

Table 2-3: Summary of non-catalytic *ex-situ* vapour upgrading processes

Vapour upgrading method	**Results**	**References**
Hot gas filtration	Removal of char from FPBO slows ageing Improved combustion characteristics 10-30 wt% of liquid product yield is lost due to cracking of vapours on alkali metals in char Plugging issues Acid resistant filters required	Bridgwater [1] Czernik and Bridgwater [18] Baldwin and Feik [95]
Addition of reactive gases (H2, CO2, CO, CH4, syngas, or steam)	Steam increases oil yield and reduced coke formation by 30-45 wt% CO decreases oil yield by 7.5 wt% CH4 increases oil yield by 1.6 wt% H2 and CO reduce oxygen content of oil and increase HHV from 17.8 MJ/kg to 24.4 and 23.7 MJ/kg, respectively Cost of process modification and gas feed	Liu et al. [14] Zhang et al. [97]
Tail-gas reactive pyrolysis (TGRP, recycling of 50-70 % of NCG to reactor)	Improved FPBO quality: Increased thermal stability, HHV, and significant reduction in oxygen content and TAN but increase in water content Increased char yield Decreased gas yield Chemical mechanism of deoxygenation similar to HZSM-5: an acid catalyzed process initiated by protonation of oxygen functional group, followed by dehydration and dehydrogenation forming olefins	Mullen et al. [98] Elkasabi et al. [99]

2.4.3.2.2 Catalytic *ex-situ* vapour upgrading

A comprehensive review on *ex-situ* pyrolysis catalytic vapour upgrading (prior to condensation, at atmospheric pressure and temperatures between 350 and 500 °C) focusing on HDO was carried out by Ruddy et al. [72]. Catalysts investigated include transition metal sulphide catalyst (TMS), noble metal catalysts, and transition metal carbide, nitride, and phosphide (C/N/P) catalysts summarized in Table 2-4. The authors conclude that more studies are needed on catalyst functionality with whole FPBO vapours opposed to model compounds [72].

Table 2-4: Comparison of catalysts for *ex-situ* pyrolysis vapour upgrading via hydrodeoxygenation from [72]

Catalyst type / Parameter	TMS	Noble metals	Transition metal C/N/P
Cost	Low	High	Intermediate
Synthetic complexity	Low-intermediate	Low	Intermediate-high
Bifunctionality	Saturated plane and edge sites for HYD (S-H)	Metallic sites for HYD	Metallic sties for HYD
	Vacancy sites for C-O activation	Support introduces acid sites	Oxygen-modified sites (-OH) provide acid function
Activation energy for H_2 dissociation	0.55-0.97 eV MoS 0.34-0.52 eV Co-MoS 0.32-0.74 eV NiMoS	0.19 eV Pt(111) 0.12 eV Pd(111) 0 eV Ru(0001)	0 eV MoP(001)
Deactivation pathways	Surface oxidation Coking	Sintering Sulphur poisoning Coking	Surface oxidation C/N/P loss Coking

Lu et al. screened 6 nano-metal catalysts (MgO, CaO, TiO_2, Fe_2O_3, NiO, ZnO) in an *ex-situ* vapour upgrading system based on py-GC/MS using poplar wood (Table 2-5). Nano-metals were chosen due to low cost and decreased susceptibility to coking. At a pyrolysis temperature of 500 °C and heating rate of 20 °C/ms, CaO was the most promising catalyst reducing the acid content while increasing the hydrocarbon content (Table 2-5).

Table 2-5: Comparison of different nano-metal catalysts for *ex-situ* pyrolysis vapour upgrading during py-GC/MS with poplar wood compared to pure poplar wood [100]

Chemicals \ **Catalyst**	**MgO**	**CaO**	**TiO_2**	**Fe_2O_3**	**NiO**	**ZnO**
Anhydrosugars	↓	↓↓	↓↓	↓	↑	↓
Furans	↑	↓	↑	↓	↓	↑
Aldehydes	↓↓	↑	↓	↓↓	↓↓	↓
Ketones	↑	↑↑	↑	↑	↑	↑
Phenols	↑	↓↓	↑	↑	↑	↑
Acids	↓	↓↓	↑	↑	↓	↑
Alcohols	↑	↑	↓	↓	↓	↑
Hydrocarbons	↑	↑↑	↑	↑↑	↑	↑
Cyclopentenones	↑	↑↑	↑	↑	↑	↑

↑ small to intermediate increase in peak area% ↑↑ intermediate to large increase in peak area %

↓ small to intermediate decrease in peak area% ↓↓ intermediate to large decrease in peak area%

2.4.4 Naturally occurring and process waste additives

Catalysts or other additive composed of high-end metals, strong acids or bases, or requiring intensive production processes, can be cost prohibitive in terms of handling, capital cost, regeneration, and/or disposal. Ideally, non-synthetic additives/catalysts, produced as a by-product or waste stream from another process, with similar chemical make-up of the aforementioned additives/catalysts could be a sustainable option. In the subsequent sections, two waste streams: an industrial waste stream (bauxite mining waste), and wastes associated with shellfish processing (calcium carbonate) are reviewed as possible co-pyrolysis materials. It should be noted that the impact on the pyrolysis reaction mechanisms with these non-synthetic additives is unknown and/or difficult to assess due to the complex nature of the additives. As such, the discussion below has been limited to these two waste streams as there is most published work in these areas with respect to impact on oil and char quality and comparison with synthetic catalysts.

2.4.4.1 Red mud

Red mud is a bauxite mining waste. Approximately 3 Gt is generated per year worldwide. Stored as a slurry in lagoons or sludge in dry-stacking storage sites, the mud represents a waste disposal issue [53]. Due to high alkalinity, red mud storage sites are safety and environmental hazards [53]. Mineralogically red mud is a complex mixture of iron, aluminum, silicon, titanium, and calcium oxides [53]. Undergoing fast pyrolysis at approximately 500 °C, red mud (iron III oxides (hematite Fe_2O_3 and goethite)) converts to iron II oxides (magnetite Fe_3O_4 and wüstite), iron carbides, or iron metals.

These compounds are known as reducing catalysts for Fischer-Tropsch, water gas shift reaction, cracking, and hydrogenation catalysts for carboxylic acids [53–55].

Veses et al. (2015) pyrolyzed pine wood chips and bark in an auger reactor at 450 °C with a constant ratio of sand/additive:biomass of 3:1 by mass [8]. Sand is used as a heat carrier. The catalytic activity of a number of clay mineral additives including: sepiolite (magnesium silicate $Mg_4Si_6O_{15}(OH)_2 \cdot 6H_2O$), bentonite (aluminum phyllosilicate, mostly montmorillonite), attapulgite (magnesium aluminium phyllosilicate $(Mg,Al)_2Si_4O_{10}(OH) \cdot 4(H_2O)$), and red mud (bauxite waste, Fe-based, also aluminum and titanium oxide, and Si, Ca, Na) was studied [8]. Additive:biomass ratios of 3:1, 1:3, and 1:6 were used. The pyrolysis oil yield decreased, and char yield increased by 10 wt% with a sepiolite:biomass ratio 3:1 [8]. All additives except red mud slightly decreased liquid yield. The optimum additive:biomass ratio was selected at 1:6 to limit the reduction in liquid yield [8]. With the addition of red mud, the liquid yield increased, due to increased water content in the oil, while char and gas yield decreased [8]. The CO_2 content in the NCGs increased, while CO decreased for all feedstock mixtures studied. H_2 decreased, except for red mud, where it was roughly constant compared to the biomass feedstock [8]. The char composition did not change between catalysts. The oil showed heterogeneous behaviour with two separated phases (aqueous top phase and organic bottom phase). Sepiolite and red mud reduced TAN and increased pH [8]. Mineral clays and red mud increased the cracking of heavy compounds [8] and increased phenolics and BTX while decreasing esters. The increase in phenolics, which make up the majority of the pyrolysis oil, leads to an increase in overall molecular weight and

viscosity and is not desirable [8]. Specifically, red mud reduced acids and increased furans and ketones leading to increased stability of the oil while PAHs in the oil were reduced, indicating tar cracking reactions [8].

Yathavan et al. [54,56] compared HZSM-5 and red mud as catalysts in the pyrolysis of a 50:50 w/w juniper:pine mixture. The material was processed in a 150 g/h fluidized bed reactor at 475 °C using a sand heat carrier. ZSM-5 was calcinated at 550 °C for 5 h while the dried red mud water slurry (pH 9) was heated in the reactor for 2 h prior to pyrolysis, thereby converting it from hematite (Fe_2O_3) to magnetite (Fe_3O_4) [54]. The red mud is regenerated for re-use by heating in air to remove coke [54]. The total liquid yield reduced from 60.3 wt% for sand heat carrier to 49.3 and 44.4 wt% for HZSM-5 and red mud, respectively [54]. Water content increased from approximately 20 wt% to 23.5 wt% for both catalysts. Dynamic viscosity at 40 °C was reduced (by a factor of 7 with red mud (97 cP) and a factor of 3 with HZSM-5 (214 cP)) compared to sand heat carrier (686 cP) and stability increased for both oils [54]. The reaction pathways were identified as decarboxylation (red mud) and decarbonylation (HZSM-5) [54].

Lim et al. (2014) [55] studied the pyrolysis of oil palm empty fruit bunch (EFB) with red mud slurry (at pH 14) in a tube furnace reactor at 400 °C with 1 L/min N_2 flow. The EFB was pretreated with acid washing (water and alkali washing also leads to demineralization) to remove inherent metals (K, Na, Ca, Mg, Cl) and impregnating with metals from red mud (Fe, Al, Ti) [55]. The oil yield increased from 39 wt% (no pretreatment) to 52 wt% (pretreatment) [55]. Fe was identified as the catalyst involved in oil cracking. Reduction of the gas and char yield is due to the formation of a tar liquid when Fe is

present, reducing char formation [55]. The metals formed complexes with phenols, reducing the phenol concentration in the pyrolysis oil [55]. The acid washing and treatment with red mud lead to an increase in sugars and O-ring structures and reduce phenol content [55].

Karimi et al. [53] studied the upgrading of pyrolysis oil using red mud in a 300 mL pressurized (10 to 21 MPa) reactor at a final reaction temperature of 365 °C and a ramp of 3 °C/min (slow pyrolysis). Acidity and oxygen content was reduced while energy density increased. However, the study resulted in a two-phase oil with high water content (82-90 wt%) aqueous top phase and low yield of organic bottom phase [53]. Red mud is suitable for the selective production of chemicals from crude pyrolysis oil. However, the produced oil is not suitable as a direct fuel due to increased water content and phase separation [55].

2.4.4.2 Calcium oxide

Lin et al. (2010) discovered a 21% reduction in oxygen content of the FPBO when they pyrolyzed white pine with CaO at a 5:1 ratio in a fluidized bed at 520 °C with 50 mL/min carrier gas flow compared to pure pine [51]. Veses et al. (2014) co-pyrolysed pine softwood with CaO in an auger reactor at temperatures higher than 450 °C increasing secondary reactions and tar production compared to pure pine feedstock [52]. Both calcined calcite (CaO) and calcined dolomite (CaO MgO) as a co-pyrolysis additive were investigated. The char carbon content decreased by 2.5 wt% for sand-CaO and 4.3 wt% for sand-CaO·MgO compared to 79.2 wt% with sand [52]. While oxygen content in char increased by roughly the same percentage to 19.7 and 21.9 wt% due to the

higher oxygen content of $CaCO_3$ [52]. Yields for liquid (48-50 wt.%), char (25-27 wt.%), and gas (26-27 wt.%) were unaffected by the additive [52]. The oil showed reduced acidity (pH and TAN) and oxygen content and increased LHV and viscosity [52]. Reduction of high oxygen content phenolics (creosol, guaiacol, ethyl-methoxyphenol) was observed, while no influence of CaO or Cao MgO on the stability of the oil could be detected. The usually endothermic pyrolysis process becomes exothermic with CaO additive [52]. In a follow-up experiment, Veses et al. (2016) carried out char combustion and reactivation of CaO for recirculation in a fluidized bed at 800 °C [48]. The authors suggest reducing the moderate deactivation of the additive by addition of a purge and an inlet of fresh heat carrier (CaO and sand) [48].

Calcium oxide can be produced via calcination of calcium carbonate containing shells such as mussel shells [101,102]. In Canada, 23 kt blue mussels worth 34 million USD were farmed in 2015 [35]. Rural, coastal regions can benefit economically from turning fisheries waste streams into value-added products [38,41]. In NL, mussel shells are disposed of in landfills, wasting a valuable by-product and incurring costs [43]. CaO is also present in clay minerals such as calcite and dolomite [52]. At temperatures above 700 °C, calcium carbonate forms lime (calcium oxide, CaO) and carbon dioxide.

Barros et al. transformed waste mussel shells into purer calcium carbonate ($CaCO_3$) limiting kiln temperature to 600 °C to prevent calcination of $CaCO_3$ to CaO and CO_2 at temperatures between 700-900 °C [103]. Mussel shells can be used in construction materials, phosphate removal from wastewater, soil conditioning, and aquaculture or animal feed additive [38,43,103]. Mussel shells consist of 95-99 wt% calcium carbonate

($CaCO_3$) and 1-5 wt% organic matrix composed of β-chitin fibrils in silk fibroin-like proteins that determine crystallization structure and counteract calcite brittleness [43]. Given the positive impact on the oil quality using CaO as an additive, there is potential to use waste mussel shells in co-pyrolysis [48–52].

2.5 Conclusions

The enhancement of FPBO, derived from forestry residues, is required to expand the market for FPBO from low-grade heating oil to transport fuel quality. Upgrading FPBO quality has been investigated using commercially available catalysts such as HZSM-5 to promote deoxygenation reactions. The main issues of biomass conversion to fuels or chemicals are product selectivity and catalyst deactivation [80]. The high oxygen (40-50 wt%) content of the feedstock biomass and the need to process aqueous streams or vapours with non-neutral pH requires processing in multiple steps and severe conditions [80]. Catalytic fast pyrolysis (CFP) or mild hydrotreatment (without hydrogen) prior to HDO and/or FCC liquid upgrading is one option to combine upgrading steps. FPBO upgraded in CFP can be more easily hydrodeoxygenated, demanding less hydrogen and lower pressures [68,76,93]. However, the bio-oil and energy yield is reduced with each step, including losses of valuable carbon in form of CO/CO_2 and char/coke. More research on the combination and integration of different vapour and liquid phase upgrading technologies is needed [68]. Generally, decarbonylation (CO) should be avoided to limit the loss of carbon and hydrogen (energy) due to coke formation and gaseous hydrocarbon production due to vapour cracking [86]. Therefore, decarboxylation and dehydration are preferred routes of FPBO deoxygenation [68,86]. Many studies

have been completed on the catalytic pyrolysis of individual biomass components. However, more research is needed with whole biomass/FPBO to account for simultaneously occurring reactions and impurities (e.g. deactivation of catalyst due to ash/metal content) [68].

All upgrading steps will need to find a balance of mass and energy yields, FPBO oxygen content, carbon loss, and hydrogen demand, as well as feed/production and product cost. Catalysts required for catalytic pyrolysis and liquid upgrading and the operation of catalytic reactions are often expensive (high temperature and pressure). Therefore, compared to the market price of the pyrolysis oil (and char) products, using commercial catalysts in oil upgrading is not economically feasible at this point. Instead, alternatives derived from waste streams with similar chemical make-up compared to suitable catalysts as co-pyrolysis additives are potentially viable options. Examples of these additives are red mud (bauxite mining waste stream) and calcium oxide (clay minerals or calcined mussel shells). These additives would shift the balance towards high yield and low cost while still achieving some reduction in FPBO oxygenated compounds. However, more work is required into the reaction mechanisms, particularly identifying possible catalytic reactions when natural additives are used. A comparison to synthetic catalysts, investigation of the fate of the additives (in oil, char and/or gas), and overall techno-economic feasibility are needed. Research in the production of green chemicals and transportation fuels via catalytic upgrading of the pyrolysis liquid or vapours could improve the environmental and economic feasibility of the pyrolysis process overall. However, the economic incentive for the use of FPBO in heat and power production is currently stronger

and upgrading with the use of co-pyrolysis additive is the least costly option. If co-pyrolysis additives enhance pyrolysis oil as well as char quality, and if the additives are incorporated within the char, an additional separation step is not necessary decreasing operational cost further compared to catalytic upgrading processes.

2.6 Bibliography

[1] Bridgwater A V. Review of fast pyrolysis of biomass and product upgrading. Biomass and Bioenergy 2012;38:68–94. doi:10.1016/j.biombioe.2011.01.048.

[2] Butler E, Devlin G, Meier D, McDonnell K. A review of recent laboratory research and commercial developments in fast pyrolysis and upgrading. Renew Sustain Energy Rev 2011;15:4171–86. doi:10.1016/j.rser.2011.07.035.

[3] Elliott DC, Meier D, Oasmaa A, Van De Beld B, Bridgwater A V., Marklund M. Results of the International Energy Agency Round Robin on Fast Pyrolysis Bio-oil Production. Energy & Fuels 2017;31:5111–9. doi:10.1021/acs.energyfuels.6b03502.

[4] Huber GW, Iborra S, Corma A. Synthesis of transportation fuels from biomass: Chemistry, catalysts, and engineering. Chem Rev 2006;106:4044–98. doi:10.1021/cr068360d.

[5] Branca C, Giudicianni P, Di Blasi C. GC/MS characterization of liquids generated from low-temperature pyrolysis of wood. Ind Eng Chem Res 2003;42:3190–202. doi:10.1021/ie030066d.

[6] Zhang L, Liu R, Yin R, Mei Y. Upgrading of bio-oil from biomass fast pyrolysis in China : A review. Renew Sustain Energy Rev 2013;24:66–72. doi:10.1016/j.rser.2013.03.027.

[7] Staš M, Kubička D, Chudoba J, Pospíšil M. Overview of analytical methods used for chemical characterization of pyrolysis bio-oil. Energy and Fuels 2014;28:385–402. doi:10.1021/ef402047y.

[8] Veses A, Aznar M, López JM, Callén MS, Murillo R, García T. Production of upgraded bio-oils by biomass catalytic pyrolysis in an auger reactor using low cost materials. Fuel 2015;141:17–22. doi:10.1016/j.fuel.2014.10.044.

[9] Xu X, Zhang C, Zhai Y, Liu Y, Zhang R, Tang X. Upgrading of Bio-Oil Using Supercritical 1-Butanol over a Ru/C Heterogeneous Catalyst: Role of the Solvent. Energy & Fuels 2014;28:4611–21. doi:10.1021/ef500968a.

[10] Cruz Ceballos DC, Hawboldt K, Helleur R. Effect of production conditions on self-heating propensity of torrefied sawmill residues. Fuel 2015;160:227–37. doi:10.1016/j.fuel.2015.07.097.

[11] Bamdad H, Hawboldt K, MacQuarrie S. A review on common adsorbents for acid gases removal: Focus on biochar. Renew Sustain Energy Rev 2018;81:1705–20. doi:10.1016/j.rser.2017.05.261.

[12] Bamdad H, Hawboldt K. Comparative study between physicochemical characterization of biochar and metal organic frameworks (MOFs) as gas adsorbents. Can J Chem Eng 2016;94:2114–20. doi:10.1002/cjce.22595.

[13] Basu P. Biomass gasification and pyrolysis: Practical design and theory. Oxford

UK: Elsevier Inc.; 2010.

[14] Liu C, Wang H, Karim AM, Sun J, Wang Y. Catalytic fast pyrolysis of lignocellulosic biomass. Chem Soc Rev 2014;43:ASAP. doi:10.1039/c3cs60414d.

[15] Yang Y, Brammer JG, Wright DG, Scott JA, Serrano C, Bridgwater A V. Combined heat and power from the intermediate pyrolysis of biomass materials: performance, economics and environmental impact. Appl Energy 2017;191:639–52. doi:10.1016/j.apenergy.2017.02.004.

[16] Wiggers VR, Wisniewski A, Madureira LAS, Chivanga Barros AA, Meier HF. Biofuels from waste fish oil pyrolysis: Continuous production in a pilot plant. Fuel 2009;88:2135–41. doi:10.1016/j.fuel.2009.02.006.

[17] Chiaramonti D, Bonini M, Fratini E, Tondi G, Gartner K, Bridgwater A V., et al. Development of emulsions from biomass pyrolysis liquid and diesel and their use in engines - Part 2: Tests in diesel engines. Biomass and Bioenergy 2003;25:101–11. doi:10.1016/S0961-9534(02)00184-8.

[18] Czernik S, Bridgwater A V. Overview of applications of biomass fast pyrolysis oil. Energy & Fuels 2004;18:590–8. doi:Doi 10.1021/Ef034067u.

[19] Beld B van de, Holle E, Florijn J. The use of a fast pyrolysis oil – Ethanol blend in diesel engines for CHP applications. Biomass and Bioenergy 2018;110:114–22. doi:10.1016/j.biombioe.2018.01.023.

[20] Xiu S, Shahbazi A. Bio-oil production and upgrading research : A review. Renew Sustain Energy Rev 2012;16:4406–14. doi:10.1016/j.rser.2012.04.028.

[21] Lehto J, Oasmaa A, Solantausta Y, Kytö M, Chiaramonti D. Review of fuel oil quality and combustion of fast pyrolysis bio-oils from lignocellulosic biomass. Appl Energy 2014;116:178–90. doi:10.1016/j.apenergy.2013.11.040.

[22] Mei Y, Liu R, Zhang L. Influence of industrial alcohol and additive combination on the physicochemical characteristics of bio-oil from fast pyrolysis of pine sawdust in a fluidized bed reactor with hot vapor filter. J Energy Inst 2017;90:923–32. doi:10.1016/j.joei.2016.08.002.

[23] Lujaji FC, Boateng AA, Schaffer M, Mtui PL, Mkilaha ISN. Spray atomization of bio-oil/ethanol blends with externally mixed nozzles. Exp Therm Fluid Sci 2016;71:146–53. doi:10.1016/j.expthermflusci.2015.10.020.

[24] Krutof A, Hawboldt K. Blends of pyrolysis oil, petroleum, and other bio-based fuels: A review. Renew Sustain Energy Rev 2016;59:406–19. doi:10.1016/j.rser.2015.12.304.

[25] Oasmaa A, Fonts I, Pelaez-Samaniego MR, Garcia-Perez ME, Garcia-Perez M. Pyrolysis Oil Multiphase Behavior and Phase Stability: A Review. Energy and Fuels 2016;30:6179–200. doi:10.1021/acs.energyfuels.6b01287.

[26] Peralta J, Williams RC, Rover M, Silva HMRD. Development of Rubber-

Modified Fractionated Bio-Oil for Use as Noncrude Petroleum Binder in Flexible Pavements. Washington, D.C.: Transportation Research Board; 2012. doi:10.17226/22725.

[27] IEA Bioenergy Task 34 Direct Thermochemical Liquefaction. Pyrolysis Demoplant Database 2016. http://task34.ieabioenergy.com/publications/pyrolysis-demoplant-database/ (accessed May 17, 2018).

[28] Bakuzis E V., Hansen HL. Balsam Fir: A Monographic Review. St. Paul Minnesota: University of Minnesota; 1965.

[29] Economy SF. Provincial Sustainable Forest Management Strategy. Corner Brook, NL, Canada: 2014.

[30] Krigstin S, Hayashi K, Tchórzewski J, Wetzel S. Current inventory and modelling of sawmill residues in Eastern Canada. For Chron 2012;88:626–35. doi:10.5558/tfc2012-116.

[31] Parzei S, Krigstin S, Hayashi K, Wetzel S. Forest harvest residues available in Eastern Canada - A critical review of estimations. For Chron 2014;90:778–84. doi:10.5558/tfc2014150.

[32] Butler L, Altdorff D, Young E, Galagedara L, Hawboldt K, Helleur R, et al. Organic Waste in Newfoundland: A Review of Available Agriculture, Fishery, Forestry and Municipal Waste Literature. St. John's, NL: 2017.

[33] Jayasinghe P. Provincial Inventory of Forest Biomass Residues. 2011.

[34] Food and Agriculture Organization. FAO Global Capture Production database updated to 2015. Summary information. Fisheries and Aquaculture Department. 2017.

[35] Food and Agriculture Organization. Fisheries and Aquaculture Department. Statistics. 2017. www.fao.org/fishery/statistics/en (accessed May 1, 2017).

[36] AMEC Earth & Environmental Limited. Management of wastes from Atlantic seafood processing operations. Dartmouth, Nova Scotia: 2003.

[37] Ferraz De Arruda L, Borghesi R, Oetterer M. Use of fish waste as silage - A review. Brazilian Arch Biol Technol 2007;50:879–86. doi:10.1590/S1516-89132007000500016.

[38] Kerton FM, Liu Y, Murphy JN, Hawboldt K. Renewable resources from the oceans: Adding value to the by-products of the aquaculture and fishing industries. 2014 Ocean - St John's, Ocean 2014 2015:14–6. doi:10.1109/OCEANS.2014.7002983.

[39] Jayasinghe P, Hawboldt K. A review of bio-oils from waste biomass: Focus on fish processing waste. Renew Sustain Energy Rev 2012;16:798–821. doi:10.1016/j.rser.2011.09.005.

[40] Jayasinghe P, Adeoti IA, Hawboldt K. A Study of Process Optimization of

Extraction of Oil from Fish Waste for Use as A Low-Grade Fuel. J Am Oil Chem Soc 2013;90:1903–15. doi:10.1007/s11746-013-2321-1.

[41] Kerton FM, Liu Y, Omari KW, Hawboldt K. Green chemistry and the ocean-based biorefinery. Green Chem 2013;15:860–71. doi:10.1039/c3gc36994c.

[42] Shell-Ex. Shell-Ex. Newfoundland's Marine Bio-refinery n.d. http://www.shell-ex.com/ (accessed May 3, 2017).

[43] Abeynaike A, Wang L, Jones MI, Patterson DA. Pyrolysed powdered mussel shells for eutrophication control: effect of particle size and powder concentration on the mechanism and extent of phosphate removal. Asia-Pacific J Chem Eng 2011;6:231–43. doi:10.1002/apj.426.

[44] Barros MC, Bello PM, Bao M, Torrado JJ. From waste to commodity: transforming shells into high purity calcium carbonate. J Clean Prod 2009;17:400–7. doi:10.1016/j.jclepro.2008.08.013.

[45] Murphy JN. Adding value to waste from the mussel aquaculture industry using clean technologies. 2015.

[46] Weiner S, Addadi L. Design strategies in mineralized biological materials. J Mater Chem 1997;7:689–702. doi:10.1039/a604512j.

[47] Nebel H, Neumann M, Mayer C, Epple M. On the structure of amorphous calcium carbonate--a detailed study by solid-state NMR spectroscopy. Inorg Chem 2008;47:7874–9. doi:10.1021/ic8007409.

[48] Veses A, Aznar M, Callén MS, Murillo R, García T. An integrated process for the production of lignocellulosic biomass pyrolysis oils using calcined limestone as a heat carrier with catalytic properties. Fuel 2016;181:430–7. doi:10.1016/j.fuel.2016.05.006.

[49] Zhang L, Zhang B, Yang Z, Yan Y. Pyrolysis behavior of biomass with different Ca-based additives. RSC Adv 2014;4:39145–55. doi:10.1039/C4RA04865B.

[50] Han L, Wang Q, Ma Q, Yu C, Luo Z, Cen K. Influence of CaO additives on wheat-straw pyrolysis as determined by TG-FTIR analysis. J Anal Appl Pyrolysis 2010;88:199–206. doi:10.1016/j.jaap.2010.04.007.

[51] Lin Y, Zhang C, Zhang M, Zhang J. Deoxygenation of bio-oil during pyrolysis of biomass in the presence of CaO in a fluidized-bed reactor. Energy & Fuels 2010;24:5686–95. doi:10.1021/ef1009605.

[52] Veses A, Aznar M, Martínez I, Martínez JD, López JM, Navarro M V., et al. Catalytic pyrolysis of wood biomass in an auger reactor using calcium-based catalysts. Bioresour Technol 2014;162:250–8. doi:10.1016/j.biortech.2014.03.146.

[53] Karimi E, Teixeira IF, Gomez A, de Resende E, Gissane C, Leitch J, et al. Synergistic co-processing of an acidic hardwood derived pyrolysis bio-oil with alkaline Red Mud bauxite mining waste as a sacrificial upgrading catalyst. Appl

Catal B Environ 2014;145:187–96. doi:10.1016/j.apcatb.2013.02.007.

[54] Yathavan B, Agblevor FA. Catalytic pyrolysis of pinyon-juniper using red mud and HZSM-5. Energy & Fuels 2013;27:6858–65. doi:10.1021/ef401853a.

[55] Lim X, Sanna A, Andrésen JM. Influence of red mud impregnation on the pyrolysis of oil palm biomass-EFB. Fuel 2014;119:259–65. doi:10.1016/j.fuel.2013.11.057.

[56] Yathavan B. Conventional and Catalytic Pyrolysis of Pinyon Juniper Biomass. All Grad Theses Diss 2013:Paper 2053.

[57] Sharma A, Pareek V, Zhang D. Biomass pyrolysis - A review of modelling, process parameters and catalytic studies. Renew Sustain Energy Rev 2015;50:1081–96. doi:10.1016/j.rser.2015.04.193.

[58] Zhang L, Kong SC. Multicomponent vaporization modelling of bio-oil and its mixtures with other fuels. Fuel 2012;95:471–80. doi:10.1016/j.fuel.2011.12.009.

[59] Nguyen TB, De Hemptinne JC, Creton B, Kontogeorgis GM. Improving GC-PPC-SAFT equation of state for LLE of hydrocarbons and oxygenated compounds with water. Fluid Phase Equilib 2014;372:113–25. doi:10.1016/j.fluid.2014.03.028.

[60] Wang S, Dai G, Yang H, Luo Z. Lignocellulosic biomass pyrolysis mechanism: A state-of-the-art review. Prog Energy Combust Sci 2017;62:33–86. doi:10.1016/j.pecs.2017.05.004.

[61] Collard FX, Blin J. A review on pyrolysis of biomass constituents: Mechanisms and composition of the products obtained from the conversion of cellulose, hemicelluloses and lignin. Renew Sustain Energy Rev 2014;38:594–608. doi:10.1016/j.rser.2014.06.013.

[62] Bridgwater A V. Challenges and Opportunities in Fast Pyrolysis of Biomass : Part I. Johnson Mathhey Technol Rev 2018;62:118–30. doi:10.1595/205651318X696693.

[63] Piskorz J., Scott D. S., Radlein D. Pyrolysis Oils from Biomass. Pyrolysis Oils from Biomass 1988;376:167–78. doi:10.1021/bk-1988-0376.

[64] Garcìa-Pérez M, Chaala A, Pakdel H, Kretschmer D, Rodrigue D, Roy C. Multiphase structure of bio-oils. Energy and Fuels 2006;20:364–75. doi:10.1021/ef050248f.

[65] Fratini E, Bonini M, Oasmaa A, Solantausta Y, Teixeira J, Baglioni P. SANS analysis of the microstructural evolution during the aging of pyrolysis oils from biomass. Langmuir 2006;22:306–12. doi:10.1021/la051990a.

[66] Alsbou E, Helleur R. Whole sample analysis of bio-oils and thermal cracking fractions by Py-GC/MS and TLC-FID. J Anal Appl Pyrolysis 2013;101:222–31. doi:10.1016/j.jaap.2013.01.003.

[67] Elliott DC, Oasmaa A, Preto F, Meier D, Bridgwater A V. Results of the IEA

Round Robin on Viscosity and Stability of Fast Pyrolysis Bio-Oils. Energy & Fuels 2012;26:3769–76. doi:10.1021/ef300384t.

[68] Fermoso J, Pizarro P, Coronado JM, Serrano DP. Advanced biofuels production by upgrading of pyrolysis bio-oil. Wiley Interdiscip Rev Energy Environ 2017;6. doi:10.1002/wene.245.

[69] Abnisa F, Wan Daud WMA. A review on co-pyrolysis of biomass: An optional technique to obtain a high-grade pyrolysis oil. Energy Convers Manag 2014;87:71–85. doi:10.1016/j.enconman.2014.07.007.

[70] Oasmaa A, Källi A, Lindfors C, Elliott DC, Springer D, Peacocke C, et al. Guidelines for transportation, handling, and use of fast pyrolysis bio-oil. 1. flammability and toxicity. Energy & Fuels 2012;26:3864–73. doi:10.1021/ef300418d.

[71] Bridgwater A V. Upgrading fast pyrolysis liquids. In: Brown RC, editor. Thermochem. Process. biomass Convers. into fuels, Chem. power, Chichester: John Wiley & Sons, Ltd.; 2011, p. 157–99.

[72] Ruddy DA, Schaidle JA, Ferrell III JR, Wang J, Moens L, Hensley JE. Recent advances in heterogeneous catalysts for bio-oil upgrading via “ex situ catalytic fast pyrolysis”: catalyst development through the study of model compounds. Green Chem 2014;16:454–90. doi:10.1039/C3GC41354C.

[73] Mohan D, Pittman CU, Steele PH. Pyrolysis of Wood / Biomass for Bio-oil : A Critical Review. Energy & Fuels 2006;20:848–89. doi:10.1021/ef0502397.

[74] Diebold JP. A Review of the Chemical and Physical Mechanisms of the Storage Stability of Fast Pyrolysis Bio-Oils. Golden, Colorado: 2000. doi:NREL/SR-570-27613.

[75] Butcher T. Ensyn bio-oil powering New Hampshire hospital. IEA Bioenergy Agreem Task 34 Newsl - PyNe 37 2015:1–34.

[76] Venderbosch RH, Ardiyanti AR, Wildschut J, Oasmaa A, Heeres HJ. Stabilization of biomass-derived pyrolysis oils. J Chem Technol Biotechnol 2010;85:674–86. doi:10.1002/jctb.2354.

[77] Gollakota ARK, Reddy M, Subramanyam MD, Kishore N. A review on the upgrading techniques of pyrolysis oil. Renew Sustain Energy Rev 2016;58:1543–68. doi:10.1016/j.rser.2015.12.180.

[78] Yang Z, Kumar A, Huhnke RL. Review of recent developments to improve storage and transportation stability of bio-oil. Renew Sustain Energy Rev 2015;50:859–70. doi:10.1016/j.rser.2015.05.025.

[79] Zhang J, Toghiani H, Mohan D, Pittman CU, Toghiani RK. Product Analysis and Thermodynamic Simulations from the Pyrolysis of Several Biomass Feedstocks Product Analysis and Thermodynamic Simulations from the Pyrolysis of Several Biomass Feedstocks. Energy 2007:2373–85. doi:10.1021/ef0606557.

[80] Serrano DP, Melero JA, Morales G, Iglesias J, Pizarro P. Progress in the design of zeolite catalysts for biomass conversion into biofuels and bio-based chemicals. Catal Rev - Sci Eng 2017;60:1–70. doi:10.1080/01614940.2017.1389109.

[81] Stefanidis SD, Heracleous E, Patiaka DT, Kalogiannis KG, Michailof CM, Lappas AA. Optimization of bio-oil yields by demineralization of low quality biomass. Biomass and Bioenergy 2015;83:105–15. doi:10.1016/j.biombioe.2015.09.004.

[82] Zhou S, Wang Z, Liaw SS, Li CZ, Garcia-Perez M. Effect of sulfuric acid on the pyrolysis of Douglas fir and hybrid poplar wood: Py-GC/MS and TG studies. J Anal Appl Pyrolysis 2013;104:117–30. doi:10.1016/j.jaap.2013.08.013.

[83] Zhou S, Osman NB, Li H, McDonald AG, Mourant D, Li CZ, et al. Effect of sulfuric acid addition on the yield and composition of lignin derived oligomers obtained by the auger and fast pyrolysis of Douglas-fir wood. Fuel 2013;103:512–23. doi:10.1016/j.fuel.2012.07.052.

[84] Raveendran K, Ganesh A, Khilar KC. Influence of mineral matter on biomass pyrolysis characteristics. Fuel 1995;74:1812–22. doi:10.1016/0016-2361(95)80013-8.

[85] Mullen CA, Tarves PC, Boateng AA. Role of Potassium Exchange in Catalytic Pyrolysis of Biomass over ZSM-5: Formation of Alkyl Phenols and Furans. ACS Sustain Chem Eng 2017;5:2154–62. doi:10.1021/acssuschemeng.6b02262.

[86] Fermoso J, Hernando H, Jiménez-Sánchez S, Lappas AA, Heracleous E, Pizarro P, et al. Bio-oil production by lignocellulose fast-pyrolysis: Isolating and comparing the effects of indigenous versus external catalysts. Fuel Process Technol 2017;167:563–74. doi:10.1016/j.fuproc.2017.08.009.

[87] Oasmaa A, Sundqvist T, Kuoppala E, Garcia-Perez M, Solantausta Y, Lindfors C, et al. Controlling the phase stability of biomass fast pyrolysis bio-oils. Energy and Fuels 2015;29:4373–81. doi:10.1021/acs.energyfuels.5b00607.

[88] Zhang M, Wu H. Phase behavior and fuel properties of bio-oil/glycerol/methanol blends. Energy & Fuels 2014;28:4650–6. doi:10.1021/ef501176z.

[89] Krutof A. Blending of bio-oils derived from pyrolysis of woody biomass with oil extracted from fish waste to determine applicability as a fuel oil. Mannheim University of Applied Sciences, Germany, 2014.

[90] Furimsky E. Hydroprocessing challenges in biofuels production. Catal Today 2013;217:13–56. doi:10.1016/j.cattod.2012.11.008.

[91] Joyce BL, Stewart CN. Designing the perfect plant feedstock for biofuel production: Using the whole buffalo to diversify fuels and products. Biotechnol Adv 2012;30:1011–22. doi:10.1016/j.biotechadv.2011.08.006.

[92] de Miguel Mercader F, Groeneveld MJ, Kersten SRA, Way NWJ, Schaverien CJ, Hogendoorn JA. Production of advanced biofuels: Co-processing of upgraded

pyrolysis oil in standard refinery units. Appl Catal B Environ 2010;96:57–66. doi:10.1016/j.apcatb.2010.01.033.

[93] Pinho ADR, De Almeida MBB, Mendes FL, Ximenes VL, Casavechia LC. Co-processing raw bio-oil and gasoil in an FCC Unit. Fuel Process Technol 2015;131:159–66. doi:10.1016/j.fuproc.2014.11.008.

[94] Li B, Lv W, Zhang Q, Wang T, Ma L. Pyrolysis and catalytic upgrading of pine wood in a combination of auger reactor and fixed bed. Fuel 2014;129:61–7. doi:10.1016/j.fuel.2014.03.043.

[95] Baldwin RM, Feik CJ. Bio-oil stabilization and upgrading by hot gas filtration. Energy & Fuels 2013;27:3224–38. doi:10.1021/ef400177t.

[96] Adjaye JD, Sharma RK, Bakhshi NN. Characterization and stability analysis of wood-derived bio-oil. Fuel Process Technol 1992;31:241–56. doi:10.1016/0378-3820(92)90023-J.

[97] Zhang H, Xiao R, Wang D, He G, Shao S, Zhang J, et al. Biomass fast pyrolysis in a fluidized bed reactor under N2, CO2, CO, CH4and H2atmospheres. Bioresour Technol 2011;102:4258–64. doi:10.1016/j.biortech.2010.12.075.

[98] Mullen CA, Boateng AA, Goldberg NM. Production of deoxygenated biomass fast pyrolysis oils via product gas recycling. Energy and Fuels 2013;27:3867–74. doi:10.1021/ef400739u.

[99] Elkasabi Y, Mullen CA, Boateng AA. Distillation and isolation of commodity chemicals from bio-oil made by tail-gas reactive pyrolysis. ACS Sustain Chem Eng 2014;2:2042–52. doi:10.1021/sc5002879.

[100] Lu Q, Zhang Z-FF, Dong C-QQ, Zhu X-FF. Catalytic Upgrading of Biomass Fast Pyrolysis Vapors with Nano Metal Oxides: An Analytical Py-GC/MS Study. Energies 2010;3:1805–20. doi:10.3390/en3111805.

[101] Tangboriboon N, Kunanuruksapong R, Sirivat A, Kunanuruksapong R, Sirivat A. Preparation and properties of calcium oxide from eggshells via calcination. Mater Sci Pol 2012;30:313–22. doi:10.2478/s13536-012-0055-7.

[102] Tekin K. Hydrothermal conversion of Russian olive seeds into crude bio-oil using a CaO catalyst derived from waste mussel shells. Energy and Fuels 2015;29:4382–92. doi:10.1021/acs.energyfuels.5b00724.

[103] Barros MC, Bello PM, Bao M, Torrado JJ. From waste to commodity: transforming shells into high purity calcium carbonate. J Clean Prod 2009;17:400–7. doi:10.1016/j.jclepro.2008.08.013.

Chapter 3 Co-pyrolysis screening experiments

Parts of this chapter have been submitted for publication; K. A. Hawboldt, S. MacQuarrie, S. Papari, H. Bamdad, A. Krutof. Biomass residues to bioproducts – challenges and opportunities in rural regions.

Abstract

Pyrolysis bio-oil from forestry residue has been investigated as a possible alternative or blend for fossil fuels and chemical feedstock. However, challenges in direct use as a fuel such as high acid, oxygen, and water content cause instability and corrosion. In addition, the biomass may be in a region where there is a supply of different feedstocks as opposed to sufficient supply the forestry residues. To improve the economics of the pyrolysis process and enhance the oil quality we are studying the co-processing of the biomass with additives in the form of by-products from the fisheries and/or mining industry to enhance oil and char quality. This chapter presents the results of a screening analysis of co-pyrolysis with shrimp residues, mussel shells, and red mud both *in-situ* (softwood mixed directly with the shells/red mud) and *ex-situ* (contact of only the softwood pyrolysis vapours with the additive). The oil and char were analyzed to determine the impact on the quality as fuel (oil and char) and adsorbent/soil amendment (char). Preliminary experiments indicate that red mud is not a viable additive for fuel applications due to cracking of high molecular weight compounds leading to high water content. Oil produced with shrimp shell additive showed nitrogenous compounds that would cause issues in refining and blending application of the pyrolysis oil. Mussel shells as a co-pyrolysis additive showed a promising slight increase in oil yield, water content, and high heating value of the water free oil indicating a reduction of oxygenated organic compounds.

Keywords: Pyrolysis bio-oil, co-pyrolysis, mussel shell, shrimp shell, red mud

3.1 Feedstock preparation, particle size, and moisture analysis

This study focused on improving the quality of pyrolysis oil and char by addition of additives (red mud, shrimp shell, and mussel shell) to the softwood feedstock. The sample preparation, moisture analysis of the feedstocks, preliminary py-GC/MS studies, and tube furnace experiments have been carried out. MS was found to be the most promising additive to improve the pyrolysis oil fuel properties, and a DoE was developed (*Chapters 4 and 5*) to produce oil and char in a laboratory scale tube furnace reactor.

3.1.1 Sample preparation

The dried SW is ground to a fine powder in a ball mill for 8 min with two ¼ in stainless steel balls (for py-GC/MS) and ground to < 2 mm in a cutting mill (for tube furnace). The additive is ground in the ball mill for 8 min with two ¼ in stainless steel balls for both lab scale pyrolysis reactors. After grinding, the wood and additive are dried at 75 °C for at least 2 hours.

3.1.2 Sieve analysis

Particle sizes of the dry feedstock were determined by sieve analysis with sieve sizes 0.125, 0.25, 0.5, 1.0, 1.2, and 2.0 mm for wood and 45, 63, 90, and 125 µm for MS. The sieve times of wood and mussel shell were 3 min and 5 min, respectively; determined as ΔResidue/min < 0.1 wt%. The start weight was selected according to DIN 66165 and chosen to be 100 g for wood and 20 g for mussel shells. Rubber cylinder sieve aids (length 10 mm, diameter 5 mm) were required for mussel shells. The amplitude was 1.3 mm/g for both wood and mussel shell. The results were analyzed via a Rosin-

Rammler-Sperling-Bennet (RRSB) distribution and particle sizes were d_{10} = 0.28 mm, d_{50} = 0.67 mm, d' = $d_{63.2}$ = 0.75 mm, and d_{80} = 1.2 mm for wood; and d_{10} = 9 µm, d_{50} = 51 µm, d' = $d_{63.2}$ = 70 µm, and d_{80} = 170 µm for MS.

3.1.3 Moisture analysis feedstock

Drying experiments of co-pyrolysis feedstocks MS, RM, SS, and SW were carried out at 60, 75, and 90 °C for 0, 1, 2, 6, and 18 hours in a Blue M Stabil-Therm Oven. Two particle sizes were tested for MS, SS, and SW, as received and ground in a ball mixer mill (Section 3.1.1). The moisture content was analyzed in a Mettler Toledo HB 43-S Halogen Moisture Analyzer at 105 °C. The sample size was 2 g per moisture analysis. The moisture content does not decrease further after 2 hours of drying time or when the temperature is increased from 75 to 90 °C. Therefore, the recommended drying temperature and time are 75 °C for at least 2 hours. The final moisture content for all feedstocks is below 2 wt% (Figure 3-1).

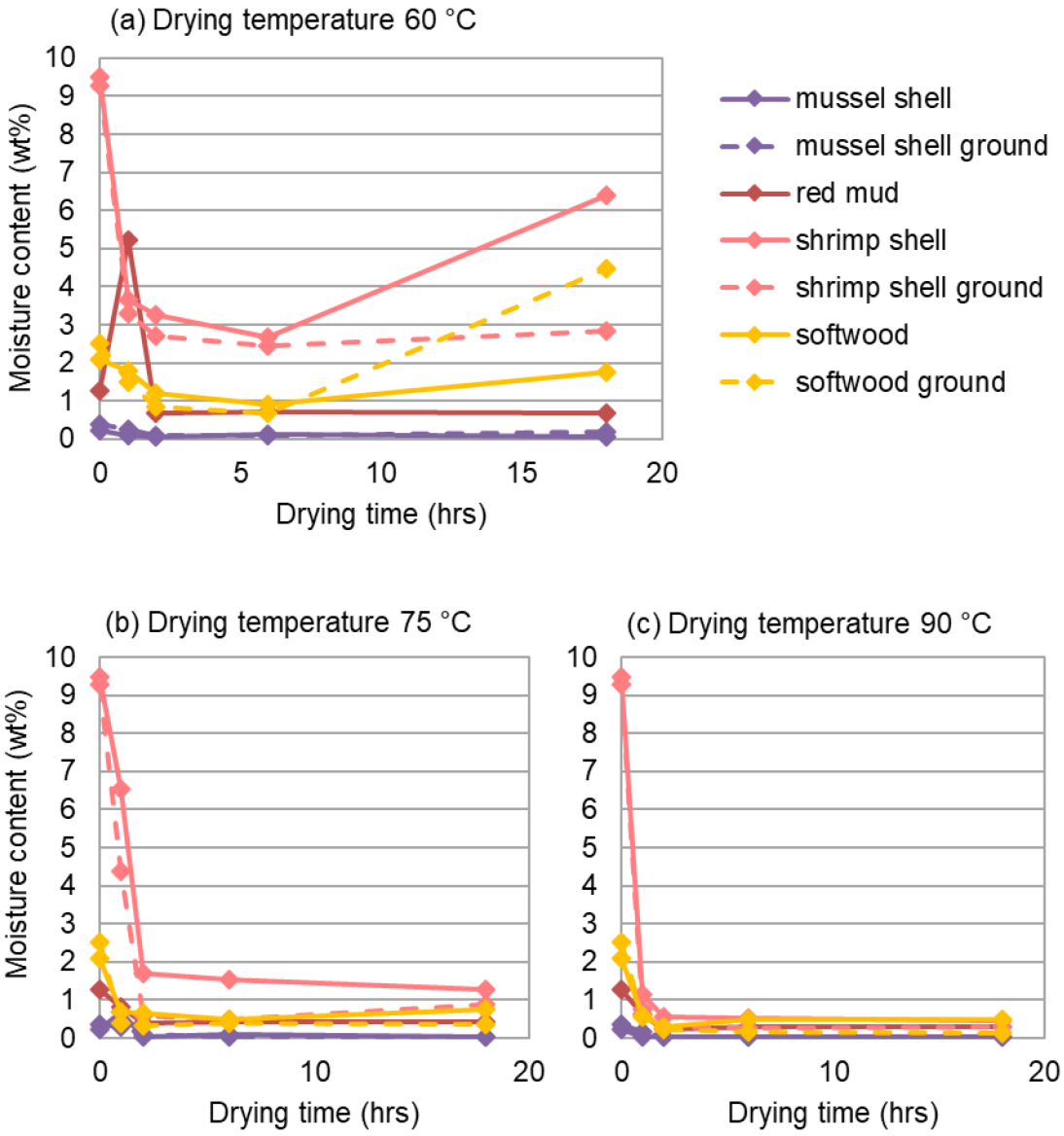

Figure 3-1: Moisture content of co-pyrolysis feedstocks at (a) 60 °C, (b) 75 °C, and (c) 90 °C drying temperature

3.2 Preliminary py-GC/MS experiment

To investigate the influence of different additives, RM, MS and SS were co-pyrolysed with SW in a GC/MS preheated to 500 °C. For compositional analysis, the vapours were passed through a GC column at 270 °C. The four SW-to-additive ratios investigated were 9:1, 5:1, 3:1, 1:1, w/w and pures (Figure 3-2). The feedstocks were mixed and ground simultaneously in a ball mill (*Section 3.1.1*).

Figure 3-2: Feedstock for py-GCMS at 1:0, 9:1, 5:1, 3:1, 1:1, and 0:1 softwood-to-additive ratio with (a) red mud and (b) mussel shell

The sample mass of SW was kept constant at 1 mg, and the weight of the complete sample adjusted accordingly. The detected chemicals were grouped into the following chemicals groups by summation of area%: Nonaromatic alcohols, carboxylic acids,

nonaromatic aldehydes, ketones, ethers, and esters, furans, pyrans, heterocyclic carbohydrates, oxygenated aromatic compounds, aromatic aldehydes, anisols, phenols, benzenediols, methoxy-, di-methoxy phenol derivatives, and PAHs [1]. The components are identified manually via a comprehensive database of pyrolysis oil compounds based on NIST webbook data with T_b, MW, and electron ionization spectrum.

3.2.1 Results

The average deviation in area% between two py-GC/MS runs with 9:1 and 7:3 ratios of SW-to-SS is 0.93 and 0.35 area% respectively. GC analyses will be carried out in duplicate and repeatability improved by integrating some of the peaks (e.g. levoglucosan peak) manually. Figure 3-3 summarizes the GC/MS spectra for the preliminary experiments with SS, MS, and RM additive per chemical family. Individual GC/MS spectra can be found in *Appendix C.1*.

3.2.2 Conclusions

The characterization of the chemical composition for the whole oil was impractical, time-consuming, and inaccurate. Only the generation of a general idea or tracking of individual compounds was possible. The GC/MS analysis is more viable when studying the bio-refinery concept, where yields of specific compounds are more important. For future oil studies elemental (CHN(O)) analysis will be investigated as an option to determine the reduction in oxygenated compounds. Moreover, at least duplicates of each py-GC/MS sample should be recorded, and the average used for analysis to reduce and identify measurement errors.

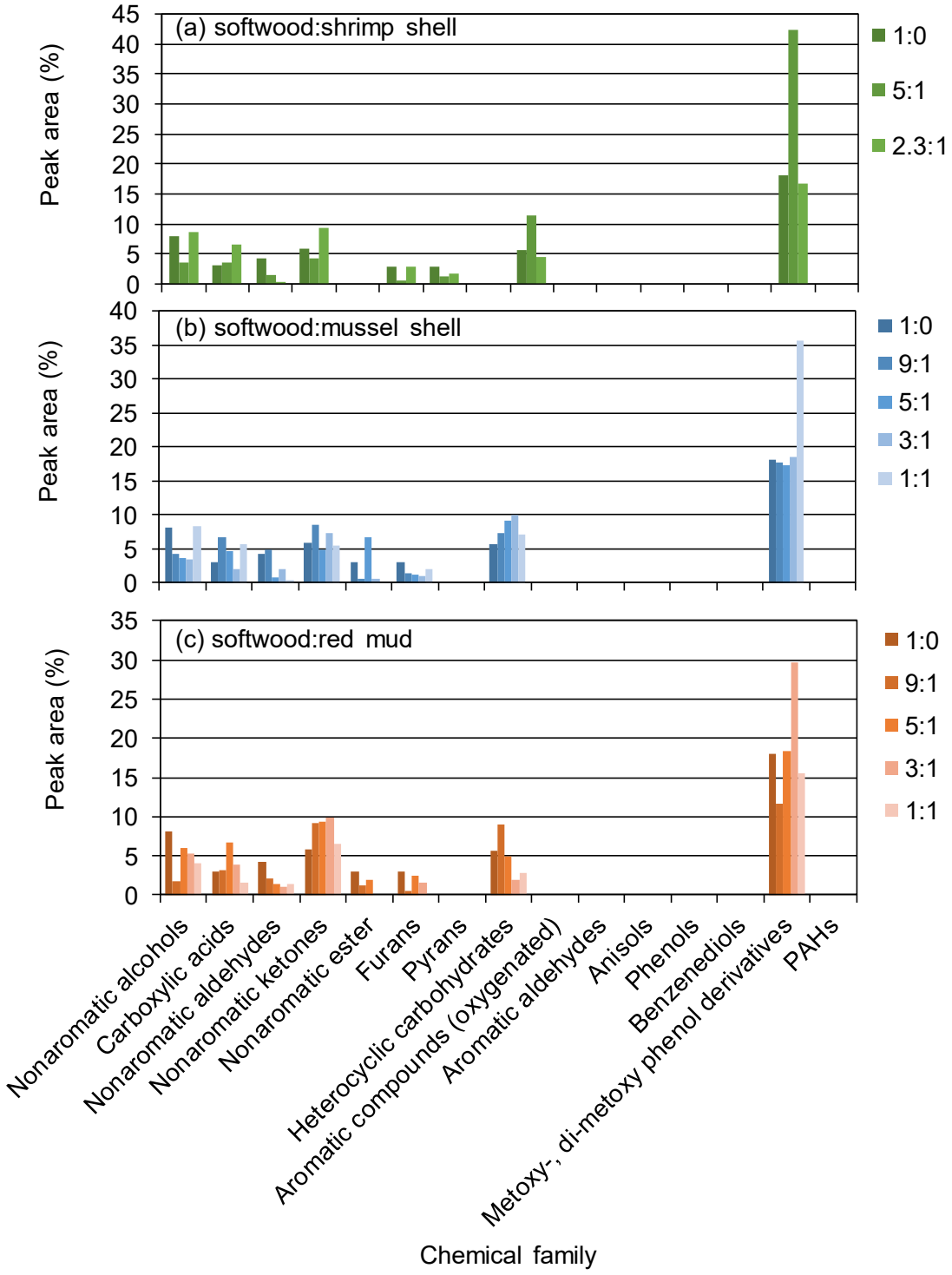

Figure 3-3: Chemical families in pyrolysis vapours from py-GC/MS for different ratios of (a) SW-to-SS, (b) SW-to-MS, and (c) SW-to-RM

3.3 Preliminary tube furnace experiment

The tube furnace sample boats were modified from open sample boats to closed tubes to allow for *ex-situ* pyrolysis vapour quality improvement by passing them through a plug of quartz wool and additive. An SW-to-additive ratio of 5:1 w/w, pyrolysis temperature (500 °C), and nitrogen flow (50 mL/min) were set as operating parameters for all experiments. The oil was analyzed for chemical composition (GC/MS), water content, and HHV. Oil and char yields were recorded, while gas yield was determined by difference. The GC/MS spectrum for pure SW is shown in Figure 3-4. The other GC/MS spectra can be found in *Appendix C.2*.

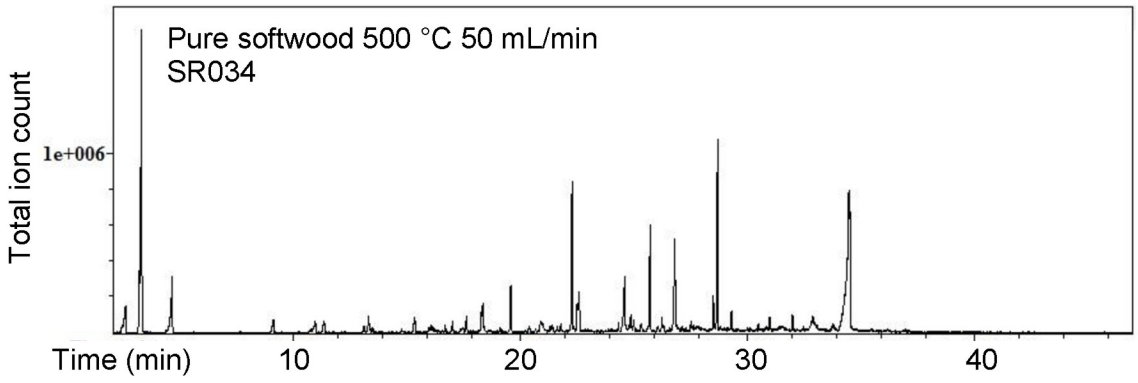

Figure 3-4: GC/MS of pyrolysis oil from pure SW (500 °C, 50 mL/min N2 flow)

3.3.1 Results

The results of the oil analyses are summarized in Table 3-1.

Table 3-1: Summary of preliminary tube furnace co-pyrolysis experiments, co-pyrolysis of SW with RM and SW with SS yielded phase separated FPBOs that were analysed individually and as a whole oil after vigorous mixing

Sample \ Properties	Yield (wt%)	Water content (wt%)		HHV (MJ/kg)		HHV of water-free oil (MJ/kg)
		Mean	95%	Mean	95%	
Pure Softwood	64.4	30.8	2.0	15.0	0.2	21.7
Pure Shrimp shell	42.9	65.7	32.4	10.2	NA	29.8
Whole Oil SW: RM *in-situ*	58.1	43.9	NA	12.6	NA	22.4
SW: RM *in-situ* aqueous	NA	50.9	7.5	9.8	5.1	19.9
SW: RM *in-situ* oily	NA	23.0	9.6	20.8	NA	27.0
Whole Oil SW: RM ex-situ	63.1	41.4	NA	12.7	NA	21.7
SW: RM *ex-situ* aqueous	NA	43.8	2.1	11.8	1.1	20.9
SW: RM *ex-situ* oily	NA	32.0	9.5	16.5	NA	24.2
SW: Mussel shell *in-situ*	58.7	35.1	1.1	14.4	0.9	22.2
SW: Mussel shell *ex-situ*	59.4	38.7	0.4	14.1	0.9	22.9
Whole Oil SW: SS *in-situ*	69.2	45.1	NA	12.6	NA	23.0
SW: SS *in-situ* aqueous	NA	53.2	1.4	10.4	0.3	22.2
SW: SS *in-situ* oily	NA	26.1	5.5	17.9	NA	24.2
Whole Oil SW: SS *ex-situ*	64.4	42.2	NA	12.4	NA	21.5
SW: SS *ex-situ* aqueous	NA	49.0	10.2	10.2	2.5	20.1
SW: SS *ex-situ* oily	NA	26.2	25.0	17.6	NA	23.9

The moisture, ash, volatile and fixed carbon content of the produced chars were analyzed along with HHV and BET surface area (Table 3-2).

Table 3-2: Results preliminary experiment char

Feed	Moisture content (wt%)	Ash (wt%)	Volatile (wt%)	Fixed carbon (wt%)	HHV (kJ/g)	BET m^2/g
Softwood	2.8	5.5	14.9	76.7	25.4	6.1
SW: SS	2.9	12.7	17.2	67.2	23.3	NA
SW: MS	3.4	9.2	25.9	61.5	17.0	6.8
SW:RM	2.1	1.6	30.9	70.7	NA	11.9

3.3.2 Other additives

Additonally to SS, MS, and RM, the influences of SW char, Hardwood (HW) char, and steel shot on the pyrolysis of pure softwood was investigated. Results show that oil production in the *in-situ* mode with SW char and steel shot reduces water content and that the *ex-situ* mode increase water content and leads to phase separation for all additives. In conclusion, softwood is in constant contact with SW char and steel shot in the auger reactor, reducing the water content of the produced oil.

3.3.3 Conclusions

Red mud is not a viable additive for fuel applications due to cracking of high molecular weight compounds leading to high water content. Oil produced with shrimp shell additive showed nitrogenous compounds that would cause issues in refining and blending application of the pyrolysis oil [2]. Both RM and SS co-pyrolysis with SW yielded two-phase FPBOs, while co-pyrolysis of SW with MS yielded a one-phase oil. Mussel shell was the most promising additive to improve oil and char quality. Oxygen content (HHV of water-free oil) in the oil was improved and the char has the potential to be used for high-value applications, such as adsorption, rather then combustion. Therefore, MS will be further investigated as a pyrolysis additive for *in-situ* and *ex-situ* operational mode. The *ex-situ* operational mode increases while i*n-situ* reduces water content in the FPBO. For future studies, acidic acid will be studied by GC/MS as an indicator of acid production. Closed tube boats reduced oil yield and quality due to poorer heat transfer compared to open boats.

3.4 Bibliography

[1] Staš M, Kubička D, Chudoba J, Pospíšil M. Overview of Analytical Methods Used for Chemical Characterization of Pyrolysis Bio-oil. Energy & Fuels 2014;28:385–402. doi:10.1021/ef402047y.

[2] Hsieh PY, Bruno TJ. Pressure-controlled advanced distillation curve analysis and rotational viscometry of swine manure pyrolysis oil. Fuel 2014;132:1–6. doi:10.1016/j.fuel.2014.04.039.

Chapter 4 Co-pyrolysis of softwood with waste mussel shells: Part 1 liquid analysis

A modified version of this chapter has been published; A. Krutof, K. A. Hawboldt. Co-pyrolysis of softwood with waste mussel shells: Liquid analysis. Fuel. May 30, 2019. 254.

Abstract

Fast pyrolysis bio-oil (FPBO) from lignocellulosic feedstocks can be limited to applications such as heating due in part to the high oxygen and resulting acid content of the oil which complicates storage, handling, and use in traditional petroleum-based systems. Research has been carried out to enhance the oil quality, both catalytically and non-catalytically. This work focuses on utilizing by-product from the fisheries industry as a co-pyrolysis additive to enhance oil quality. Mussel shells (MS) were co-pyrolyzed with softwood forestry residues in a lab-scale, tube furnace reactor. The pyrolysis temperature (400-525 °C), nitrogen flow rate (50-300 mL/min), wood-to-MS ratio (0-50 wt% MS), and operational mode (*in-situ* and *ex-situ*) were varied in a designed experiment. The produced pyrolysis oils were analyzed for water content (Karl-Fischer titration), high heating value (HHV), total acid number (TAN), pH, density, volatility and ash content via thermogravimetric analysis (TGA), and chemical composition via gas chromatography-flame ionization detector (GC-FID) and C/H/N(O) elemental analysis. Co-pyrolysis with MS *in-situ* decreased the TAN of FPBO from 68 to 48 mgNaOH/gOil), while the water content increased from 29 wt% to 39 wt%. However, the HHV of the water-free oil increased from 22.4 to 23.6 MJ/kg, indicating a reduction in oxygenated compounds, and therefore, an improvement in fuel quality of FPBO.

Keywords: Fast pyrolysis bio-oil; oil upgrading; co-pyrolysis; mussel shell; calcium carbonate; design of experiment (DoE)

4.1 Highlights

- Mussel shells, a fisheries by-product, reduce fast pyrolysis bio-oil acidity
- Deoxygenation of fast pyrolysis bio-oil through decarboxylation and dehydration
- Co-pyrolysis additives are potentially less costly compared to commercial catalysts
- GC-FID combined with response surface methodology show trends in composition

4.2 Introduction

Biomass is the world's largest, most widely available, and the only renewable energy source that can be converted into several fuels (including liquids) and chemicals [1–4]. An inventory in 2009 showed over 250 kt of residues (bark, sawdust, sludge, etc.) per year generated by sawmill and forestry operations in Newfoundland and Labrador alone [5–7]. In 2016, 171 million tonnes of fisheries products were harvested globally, with 88% for human consumption, 35-70% of which was by-product [8,9]. Fisheries by-products have the potential to be used in a variety of applications including fuels, industrial chemicals, oil spill cleanup, food industry, cosmetics, feed additives, and biotechnology [10].

Fast pyrolysis is a proven process for the conversion of forestry and agricultural residues [4,11–13]. Fast pyrolysis bio-oil (FPBO) (yield of 50-75 wt%) is the main product with by-products of biochar (12-20 wt%) and non-condensable gas (NCG) (13-16 wt%) [14–17]. FPBO is an organic liquid containing water, oxygenated compounds, and trace inorganics [12,16,18,19]. Biomass-derived FPBO is a feasible alternative to petroleum-

based heating oils requiring minimal modifications to the combustion systems and resulting in lower overall CO_2 emissions and close to zero sulphur content depending on the source of the biomass [12,20].

Improving the quality of FPBO is required to expand its use into transportation and higher end fuel markets [17]. A detailed review of FPBO fuel quality refinement can be found in [20]. Processes to improve FPBO can be grouped into catalytic and non-catalytic processes and further subdivided into upgrading of pyrolysis oil post or during pyrolysis. During pyrolysis, the vapours can be upgraded prior to condensation (*ex-situ* vapour upgrading), or the additive/catalyst can be in contact with the biomass during *in-situ* upgrading (catalytic fast pyrolysis (CFP), or co-pyrolysis) (Figure 4-2) [20]. The primary advantage of upgrading with a commercial or specially designed catalyst is the control over oil quality. However, these processes can be expensive due to catalyst replacement, high or vacuum operating pressures, and the potential requirement for hydrogen [4,11,21]. Non-synthetic additives/catalysts, produced as a by-product or waste stream from another process, with similar chemical make-up of the commercial additives/catalysts, could be a sustainable option [20]. The additive proposed in this work is mussel shells (MS). In general, studies of the pyrolysis of waste fin and shellfish and co-pyrolysis of fishery and forestry are limited.

Fast pyrolysis of waste fish oil was carried out by Wiggers and Wisniewski et al. [8,22,23] yielding 72-72.8 wt% liquid fuel, 15.9 wt% NCG, and 11.3 wt% char. The FPBO was separated into two fuels with properties comparable to gasoline and diesel via distillation; however, the fuels were highly acidic [8,22,23]. As such, the FPBO was

upgraded via reactive distillation and esterification, which reduced acid content by 95% for gasoline range and 43% for diesel range oil [8]. Fadhil et al. produced pyrolysis oil and activated carbon (via steam activation of biochar) from de-oiled fish waste in a fixed-bed laboratory scale slow pyrolysis reactor at 500 °C [24]. Rowland et al. gasified salmon processing waste (comparing whole fish to heads, viscera, and frames) and mixtures of salmon waste and pine wood pellets to produce bio-syngas [25]. Kraiem et al. pyrolyzed waste tuna lipids in a fixed-bed laboratory scale reactor at 500 °C [26,27]. Varuvel et al. used *ex-situ* pyrolysis (catalytic cracking of slow pyrolysis vapours on $Na_2Co_3/MgSO_4$ catalyst) of waste fish fat to produce a liquid for blending with diesel fuel [28,29]. Abeynaike et al. [30] and Currie et al. [31] partially calcined powdered mussel shells via slow pyrolysis at 650-800 °C to produce biochar for phosphate removal from wastewater. Pine sawdust, microalgae (*Spirulina platensis*), seaweed (*Ulva lactuca.*), and marine fish waste generated FPBO were compared [32]. The oils were generated in a fixed-bed laboratory scale reactor at 460 °C (with 10 min hold) followed by vapour upgrading on H-ZSM5 catalyst [32]. The upgrading had a dehydrating, deoxygenating, and denitrogenating (nitriles, amines, and amides) effect on the FPBO [32].

Forestry residues have been co-pyrolyzed with waste materials such as plastic and tire rubber waste [33–38], waste printed circuit boards [39], glycerol [40], sewage sludge [41], bituminous coal [42], seaweed bio-coke [43], calcium-based minerals [44,45], and mineral clays [20,46]. *Enteromorpha clathrate* sea-weed bio-coke was pyrolyzed with rice husk volatiles (*ex-situ*) in a fixed bed, laboratory scale, reactor at 550 °C, increasing the aldehydes, furans, carboxylic acids, ketones and phenols in the liquid product, while

the saccharide content decreased [43]. Co-pyrolysis of 30 wt% polypropylene with 70 wt% alder or pine wood in a laboratory scale, fixed bed, slow pyrolysis reactor at 600 °C resulted in a decrease in concentration of oxygenated organics in oil [38]. Pyrolysis of fir sawdust with waste printed circuit boards at 500 °C under 10kPa vacuum in a fixed bed, slow pyrolysis reactor produced value-added brominated aromatic compounds [39]. Co-pyrolysis of forestry waste (pine) and waste tire rubber at 500 °C improved the liquid product fuel quality compared to pyrolysis of neat pine (reduction in acidity, density, oxygen, aldehyde, and phenolic content, while pH and calorific value increased) [35]. Fast pyrolysis of sawdust pellets with 20 and 40 wt% glycerol content at 600 °C in a batch reactor decreased the FPBO and char yields and increased NCG yield as glycerol was increased [40]. In the co-pyrolysis of sewage sludge with wood or rapeseed at a ratio of 6:4 (sewage sludge to forestry/agro feed) in a fixed bed, slow pyrolysis reactor at 450 °C the fuel properties of the organic phase were improved [41].

In this work, we investigate the impact on the FPBO in the co-pyrolysis of mussel by-product (shells) with forestry residues. In Canada, 23 kt blue mussels worth 34 million USD were farmed in 2015 [47]. Once the meat is removed, the shells represent 30-50 wt% of the harvested material [48,49]. In Newfoundland, MS are disposed of in landfills, wasting a valuable by-product and incurring costs [9,30]. MS consist of 95-99 wt% mineral phase (mainly $CaCO_3$ >90%) and 1-5 wt% organic matrix composed of β-chitin fibrils in silk fibroin-like proteins that determine crystallization structure and counteract calcite brittleness [30,49–53]. Since the anhydrous $CaCO_3$ polymorphs contain little to no water, they would not directly contribute to the water content

of FPBO [54,55]. Calcium oxide can be produced along with carbon dioxide via calcination (> 700 °C) of $CaCO_3$ containing shells such as MS [50]. Zhang et al. investigate the decarboxylation (DCO) of FPBO, produced from rice husk in a fluidized bed reactor at 500 °C, with $CaCO_3$ [56]. Calcium oxide has been investigated as a co-pyrolysis additive, successfully improving the pyrolysis oil quality, reducing acid content and increasing FPBO stability [20,44,45,57–59].

Response surface methodology (RSM) was used to determine the impact of temperature, nitrogen flow (i.e. vapour residence time), softwood-to-MS ratio, and operational mode on the properties of oil and char from the co-pyrolysis of MS and forestry residues. Produced oils are analyzed for physical, chemical, and thermal properties, and fuel quality.

4.3 Materials and methods

4.3.1 DoE factors and levels

Factors that influence the yield and properties of the pyrolysis products are temperature, moisture and ash content of softwood and additive, particle size and shape of softwood and additive, total sample mass, solid and vapour residence times, age of softwood and additive, and type of reactor and condenser system [60–63]. The four main factors selected for this study were temperature (400-525 °C), nitrogen flow rate (50-300 mL/min), softwood-to-MS ratio (0-50 wt% additive), and operational mode (*in-situ* vs. *ex-situ*). This temperature range was selected to maximize the oil yield based on previous experiments and literature [12,64]. To avoid damage to the pyrolysis reactor (Figure 4-1) and glassware, the reaction temperature was limited to 525 °C.

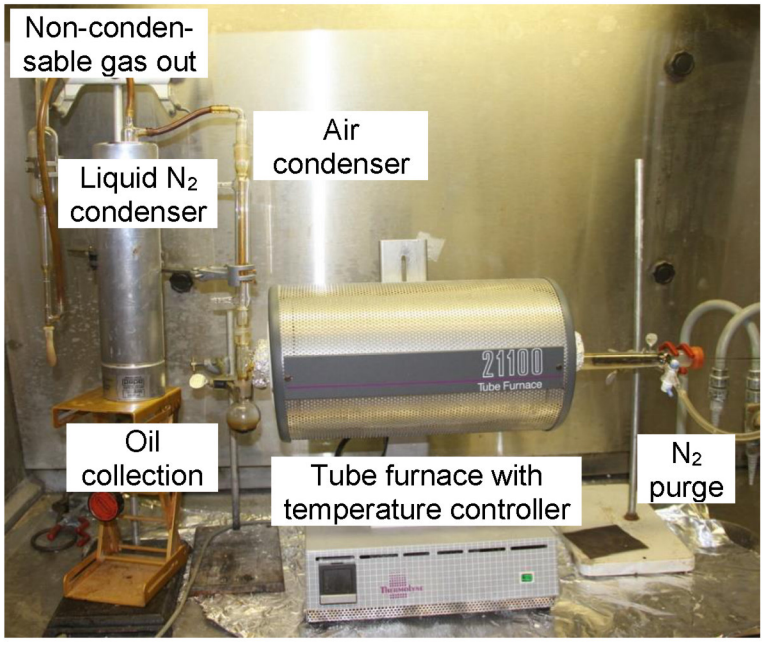

Figure 4-1: Fixed bed tube furnace reactor and condenser system set-up

For very low nitrogen flow rate (high residence time of pyrolysis vapours) secondary cracking reactions occur reducing the oil yield and increasing the char yield and water content of the oil; while for very high nitrogen flow rates, the vapours are swept out of the condenser system prior to condensation resulting in lower oil yield [12,64]. The reaction and solid residence time are covariates/concomitant variables. They can be measured/calculated, but they can not be changed [65]. The solid residence time was varied from 3.0-4.5 min. The vapour residence time is a function of the reaction temperature (higher temperatures leading to shorter reaction times) and nitrogen flow rate (higher flow rates leading to shorter reaction time). The vapours are condensed in a Liebig condenser at room temperature, collected oil cooled in an ice-water-bath followed by a liquid nitrogen trap [64,66]. The nitrogen flow rate is measured at the exit of the liquid nitrogen trap at atmospheric pressure [64].

The range of softwood-to-MS ratios was selected based on preliminary experiments, and *in-situ* and *ex-situ* mode are compared to draw conclusions on the effect of MS on the pyrolysis reactions for pyrolysis vapours in/without direct contact with solid wood biomass (Figure 4-2).

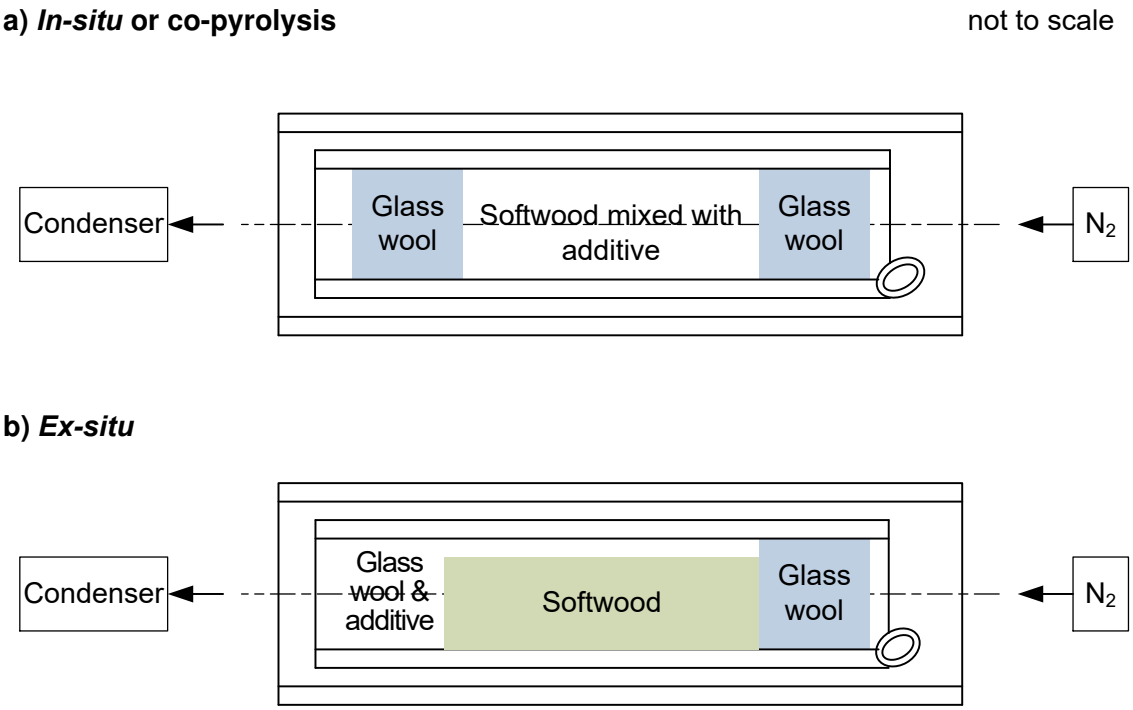

Figure 4-2: *In-situ* and *ex-situ* tube furnace operational modes

Design Expert® software (11.0.6.0) was used to determine the number of experimental runs (D-optimal design, one block, quadratic model with three lack of fit and three repetition points). The D-optimal design criterion which focuses on precise parameter estimation (maximizes determinant of the X'X matrix, best estimates effects of the factors and finds factors important to the process) was chosen over the I-optimal design criterion which focuses on precise prediction (experimental points selected that minimize the integral of the prediction variance across the design space) [65]. The fraction of design space (FDS) was larger than 0.8 for a signal-to-noise ratio of 2 and a standard deviation of 1, indicating a good design (Figure 4-3). Moreover, the design produced a relatively flat surface on the standard error plots, and therefore, this design and combination of factors will be suitable to describe the experimental region.

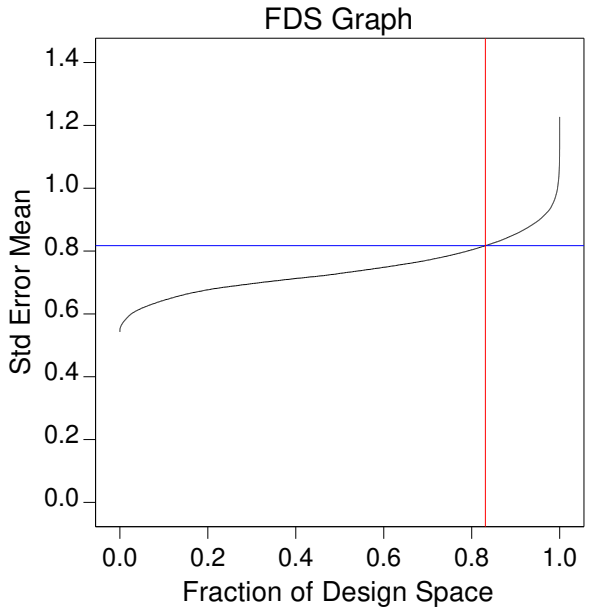

Figure 4-3: Fraction of design space (FDS) is larger than 0.8 for a signal-to-noise ratio of 2 and a standard deviation of 1 indicating a good design

Based on the ANOVA results, the factors temperature (*A*), nitrogen flow rate (*B*), amount of MS additive (*C*), and operational mode (*D*), as well as their 2 factor interactions (2FI), and quadratic effects were included in the model if the p-value was < 0.05 or between 0.05 and 0.1. To ensure hierarchy of the model factors with p-values > 0.1 were included in the model if their 2FI or quadratic effect were significant. The following three model selection criterions were applied: p-values (significance level < 5% to max. 10% with forward selection direction), Akaike information criterion (AICc, forward selection direction), and adjusted R^2. Significance of each model is defined as p-value < 0.05, F-value as 'adequately large', adjusted R^2 and predicted R^2 close to 1 with a difference between the two of < 0.2, the adequate precision coefficients as a measure for the signal-to-noise ratio (> 4), and a graphical comparison of predicted and actual values.

The responses used to compare factors are the yield of liquid, char, and gas in wt% as well as oil and char properties. Oil yield is calculated as the mass of oil collected over the mass of softwood used; char yield is the weight of the sample boat after pyrolysis minus the weight of the empty boat including quartz wool and weight of the MS (prior to pyrolysis) over the mass of softwood used; the gas yield is calculated by difference. The yields are calculated based on the softwood mass, not total biomass (softwood and MS), to allow for comparison between *in-* and *ex-situ* runs with different MS loadings, and for comparison to literature. Differences between duplicated DoE runs were 0.1-3.2 wt% for oil yields, 0.1-0.9 wt% for char yields, and 0.8-4.1 wt% for gas yields.

4.3.2 Materials and sample preparation

A mixture of Newfoundland pine and spruce softwood shavings supplied by Sexton Lumber Co Sawmill, Bloomfield NL Canada, was ground to < 2 mm in a cutting mill for use in the tube furnace reactor [64]. The MS were treated with enzymes to remove any residual organics [67]. Shells were then ground to a powder in a ball mixer mill for 8 min with two ¼ in stainless steel balls. After grinding, the wood and additive were dried at 75 °C for at least 2 hours, cooled to room temperature, and stored in airtight containers. The moisture content of the MS was < 0.1 wt%, while the moisture content of the wood was 0.4-2.0 wt% (Mettler Toledo Compact Halogen Moisture Analyzer HB34-S at 105 °C). For *in-situ* operation, the softwood was mixed with ground MS, and the ends of the sample boat were closed with plugs of very loose quartz wool to avoid material loss. For *ex-situ* mode, the MS powder was mixed into the quartz wool at the

end of the sample boat to allow for pyrolysis vapour to pass through the MS (Figure 4-2 and Figure 4-4).

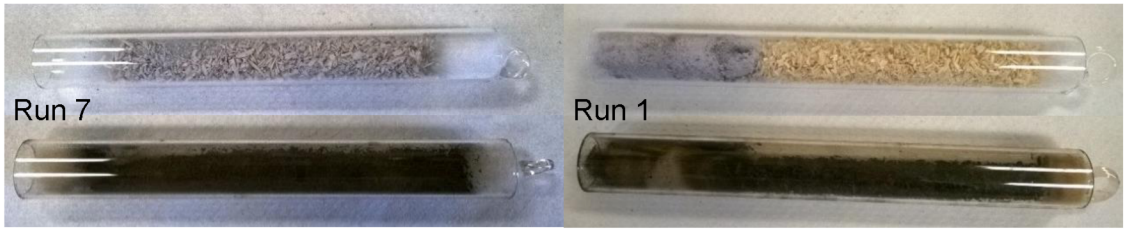

Figure 4-4: *In-situ* (left) and *ex-situ* (right) sample boats before (top) and after (bottom) pyrolysis

Loaded sample boats were dried at 75 °C for 2 hours just prior to pyrolysis. The total mass of wood per sample tube/boat was 2.0 g. The estimated weighing and handling errors were below 3 wt% for softwood and between 5-13 wt% MS (due to loss during handling). The median particle size determined via sieve analysis was 750 µm for softwood and 70 µm for MS. Other feedstock properties are analyzed analogously to the biochar [68]. The HHV of softwood was determined to be 19.51 ± 0.48 MJ/kg (triplicate measurement); MS does not combust. Carbon varied from 47.7-56.8 wt%, hydrogen from 4.7-5.8 wt%, nitrogen from 0.0-1.1 wt%, and oxygen between 37.1-46.6 wt% [69,70] for the softwood. For MS carbon was 12.9 wt%, nitrogen was 0.5 wt%, oxygen was 51.2 wt%, and calcium content was 35.3 wt%. The moisture content (< 150 °C), volatile matter (150-600 °C), fixed carbon and CO_2 content (600-800 °C), and ash and CaO content (> 800 °C) were 1.8, 84.8, 12.6, and 0.8 wt% for softwood and 0.4, 3.5, 42.0, and 54.1 wt% for MS, respectively.

4.3.3 Oil analyses

The oil was evaluated using water content, high heating value in MJ/kg (HHV), total acid number (TAN) (mgNaOH/gOil), elemental analysis (wt%), thermogravimetric analysis (TGA), and GC-FID. Density was estimated in duplicate by pipetting with a 1 mL automatic pipette and weighing on an analytical scale. Water content (free water and water of hydration) was determined in duplicate via Karl Fischer titration [71]. The difference between duplicates was no more than 1.2 wt%. HHV was determined in duplicate via ASTM D240 using a Parr B41 calorimeter with 1108 Oxygen Bomb and Model 6775 Digital Thermometer. The 95% confidence interval was determined to be ± 0.5 MJ/kg for one triplicate analysis. The TAN was analyzed according to ASTM D663 as suggested in [72] modified to use 20 mL methanol (99.9% purity) as a solvent for a 3 g FPBO sample with 0.1 M NaOH titrant. There were no duplicates due to sample volume requirements. Differences between TAN of oils produced under the same conditions (DoE runs 16 and 20, 2 and 11, and 6 and 9) were 0.2-1.9 mgNaOH/gOil. A VWR SympHony B10P pH meter with an 89231-604 electrode was used to measure pH in accordance with ASTM E70, and measurements were carried out in duplicate with an estimated error of 0.3.

The FPBO samples were analyzed for elemental composition of carbon, hydrogen, nitrogen, and oxygen (by difference) (C/H/N(O)) at the University of Alberta for samples from run 1, 3, 6, 8, 12, 13, 14, and 15. The 95% confidence interval error of the triplicate analysis of C_{wet} ranged from 0.5-3.0 wt%, H_{wet} was 0.1-1.0 wt%, and N_{wet} was

0.01-0.06 wt%. The C/H/N(O) content of the dry oil is calculated by subtracting the amount of C/H/N(O) from the water in the oil. For C (and N):

$$C_{dry} = \frac{C_{whole\ oil}}{1 - Water\ content} \tag{4.1}$$

For H:

$$H_{dry} = \frac{H_{whole\ oil} - 0.11 * Water\ content}{1 - Water\ content} \tag{4.2}$$

And for O:

$$O_{dry} = \frac{O_{whole\ oil} - 0.89 * Water\ content}{1 - Water\ content} \tag{4.3}$$

TGA and ash content analysis are carried out with a TGA Q500 (TA Instruments) operated according to ASTM E1131. An FPBO sample of 10-20 mg is heated at 20 °C/min to 600 °C under nitrogen (50 mL/min) atmosphere on a platinum pan. At 600 °C, the carrier gas is switched over to oxygen (50 mL/min), and the heat ramp continues to a maximum of 800 °C. The mass loss is recorded in the groups: highly volatile matter (< 200 °C), medium volatile matter (200-600 °C), combustible material (600-650 °C), and ash (> 650 °C). In ASTM E1131, 750 °C is suggested to determine the ash content. However, the metals in the ash oxidize with increasing temperature resulting in an increase in ash weight. Therefore, 650 °C is chosen to determine ash content in this work. Differences between five random duplicates of the same oils ranged from 2.2-5.4 wt% for highly volatiles, 1.1-3.9 wt% for medium volatiles, 0.2-2.0 wt% for combustibles, and 0.04-0.08 wt% for ash content. The FPBO samples are analyzed via GC-FID as outlined in [73] with an integration limit of $2x10^6$ area%. Glycolaldehyde, acetic acid, acetol, guaiacol, 4-methyl-guaiacol, syringol, and levoglucosan amounts

were further analyzed using Design Expert®. The standard deviation between oils produced under the same conditions (DoE runs 16 and 20, 2 and 11, and 6 and 9) averaged 0.33 ± 0.13 area%, and the triplicate analysis of a single oil resulted in a 95% confidence interval of ± 0.5 area% with a relative error < 10%.

4.4 Results and discussion

The ANOVA results and model equations are given in *Appendix D*.

4.4.1 Pyrolysis yields

The liquid yield from the pyrolysis of pure MS varied from 4.0-6.6 wt%, char yield from 94.7-95.9 wt%, while gas yield was negligible at 500 °C and 50 mL/min N_2 flow. The MS content of the char was omitted from the yield calculations for comparison of char yield between *in-* and *ex-situ*. The gas yield was determined by difference (Table 4-1). In general, the oil yield increased with temperature. The RSM analyses give a better indication of trends and interactions between parameters and are outlined for each response studied below.

Table 4-1: Oil, char, and gas yield (in wt% of wood biomass) for each run sorted by reactor temperature, amount of mussel shell additive, and operational mode

Oil	**Temp °C**	**N_2 flow mL/min**	**Mussel wt%**	**Mode *in/ex-situ***	**Oil yield wt%**	**Char yield wt%**	**Gas yield wt%**
10	400	156	0	*in*	52.6	31.6	15.8
16	400	300	0	*ex*	50.4	28.9	20.6
20	400	300	0	*ex*	53.6	29.8	16.5
2	400	50	25	*ex*	51.9	29.8	18.3
11	400	50	25	*ex*	52.0	30.5	17.5
5	400	300	50	*in*	47.0	28.8	24.2
15	400	50	50	*in*	50.0	30.7	19.3
18	428	186	50	*ex*	57.1	22.4	20.5
17	439	283	10	*in*	52.3	25.5	22.2
4	456	50	0	*ex*	61.4	22.3	16.3
8	466	260	25	*ex*	48.9	24.0	27.1
13	467	50	25	*in*	62.1	24.2	13.7
7	473	300	50	*in*	49.4	22.8	27.7
12	525	50	0	*in*	62.4	21.5	16.1
19	525	300	0	*in*	57.4	21.2	21.4
14	525	186	10	*ex*	53.4	21.9	24.7
3	525	195	50	*in*	49.8	18.4	31.8
1	525	300	50	*ex*	50.3	15.5	34.2
6	525	50	50	*ex*	61.9	17.5	20.6
9	525	50	50	*ex*	64.3	17.6	18.2

A reduced 2-factor interaction (2FI) model was found to be a good fit for the oil yield data by ANOVA (*Appendix D.1*). Temperature (*A*), nitrogen flow rate (*B*), and the interaction of temperature and nitrogen flow rate (*AB*) were the only significant factors. The yield of oil can be calculated for this system with factors normalized linearly from -1 to +1 as:

$$Yield\ of\ oil\ (wt\%) = 54.4 + 2.45\,A - 3.64\,B - 2.44\,A\,B \qquad (4.4)$$

With temperature (*A*) normalized from 400 °C (-1) to 525 °C (+1), and nitrogen flow rate (*B*) from 50 mL/min (-1) to 300 mL/min (+1). Oil yield was highest (62.9 wt%) for

high temperature (525 °C) and low nitrogen flow rate (50 mL/min). Oil yield increased with temperature until 475 °C at which point it plateaued. Higher temperatures favour gas production [17] (Figure 4-5). At high nitrogen flow rates (300 mL/min) the yield of oil was low (50.7 wt%) and increasing temperature from 400 to 525 °C did not impact the oil yield compared to a 10 wt% increase from 53.1 to 62.9 wt% with temperature at 50 ml/min flow rate. This was due to the shorter reaction time the vapours had in the reactor/condenser at high flow rates and the sweeping of vapours out of the system prior to condensation [64] (Figure 4-6). At low temperatures, the vapour production was limited, and the impact of nitrogen flow rate was small, however, at 525 °C increasing the flow from 50 to 300 mL/min decreased the gas yield by 20%. This is reflected in equation 4.4) and Figure 4-5 and Figure 4-6.

Based on RSM, the effect of temperature, and amount of MS additive on the yield of char was non-linear. The yield of char can be calculated for this system with factors normalized linearly from -1 to +1:

$$Yield\ of\ char\ (wt\%) = 24.1 - 4.98\,A - 1.07\,C - 1.00\,D + 2.34\,A^2 - 2.17\,C^2 \quad (4.5)$$

With MS additive (*C*) normalized from 0 wt% (-1) to 50 wt% (+1), and operational mode (*D*) normalized as *in-situ* (-1) and *ex-situ* (+1). The char yield was highest (*in-situ*: 29.2-32.6 wt%; *ex-situ*: 27.2-30.6 wt%) for low temperature (400 °C) consistent with literature [17] (Figure 4-5). The effect of MS was less pronounced compared to temperature. At constant MS content and mode, increasing the temperature from 400 to 525 °C increased the char yield by 10 wt%. At constant temperatures, 20 wt% MS gave

highest char yields, MS amounts higher or lower than this value decreased the char yield by up to 6% at 0 wt% MS and up to 17% at 50 wt% MS. *Ex-situ*, the fixed carbon content of the char reached a minimum at 20-25 wt% MS, while moisture, volatile, and ash content increased with MS addition. Acetic acid content in the oil was lowest when char yield was highest (low temperature and nitrogen flow rates at 20-25 wt% MS). Increased effects at high temperature and nitrogen flow rate support the theory of reactions occurring in the presence of MS. The maximum in char yield and minimum in acetic acid yield at 20-25 wt% MS could be due to the overlapping of secondary ketonization [56] and cracking reactions [64,74]. With 20-25 wt% MS ketonization reactions transform acetic acids into ketones; while at higher MS addition, secondary cracking reactions dominate, causing the increased reaction of pyrolysis vapour to char, water, and NCG. The dependence of char yield on temperature and amount of MS followed the same trend *in-* and *ex-situ* with *in-situ* values being higher by 2.0 wt%. Because the MS or operational mode did not affect the yield of oil, trapping of vapours could be ruled out. The increased char yield *in-situ* was potentially due to slightly increased vapour residence times and direct contact of vapours with the MS, leading to secondary reactions, and therefore, increased biochar, water (in oil and char), and NCG formation [64,74–76].

The yield of gas with normalized factors is:

$$Yield\ of\ gas\ (wt\%) = 21.4 + 2.35\ A + 4.04\ B + 2.82\ C + 1.89\ A\ B \quad (4.6)$$

The dependence of gas yield on temperature and nitrogen flow rate followed the same trend for all MS loadings. However, the gas yield for 25 wt% and 50 wt% MS was

2-3 wt% and 5-6 wt% higher compared to 0 wt% MS. The increased yield of gas with MS points towards secondary pyrolysis vapours reactions in both operational modes. The high gas yield and low oil yield at high nitrogen flow rates are due to incomplete condensation of pyrolysis vapours for high nitrogen flow rates [64] (Figure 4-6). Figure 4-5 shows the effect of temperature on the oil, water, char, and gas yield, while Figure 4-6 shows the effect of nitrogen content on the yields.

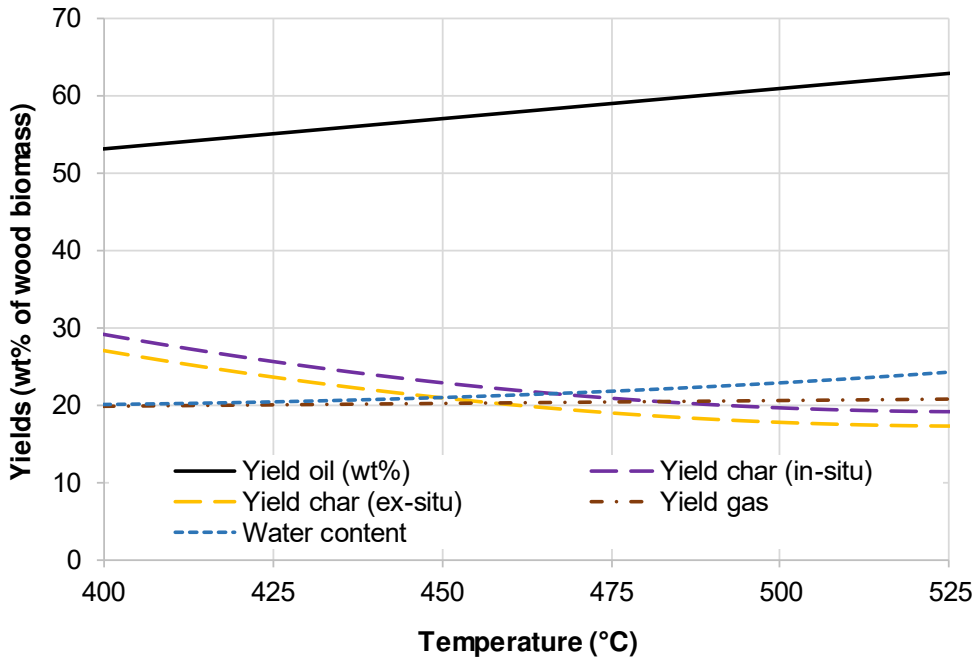

Figure 4-5: Oil, water, char, and gas yield in wt% as a function of temperature at 50 mL/min nitrogen flow rate, and 50 wt% mussel shell additive

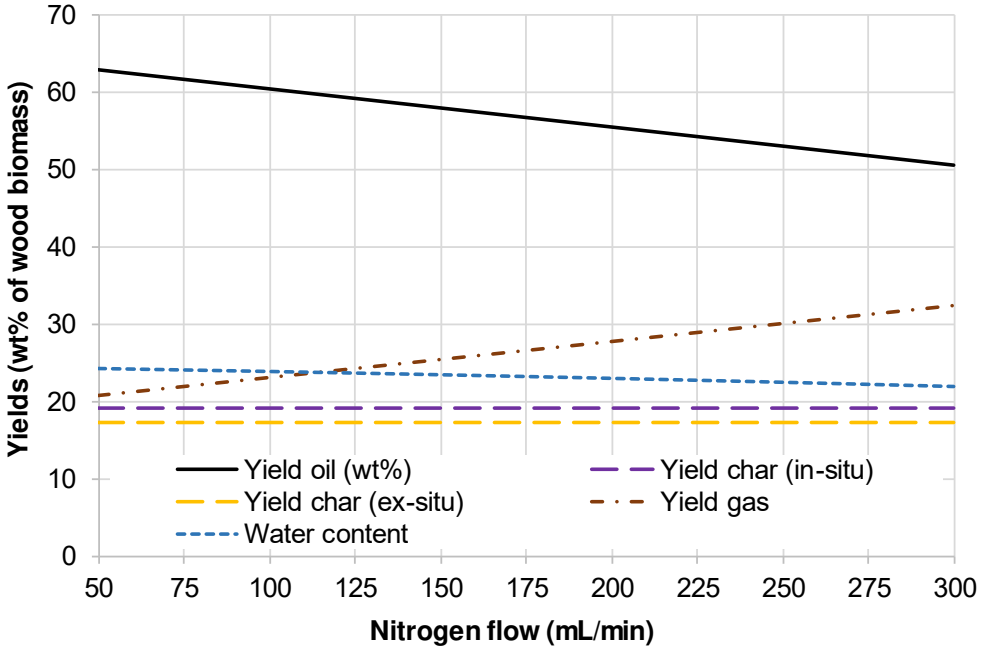

Figure 4-6: Oil, water, char, and gas yield in wt% as a function of nitrogen flow rate at 525 °C, and 50 wt% mussel shell additive

4.4.2 Oil properties

The physical oil properties investigated are outlined in *Appendix D.2*.

4.4.2.1 Water content

The normalized model is:

$$Water\ content\ (wt\%) = 33.8 - 0.700\ A + 0.562\ B + 5.22\ C + 1.27\ A\ C + 1.67\ B\ C + 1.43\ A^2 \quad (4.7)$$

Without MS additive, the water content ranged from (26.7-33.0 wt%). For constant nitrogen flow rates, the water content decreased by 12% with temperature increase from 400 to 525 °C. The impact of nitrogen flow rate at constant temperature was small (7% decrease) with increasing flow from 50 to 300 mL/min. When MS was added, the water

content increased to 33.1-36.5 wt% at 25 wt% MS, and to 36.7-43.2 wt% at 50 wt% MS. At 400 °C and 50 wt% MS the water content increased by 14-37% depending on flowrate compared to 0 wt% MS, while at 525 °C there was a 33-61% increase in water content at 50 wt% MS. At 50 wt% MS, the increase of water content with temperature over the studied range was negligible (3%) while increasing the nitrogen flow at constant temperatures resulted in a 12% increase in water content. These effects suggest dehydration (deoxygenation) reactions favoured by MS addition in both operational modes, particularly at high temperatures and nitrogen flow rates.

4.4.2.2 HHV

The normalized model for the HHV is:

$$HHV\ (MJ/kg) = 14.8 + 0.280\,A - 0.336\,B - 0.834\,C - 0.148\,D - 0.167\,A\,C - 0.157\,A\,D - 0.392\,B\,C - 0.327\,A^2 \quad (4.8)$$

In the absence of MS, nitrogen flow rate had no significant impact on HHV. The highest HHV occurred at 490-520 °C (15.4-16.1 MJ/kg), a 4-8% increase from 400 °C. At 50 wt% MS content, the effect of temperature was small (< 4% increase). However, increasing the nitrogen flow rate at constant temperatures resulted in a 10% decrease in HHV for 50 wt% MS. Regardless of operational mode and at constant temperatures, addition of 50 wt% MS reduced the HHV by 4-8% at 50 mL/min flow rate and by 14-18% at 300 mL/min, due to the increased water content resulting from dehydration reaction favoured by MS. HHV results have to be evaluated in combination with the water content to estimate the net heat of combustion.

4.4.2.3 HHV water-free oil

The HHV of the water-free oil was calculated as HHV of the wet oil over one minus water content. Through the correction of water content, this value allows for an estimation of the extent of deoxygenation reactions, including dehydration. The HHV of the water-free oil with normalized factors is:

$$HHV\ water\text{-}free\ oil\ (MJ/kg) = 22.4 + 0.264\,A - 0.299\,B + 0.418\,C - 0.0388\,D - 0.179\,C\,D \quad (4.9)$$

Regardless of MS content, increasing the temperature from 400 to 525 °C, with other factors constant, increased the HHV of the water-free oil by 2-3 %. Increasing the flow rate decreased HHV of the water-free oil by 2-3 %. At constant temperatures and flow rates, addition of 50 wt% MS increased the HHV of the water-free oil by 5% to up to 23.6 MJ/kg% *in-situ* compared to 2% to up to 23.1 MJ/kg% *ex-situ*. Though the addition of MS increased water content, the HHV of the water-free oil increased as well. This points at MS modifying the reactions pathways to deoxygenation through dehydration increasing the HHV of the water-free oil [77]. This effect was more pronounced *in-situ* due to direct contact of softwood, pyrolysis vapours, and MS.

4.4.2.4 TAN

FPBO contains 3-6 wt% weak, volatile, carboxylic acids [72]. Of the total acids in FPBO 60-70% are volatile acids, 5-10% are phenolic acids, < 5% are fatty and resin acids, and 20% are hydroxy acids [72]. The normalized model for the TAN of the oil is:

$$TAN\ (mgNaOH/gOil) = 61.4 - 3.61\ A + 2.08\ B - 7.46\ C + 1.38\ D + 2.64\ C\ D + 3.67\ C^2 \quad (4.10)$$

Without MS and at a constant nitrogen flow, the TAN decreased by 10% from 73-75 to 66-68 mgNaOH/gOil as the temperature increased from 400 to 525 °C. The impact of the nitrogen flow rate was lower compared to temperature with a 6% increase in TAN as flow rate increased from 50 to 300 mL/min (other factors constant). The trends of the impact of temperature and nitrogen flow rate on the TAN were negligible with MS addition. However, addition of MS *in-situ* decrease TAN to a great degree compared to *ex-situ*. Comparing the TAN at the same temperature and nitrogen flow rate, addition of 50 wt% MS decreased TAN by 25-30% *in-situ* and by 13-17% *ex-situ* to a minimum of 47.9 and 55.5 mgNaOH/gOil. This indicates a larger reduction of acids with direct contact of the wood with the MS demonstrated in the increased HHV of the water-free oil under the same conditions. Since the oxygen content correlates with TAN [72], decreased TAN points towards deoxygenation reactions as well as increased HHV of water-free oil.

4.4.2.5 pH

The pH of the oil with normalized factors is:

$$pH = 2.38 + 0.0640\ A + 0.493\ C - 0.214\ C^2 \quad (4.11)$$

The pH increased with the addition of MS both *in-* and *ex-situ*. The effect of increasing the temperature from 400 to 525 °C on the pH was negligibly small (5-10% increase in pH), compared to the effect of MS (60% increase in pH at 50 wt% MS). The pH was highest for 525 °C, and 50 wt% MS (2.7) and lowest at 400 °C and 0 wt% additive

(1.6). The results aligned with TAN and acidity of the oil was improved by the addition of MS at high reactor temperatures. The pH was measured to compare with TAN; however, TAN represents the acid content of FPBO more accurately [72].

4.4.2.6 Density

Temperature and operational mode did not impact density significantly. If no MS was present, the density was highest (1.17-1.20 kg/dm³). As the density is a function of water content [61], the density was lowest (1.14-1.16 kg/dm³) for high amounts of MS (> 25 wt%). The influence of the nitrogen flow rate on the density was negligible compared to the effect of MS (2.5-4.5% decrease in density).

4.4.2.7 C/H/N(O)

C/H/N(O) of the dry oil are given in Table 4-2. There was no sulphur in any of the oils. Oils produced in runs 1, 3, 6, 8, 12, 13, 14, and 15 were analyzed, and therefore, only a linear model could be developed. The model F-value for C_{dry}, H_{dry}, and O_{dry} of 0.41, 1.25, and 0.42, respectively implies that the model is not significant relative to noise, no RSM could be developed.

Table 4-2: C/H/N(O) content of the dry oil for runs 1, 3, 6, 8, 12, 13, 14, and 15

Oil	**Temp. °C**	**N_2 flow mL/min**	**Mussel wt%**	**Mode *in/ex-situ***	**C_{dry} wt%**	**H_{dry} wt%**	**N_{dry} wt%**	**O_{dry} wt%**
15	400	50	50	*in-situ*	56.3	6.5	0.66	36.6
8	466	260	25	*ex-situ*	55.2	6.5	0.49	37.8
13	467	50	25	*in-situ*	58.9	6.3	0.32	34.5
12	525	50	0	*in-situ*	55.3	6.4	< 0.3	38.3
14	525	186	10	*ex-situ*	59.0	6.3	< 0.3	34.7
3	525	195	50	*in-situ*	62.7	6.2	1.09	30.1
1	525	300	50	*ex-situ*	49.3	6.4	0.93	43.4
6	525	50	50	*ex-situ*	62.5	6.2	0.86	30.4

The carbon, hydrogen, nitrogen, and oxygen content for the softwood feedstock were 47.7-56.8, 4.7-5.8 wt%, 0.0-1.1, and 37.1-46.6 wt% [69,70]. The carbon and hydrogen content increased compared to the feedstock while the oxygen decreased. The hydrogen content ranged from 6.2-6.5 wt% and decreased slightly with increasing pyrolysis temperature. The carbon content of the oil ranged from 55.2-62.7 wt% and increased with increasing temperature and MS wt%. A high carbon content of the oil reduced the carbon to oxygen ratio, and therefore, equates to low oxygen content. At 525 °C, the oxygen content of the dry oil was reduced from 38 wt% with no MS to 30 wt% with 50 wt% MS.

The experiment at 525 °C, 300 mL/min nitrogen flow rate, and 50 wt% MS *ex-situ* showed low oil (50.3 wt%) and char (15.5 wt%) and high gas yield (34.2 wt%). The oil was low in acidity (TAN 58.3 mgNaOH/gOil and pH 2.7). However, acetic acid (15.8 area%), and acetol (17.7 area%) concentrations were high with high boiling point compounds, such as guaiacols, phenols, and syringols low compared to oils produced at lower temperatures, flow rates, or MS wt% (see *Section 4.4.2.9*). Low carbon

(49.3 wt%) and high oxygen content (43.4 wt%) of this oil align with the observed high concentration of low boiling point components and high gas yield which can be attributed to the high nitrogen flow rate and incomplete condensation, as well as increased cracking reactions at high temperatures. The high water and oxygen content can be due to cracking reactions of high molecular weight pyrolysis vapour compounds to low molecular weight compounds (e.g. NCG, water, acetic acid, acetol) due to the MS at high reaction temperatures.

The nitrogen content of the dry oil with normalized factors is:

$$N_{dry}\ (wt\%) = 0.396 + 0.144\ A + 0.411\ C \quad (4.12)$$

Not surprisingly given the residual protein material left in shells, the N_{dry} increased with the amount of MS and temperature from 0.0 wt% at 400 °C and 0 wt% MS to 0.95 wt% at 525 °C and 50 wt% MS.

4.4.2.8 TGA

Highly volatile (< 200 °C), medium volatile (200-600 °C), and combustible matter (600-650 °C), and ash content (> 650 °C) of the FPBO by TGA are given in *Appendix D.2*. The ash content was below the maximum recommended for grade G FPBO in ASTM D7544 (0.25 wt%) and ranged from 0.08 to 0.23 wt%. However, no model was significant relative to noise with respect to ash content.

The models using normalized factors are outlined below:

$$Highly\ volatile\ matter\ (wt\%) = 73.9 - 2.11\ A + 2.46\ B + 2.07\ C \quad (4.13)$$

$$Medium\ volatile\ matter\ (wt\%) = 18.9 + 0.978\ A - 2.13\ B - 2.41\ C \quad (4.14)$$

$$\frac{1}{Combustible\ matter\ (wt\%)} = 0.170 - 0.0202\ A - 0.0031\ C - 0.00866\ D - 0.0300\ C^2 \quad (4.15)$$

The highly volatile matter without MS varied from 67.2-76.4 wt% over the range of temperatures and flows investigated. Regardless of MS, the impact of temperature (4 wt% decrease over temperature range) and flow (5 wt% increase over the range of flows) was constant. When 50 wt% MS were added, a 4 wt% increase in highly volatiles to 71.4-80.5 wt% occurred compared to no MS at constant temperature and flow. The highly volatile matter correlates well with the water content of the oil. Therefore, it should be minimized to improve the fuel quality (water content, HHV, and TAN) of the FPBO while maintaining low enough viscosity to allow for pumping, atomization, and ignition of the fuel [78]. The medium volatile matter without MS varied from 18.2-24.4 wt% over the range of temperatures and flows investigated. Regardless of MS, medium volatiles increased by 2 wt% with increasing temperature from 400 to 525 °C and decreased by 4 wt% with increasing nitrogen flow rate from 50 to 300 mL/min. At 50 wt% MS, medium volatiles decreased by 5 wt% to 13.4-19.6 wt% compared to no MS (other factors constant). The medium volatile matter is inversely proportional to the highly volatile matter and water content of the oil. Therefore, high boiling point liquids (200-600 °C) react to highly volatiles (including water) with low temperature (longer

reaction times) and addition of MS. High medium volatile matter content is a rough indicator for good FPBO fuel quality because FPBO components with a boiling point range of 200-600 °C are liquids with high HHV.

High combustible matter indicates that more of the carbon from the biomass ended up in the oil instead of the char, increasing yields of gas and oil, and lowering yields of char. It also correlates with high carbon content, and therefore, low oxygen content and improved FPBO fuel quality. The difference in combustible matter between modes is negligible but follows the same trend in relation to temperature (1-2 wt% increase in combustibles with increasing temperature) and amount of MS (minimum at 25 wt% MS with 1-2 wt% lower combustible matter content compared to 0 and 50 wt% MS). It is highest at 525 °C, *ex-situ*, at 0 wt% (8.7 wt%) and 50 wt% (9.2 wt%) MS and lowest (5.0 wt%) at 400 °C, *in-situ*, at 25 wt% MS.

4.4.2.9 GC-FID

The integrated peaks of DoE oils 12 and 3 (GC-FID run 2) are shown here to represent 0 and 50 wt% MS (Figure 4-7). GC-FID integration results are given in area % for each identified component in *Appendix D.3* [73].

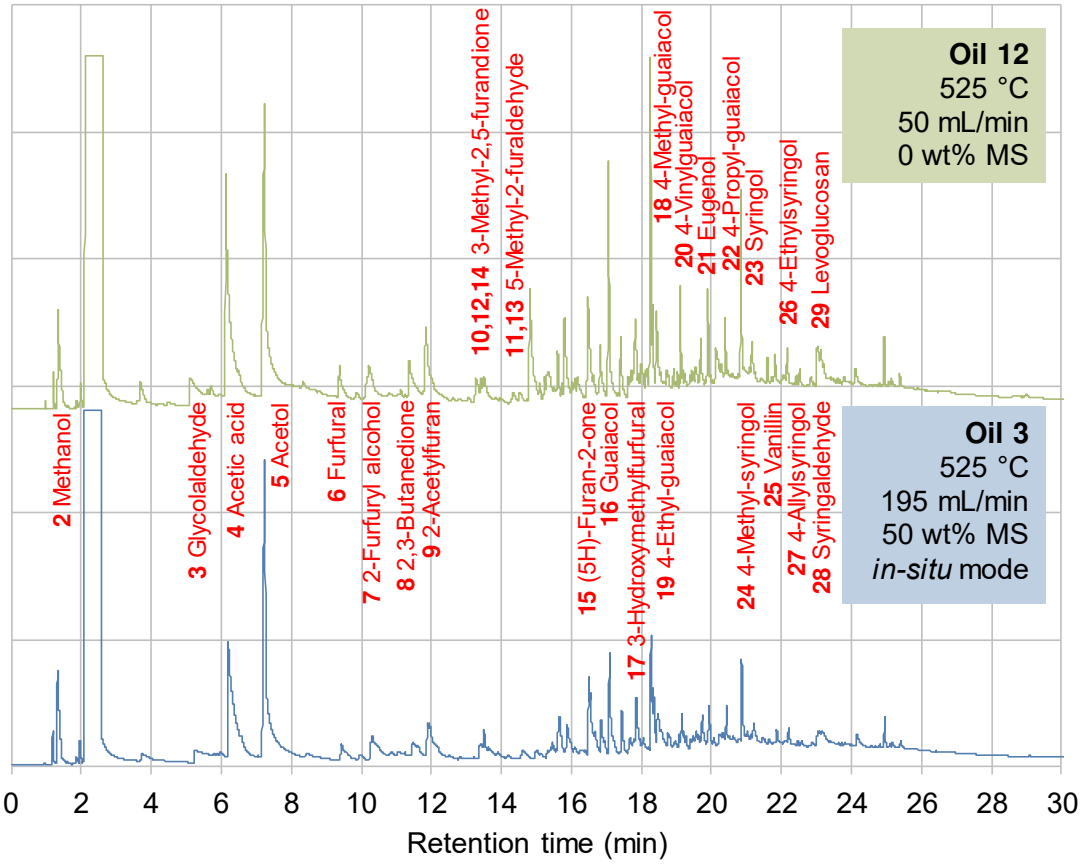

Figure 4-7: Comparison of DoE oils 3 and 12 (with and without MS)

Oil 12 showed the highest oxygen content (with exception of oil 1) and low acid and acetol contents; while oil 3 showed the lowest oxygen content and high acid and acetol contents.

4.4.2.10 Glycolaldehyde

Glycolaldehyde has potential use in the food industry and as an intermediate in the renewable ethylene glycol production [79,80]. The normalized model is:

$$\frac{1}{Glycolaldehyde\ (Area\ \%)} = 0.579 - 0.0507\ A - 0.0456\ B + 0.0780\ C - 0.0337\ D + 0.0483\ B\ D - 0.0947\ C^2 \quad (4.16)$$

The glycolaldehyde increased with increasing temperature, increasing nitrogen flow rate, and decreasing amount of MS. The glycolaldehyde content was highest (3.4 area%) at 525 °C, 300 mL/min, 0 wt% MS, and *in-situ*; and lowest (1.3 area%) at 400 °C, 50 mL/min, and 25-50 wt% MS, and *in-situ*. Increasing nitrogen flow from 50 to 300 mL/min increased the glycolaldehyde by 0.4-1.3 area% (by 30-60%) *in-situ* but negligible *ex-situ.* This requires more investigation as it is clear the contact of the MS with solid wood and/or vapours is a factor in oil composition and hence application. At 50 mL/min, 0.3-1.0 area% (20-25%) less glycolaldehyde was present *in-situ* (1.3-2.1 area%) vs. *ex-situ* (1.6-3.1 area%). However, there was no difference at 300 ml/min (other factors constant). The glycolaldehyde increase with temperature was small: up to 0.5 area% (15-25%) increase with > 20 wt% MS addition and up to 0.9 area% (25-35%) increase without MS. Keeping all other factors constant, the addition of 50 wt% MS decreased the glycolaldehyde by 0.4-1.2 area% (25-35%).

4.4.2.11 Acetic acid

The acetic acid is associated with the TAN, and hence with any deoxygenation that may be required downstream. The normalized model is:

$$Acetic\ acid\ (Area\ \%)^{-2.26} = 4.49 * 10^{-3} - 5.85 * 10^{-4}\ A - 5.78 * 10^{-4}\ B - 3.85 * 10^{-5}\ C - 2.97 * 10^{-4}\ D - 7.42 * 10^{-4}\ C^2 \quad (4.17)$$

Keeping all other factors constant, the acetic acid increased by 0.5-2.5 area% (10-20%) with temperature increasing from 400 to 525 °C and by 1.2-2.5 area% (10-20%) with flow rate increased from 50 to 300 mL/min. There was a slight increase of 0.5-1.4 area% (5-10%) *ex-situ* compared to *in-situ*. The minimum acetic acid (9.6-10.1 area%) is associated with the maximum char yield (25 wt% MS, 400 °C and 50 mL/min nitrogen flow rate). For no MS the highest acetic acid was 13.4 area% at 525 °C, 300 mL/min and for MS present at 50 wt% MS *ex-situ* (14.6 area%) at the same temperatures and flow rates. The reduction of acetic acid content with MS could be due to decarboxylation of carboxylic acids to ketones on $CaCO_3$ [56], which is favoured with the direct contact of wood and pyrolysis vapours with MS *in-situ*. At 30-50 wt% MS secondary cracking reactions are likely favoured instead of ketonization reactions leading to a different deoxygenation pathway: increase in water content due to dehydration reactions instead of a decrease in acetic acid content due to ketonization.

4.4.2.12 Acetol

Acetol levels were studied as it has been identified as a value-added chemical [81].The normalized model is:

$$Acetol\ (Area\ \%) = 15.1 - 0.0222\ A + 0.687\ B + 1.42\ C + 0.535\ A\ C + 1.11\ B\ C \quad (4.18)$$

The highest acetol (18.8 area%) occurred at 525 °C, 300 mL nitrogen flow rate, and 50 wt% MS and the lowest at 525 °C, 300 mL/min nitrogen flow rate, and 0 wt% MS.

In the absence of MS, the decrease in acetol content with increasing temperature and the increase with flow rate were small with a 5-10% change over the investigated range keeping all other factors constant. At constant temperatures, addition of 50 wt% MS increased the acetol by 4-6 area% (30-48%) at 300 mL/min nitrogen flow; this effect was much smaller (-0.5-1.7 area%) (-3% to +12% increase) at 50 mL/min flow rate. The effect of the amount of MS and its interaction with nitrogen flow rate dominated all other effects. The increase in acetol with MS addition could be due to decarboxylation of carboxylic acids to ketones on $CaCO_3$ [56].

4.4.2.13 Guaiacol

Guaiacol is one of a number of compounds used as a surrogate in the study of the hydrodeoxygenation of pyrolysis oil [82]. The normalized model is:

$$\begin{aligned} Guaiacol\ (Area\ \%) &= 4.97 - 0.328\ A - 0.0336\ B + 0.0727\ C \\ &\quad - 0.150\ D - 0.276\ A\ B - 0.163\ A\ D + 0.159\ C\ D \\ &\quad - 0.870\ A^2 + 0.407\ B^2 \end{aligned} \tag{4.19}$$

Little change (< 0.5 area% total, < 5-15% relative change) in guaiacol content occurred with MS addition for both operational modes. The highest guaiacol content (5.6 area%) occurred at 450 °C, 300 mL/min nitrogen flow rate, and 0 wt% MS, lowest (3.1 area%) was at 525 °C, 220 mL/min nitrogen flow rate, and 0 wt% MS. The temperature (*A*) and its interaction effect with nitrogen flow rate (*AB*) dominate all other effects on guaiacol content. The guaiacol was highest for moderate temperatures (450-475 °C), 0.3-1.0 area% (8-23%) higher compared to 400 °C and 0.8-1.6 area% (17-33%) higher

compared to 525 °C (keeping all other factors constant). The decrease of guaiacol content with increasing pyrolysis temperature is well studied [83–85]. At low pyrolysis temperatures (300-350 °C) cleavage/depolymerization reactions of lignin polymers result in guaiacol/syringol formation [83]. At higher temperatures (400-450 °C) guaiacol's methoxyl groups react (homolysis/rearrangement), and condensation reactions of lignin degradation products (such as guaiacol) occur with increasing temperatures reducing the initial guaiacol concentration [83].

4.4.2.14 4-Methyl-guaiacol

The normalized model for the lignin pyrolysis product, 4-methyl-guaiacol, is:

$$\begin{aligned} &4\text{-}Methyl\text{-}guaiacol\ (Area\ \%) \\ &\quad = 6.85 + 0.0525\ A - 0.382\ B - 0.392\ A\ B \\ &\quad - 0.621\ A^2 \end{aligned} \tag{4.20}$$

The 4-methyl-guaiacol content of the oil increased for mid-range temperatures and decreasing nitrogen flow rates with an interaction effect of temperature and nitrogen flow rate. At low temperatures, nitrogen flow rate did not impact the 4-methyl-guaiacol content, while at 525 °C the 4-methyl-guaiacol content decreased by 23% from 7.1 area% to 5.5 area% with nitrogen flow increase of 50 to 300 mL/min. The 4-methyl-guaiacol content was highest for 485 °C, and 50 mL/min nitrogen flow rate (7.3 area%), and lowest for 525 °C, and 300 mL/min nitrogen flow rate (5.5 area%). The decrease in 4-methyl-guaiacol content at temperatures higher 485 °C is due to the same reactions outline for guaiacol above (*Section 4.4.2.13*) [85].

4.4.2.15 Syringol

The syringol content of the oil with coded factors normalized linearly from -1 to +1 is:

$$Syringol\ (Area\ \%) = 4.18 - 0.367\ B + 0.0801\ C - 0.742\ C^2 \quad (4.21)$$

The syringol content of the oil decreased by 0.7 area% (16-20%) from 3.7-4.5 area% to 3.0-3.8 area% with increasing flow rate from 50 to 300 mL/min at constant MS content. The syringol content was highest for 50 mL/min nitrogen flow rate and 26 wt% MS (4.5 area%) and lowest for 300 mL/min and 0 and 50 wt% MS (3.0-3.1 area%) outlining the strong non-linear effect of MS (20-30% increase in syringol content at 25 wt% MS vs. 0 or 50 wt% MS at constant flow rate). As a lignin degradation product, syringol content should decrease with increasing temperature [83]. However, the temperature is insignificant in this case. Instead, the syringol follows the trend of char yield and the inverse trend of the acetic acid content: syringol production is favoured at long residence times in the presence of up to 26 wt% MS. At higher MS content, secondary reactions (cracking/dehydration) are favoured as outlined above (see *Section 4.4.1*).

4.4.2.16 Levoglucosan

Levoglucosan is the most abundantly produced pyrolytic sugar [86,87] with proposed applications in pharmaceuticals, food additives, pesticides, surfactants, and polymers [81]. The normalized model is:

$$\begin{aligned} Levoglucosan\ (Area\ \%) \\ &= 3.20 - 0.104\ A - 0.433\ B - 0.492\ C + 0.228\ D \\ &+ 0.286\ A\ B - 0.237\ B\ D + 0.402\ C\ D \end{aligned} \quad (4.22)$$

Regardless of MS content, the levoglucosan increased with decreasing nitrogen flow rate, decreasing temperature for low nitrogen flow rates, and increasing temperature for

high nitrogen flow rate (> 200 mL/min). The highest levoglucosan content occurred at 400 °C, 50 mL/min, and 0 wt% MS (4.5 area%) and lowest at 400 °C, 300 mL/min, and 50 wt% MS *in-situ* (1.7 area%) and *ex-situ* (2.5 area%). The change in levoglucosan level through an increase in temperature was < 1.0 area% (-30 to 25% relative change). At 400 °C the nitrogen flow decreased levoglucosan by 1.0 area% (20-40%) *in-situ* and by 1.9 area% (40-50%) *ex-situ*, while the effect at 525 °C was smaller: no significant change *in-situ* and decrease by 0.7 area% (20%) *ex-situ*. At constant temperatures and nitrogen flow rates, levoglucosan decreased by 1.8 area% (40-50%) with 50 wt% MS shell addition *in-situ*, but no significant change occurred *ex-situ*. Levoglucosan is the primary cellulose degradation product [88]. Alkali and alkaline earth metals (esp. Mg and Ca) catalyze pyranose ring fragmentation [86,89]. Therefore, conclusions can be drawn that the presence of MS causes ring fragmentation. The decrease of levoglucosan production with increasing temperature has also been shown by Demirbas [90].

4.5 Conclusions

In this work, mussel shell was investigated as a co-pyrolysis additive to improve the oil and char properties compared to pyrolysis of neat softwood forestry residues via a de-signed experiment (DoE). In remote maritime regions, fisheries by-product such as MS may be an alternative to commercial catalysts. To maximize the oil yield and heating value of the water-free oil (deoxygenation), the optimum reactor temperature for the studied system was found to be 500-525 °C with a low sweep gas flow rate. The amount of mussel shell additive and operational mode did not have a significant impact on the

oil yield. The highest char yield was observed *in-situ* at 400 °C, and 20 wt% MS. The presence of MS increased the NCG yield by 1 wt% per 10 wt% of MS additive.

Addition of MS notably decreased the acidity of the oil measured as pH, TAN, and acetic acid content. This effect was more pronounced *in-situ*, indicating reduction of acids due to direct contact of the pyrolysis oil vapours and wood with the MS. High amounts of MS (50 wt%) at 525 °C and 50 mL/min reduced TAN from 67 to 48-56 mgNaOH/gOil. Decreased TAN, as well as oxygen content of the dry oil (from 38 wt% at 525 °C and no MS to 30 wt% with 50 wt% MS), indicate deoxygenation reactions. The non-linear effect of the amount of MS gave a minimum of acetic acid content at 25 wt% MS for both operational modes. The MS increased the water content, decreasing the overall HHV while still producing a one phase oil. However, a small increase in the HHV of the water-free oil suggests MS favoured deoxygenation reactions through dehydration in both operational modes which is confirmed by a decrease in oxygen and increase in water content. For heat and power applications the maixmum amount of MS additive is 20 wt% to meet the ASTM D7544 standard of maximum 30 wt% water content. TGA showed that the highly volatile matter is associated with the water content of the oil. The medium volatiles in the oil were inversely proportional to highly volatiles and water content of the oil. High medium volatile content indicates good FPBO fuel quality (high HHV, low water and TAN). High combustible matter in the oil correlates with high yields of gas and oil, and low yields of char. A maximum of nitrogen in the dry oil was reached at 525 °C and 50 wt% MS. The nitrogen originates from the organics (5 wt%) in the MS and can limit fuel applications due to nitrous oxide emissions.

The addition of MS leads to decarboxylation of carboxylic acids to ketones with $CaCO_3$. Acetol has a ketone functional group; therefore, acetol increased with MS. Glycolaldehyde content in the oil decreased with increasing amount of MS, while acetol and furfural content increased. Levoglucosan content decreased *in-situ* only, while guaiacol content increased *ex-situ* only with an increased amount of MS. The acetic acid content reached a minimum, while the syringol content reached a maximum at 25 wt% MS content.

In conclusion, the addition of MS as a co-pyrolysis additive with softwood successfully deoxygenated the FPBO through decarboxylation of acids to ketones and dehydration reactions. Enhancing oil quality with the use of co-pyrolysis additive is a low cost first upgrading step that can be used for oil production on-site for heat and power application and as a biorefinery feedstock. Due to reduced oxygen and acid content the stability for transportation to central processing sites, such as biorefineries, is increased. Co-pyrolysis FPBO as a feedstock to biorefineries can reduce cost such as catalyst cost. If co-pyrolysis additives enhance pyrolysis oil as well as char quality, and if the additives are incorporated within the char, an additional separation step is not necessary decreasing operational cost further compared to catalytic upgrading processes.

4.6 Bibliography

[1] BioFuelNet. Annual report 2016. Montreal, Quebec, Canada: 2016.

[2] COP22. The COP22, the COP of Action. Marrakech, Morocco: 2016.

[3] Lee H. The IPCC's scientific assessments of Climate Change. COP22 United Nations Clim Chang Conf 2016:18–9.

[4] Abnisa F, Wan Daud WMA. A review on co-pyrolysis of biomass: An optional technique to obtain a high-grade pyrolysis oil. Energy Convers Manag 2014;87:71–85. doi:10.1016/j.enconman.2014.07.007.

[5] Butler L, Altdorff D, Young E, Galagedara L, Hawboldt K, Helleur R, et al. Organic Waste in Newfoundland: A Review of Available Agriculture, Fishery, Forestry and Municipal Waste Literature. St. John's, NL: 2017.

[6] Krigstin S, Hayashi K, Tchórzewski J, Wetzel S. Current inventory and modelling of sawmill residues in Eastern Canada. For Chron 2012;88:626–35. doi:10.5558/tfc2012-116.

[7] Jayasinghe P. Provincial Inventory of Forest Biomass Residues. 2011.

[8] Wisniewski A, Wosniak L, Scharf DR, Wiggers VR, Meier HF, Simionatto EL. Upgrade of biofuels obtained from waste fish oil pyrolysis by reactive distillation. J Braz Chem Soc 2015;26:224–32. doi:10.5935/0103-5053.20140251.

[9] Food and Agriculture Organization. The State of World Fisheries and Aquaculture. Rome, Italy: 2018.

[10] Kerton FM, Liu Y, Murphy JN, Hawboldt K. Renewable resources from the oceans: Adding value to the by-products of the aquaculture and fishing industries. 2014 Ocean - St John's, Ocean 2014 2015:14–6. doi:10.1109/OCEANS.2014.7002983.

[11] Butler E, Devlin G, Meier D, McDonnell K. A review of recent laboratory research and commercial developments in fast pyrolysis and upgrading. Renew Sustain Energy Rev 2011;15:4171–86. doi:10.1016/j.rser.2011.07.035.

[12] Basu P. Biomass gasification and pyrolysis: Practical design and theory. Oxford UK: Elsevier Inc.; 2010.

[13] Chiaramonti D, Bonini M, Fratini E, Tondi G, Gartner K, Bridgwater A V., et al. Development of emulsions from biomass pyrolysis liquid and diesel and their use in engines - Part 2: Tests in diesel engines. Biomass and Bioenergy 2003;25:101–11. doi:10.1016/S0961-9534(02)00184-8.

[14] Branca C, Giudicianni P, Di Blasi C. GC/MS characterization of liquids generated from low-temperature pyrolysis of wood. Ind Eng Chem Res 2003;42:3190–202. doi:10.1021/ie030066d.

[15] Zhang L, Liu R, Yin R, Mei Y. Upgrading of bio-oil from biomass fast pyrolysis in China : A review. Renew Sustain Energy Rev 2013;24:66–72. doi:10.1016/j.rser.2013.03.027.

[16] Staš M, Kubička D, Chudoba J, Pospíšil M. Overview of Analytical Methods Used for Chemical Characterization of Pyrolysis Bio-oil. Energy & Fuels 2014;28:385–402. doi:10.1021/ef402047y.

[17] Bridgwater A V. Review of fast pyrolysis of biomass and product upgrading. Biomass and Bioenergy 2012;38:68–94. doi:10.1016/j.biombioe.2011.01.048.

[18] Zhang L, Kong SC. Multicomponent vaporization modelling of bio-oil and its mixtures with other fuels. Fuel 2012;95:471–80. doi:10.1016/j.fuel.2011.12.009.

[19] Nguyen TB, De Hemptinne JC, Creton B, Kontogeorgis GM. Improving GC-PPC-SAFT equation of state for LLE of hydrocarbons and oxygenated compounds with water. Fluid Phase Equilib 2014;372:113–25. doi:10.1016/j.fluid.2014.03.028.

[20] Krutof A, Hawboldt KA. Upgrading of biomass sourced pyrolysis oil review: focus on co-pyrolysis and vapour upgrading during pyrolysis. Biomass Convers Biorefinery 2018;8:775–87. doi:10.1007/s13399-018-0326-6.

[21] Ruddy DA, Schaidle JA, Ferrell III JR, Wang J, Moens L, Hensley JE. Recent advances in heterogeneous catalysts for bio-oil upgrading via “ex situ catalytic fast pyrolysis”: catalyst development through the study of model compounds. Green Chem 2014;16:454–90. doi:10.1039/C3GC41354C.

[22] Wiggers VR, Wisniewski A, Madureira LAS, Chivanga Barros AA, Meier HF. Biofuels from waste fish oil pyrolysis: Continuous production in a pilot plant. Fuel 2009;88:2135–41. doi:10.1016/j.fuel.2009.02.006.

[23] Wisniewski A, Wiggers VR, Simionatto EL, Meier HF, Barros AAC, Madureira LASS, et al. Biofuels from waste fish oil pyrolysis: Chemical composition. Fuel 2010;89:563–8. doi:10.1016/j.fuel.2009.07.017.

[24] Fadhil AB, Ahmed AI, Salih HA. Production of liquid fuels and activated carbons from fish waste. Fuel 2017;187:435–45. doi:10.1016/j.fuel.2016.09.064.

[25] Rowland S, Bower CK, Patil KN, DeWitt CAM. Updraft gasification of salmon processing waste. J Food Sci 2009;74:426–31. doi:10.1111/j.1750-3841.2009.01312.x.

[26] Kraiem T, Hassen-Trabelsi A Ben, Naoui S, Belayouni H, Jeguirim M. Characterization of the liquid products obtained from Tunisian waste fish fats using the pyrolysis process. Fuel Process Technol 2015;138:404–12. doi:10.1016/j.fuproc.2015.05.007.

[27] Kraiem T, Ben Hassen-Trabelsi A, Naoui S, Belayouni H. Characterization of syngas and bio-char: Co-products from pyrolysis of waste fish fats. IREC 2014 - 5th Int Renew Energy Congr 2014. doi:10.1109/IREC.2014.6826976.

[28] Mrad N, Aloui F, Tazerout M. Upgrade of corrosiveness nature of fish waste bio-oil using a hybrid catalyst (MGO/NA2CO3) optimization process. Am Soc Mech Eng Fluids Eng Div FEDSM 2013;1 C:1–9. doi:10.1115/FEDSM2013-16391.

[29] Varuvel EG, Mrad N, Tazerout M, Aloui F. Assessment of liquid fuel (bio-oil) production from waste fish fat and utilization in diesel engine. Appl Energy 2012;100:249–57. doi:10.1016/j.apenergy.2012.05.035.

[30] Abeynaike A, Wang L, Jones MI, Patterson DA. Pyrolysed powdered mussel shells for eutrophication control: effect of particle size and powder concentration on the mechanism and extent of phosphate removal. Asia-Pacific J Chem Eng 2011;6:231–43. doi:10.1002/apj.426.

[31] Currie JA, Harrison NR, Wang L, Jones MI, Brookes MS. A preliminary study of processing seafood shells for eutrophication control. Asia-Pacific J Chem Eng 2007:460–7. doi:10.1002/apj.082.

[32] Lorenzetti C, Conti R, Fabbri D, Yanik J. A comparative study on the catalytic effect of H-ZSM5 on upgrading of pyrolysis vapors derived from lignocellulosic and proteinaceous biomass. Fuel 2016;166:446–52. doi:10.1016/j.fuel.2015.10.051.

[33] Uzoejinwa BB, He X, Wang S, Abomohra AE, Hu Y, Wang Q. Co-pyrolysis of biomass and waste plastics as a thermochemical conversion technology for high-grade biofuel production : Recent progress and future directions elsewhere worldwide. Energy Convers Manag 2018;163:468–92. doi:10.1016/j.enconman.2018.02.004.

[34] Burra KG, Gupta AK. Kinetics of synergistic effects in co-pyrolysis of biomass with plastic wastes. Appl Energy 2018;220:408–18. doi:10.1016/j.apenergy.2018.03.117.

[35] Martínez JD, Veses A, Mastral AM, Murillo R, Navarro M V., Puy N, et al. Co-pyrolysis of biomass with waste tyres: Upgrading of liquid bio-fuel. Fuel Process Technol 2014;119:263–71. doi:10.1016/j.fuproc.2013.11.015.

[36] Bernardo M, Lapa N, Gonçalves M, Mendes B, Pinto F. Study of the organic extraction and acidic leaching of chars obtained in the pyrolysis of plastics, tire rubber and forestry biomass wastes. Procedia Eng 2012;42:1739–46. doi:10.1016/j.proeng.2012.07.567.

[37] Bernardo M, Mendes S, Lapa N, Gonçalves M, Mendes B, Pinto F, et al. Leaching behaviour and ecotoxicity evaluation of chars from the pyrolysis of forestry biomass and polymeric materials. Ecotoxicol Environ Saf 2014;107:9–15. doi:10.1016/j.ecoenv.2014.05.007.

[38] Sajdak M, Muzyka R. Use of plastic waste as a fuel in the co-pyrolysis of biomass . Part I : The effect of the addition of plastic waste on the process and products. J Anal Appl Pyrolysis 2014;107:267–75. doi:10.1016/j.jaap.2014.03.011.

[39] Wu W, Qiu K. Vacuum co-pyrolysis of Chinese fir sawdust and waste printed circuit boards. Part I : Influence of mass ratio of reactants. J Anal Appl Pyrolysis 2014;105:252–61. doi:10.1016/j.jaap.2013.11.011.

[40] Bartocci P, Bidini G, Asdrubali F, Beatrice C, Frusteri F, Fantozzi F. Batch pyrolysis of pellet made of biomass and crude glycerol: Mass and energy balances. Renew Energy 2018;124:172–9. doi:10.1016/j.renene.2017.06.049.

[41] Samanya J, Hornung A, Apfelbacher A, Vale P. Characteristics of the upper phase of bio-oil obtained from co-pyrolysis of sewage sludge with wood , rapeseed and straw. J Anal Appl Pyrolysis 2012;94:120–5. doi:10.1016/j.jaap.2011.11.017.

[42] Wu Z, Yang W, Chen L, Meng H, Zhao J, Wang S. Morphology and microstructure of co-pyrolysis char from bituminous coal blended with lignocellulosic biomass: Effects of cellulose, hemicellulose and lignin. Appl Therm Eng 2017;116:24–32. doi:10.1016/j.applthermaleng.2017.01.061.

[43] Wang S, Jiang D, Cao B, Hu Y, Yuan C, Wang Q, et al. Study on the interaction effect of seaweed bio-coke and rice husk volatiles during co-pyrolysis. J Anal Appl Pyrolysis 2018;132:111–22. doi:10.1016/j.jaap.2018.03.009.

[44] Veses A, Aznar M, Martínez I, Martínez JD, López JM, Navarro M V., et al. Catalytic pyrolysis of wood biomass in an auger reactor using calcium-based catalysts. Bioresour Technol 2014;162:250–8. doi:10.1016/j.biortech.2014.03.146.

[45] Veses A, Aznar M, Callén MS, Murillo R, García T. An integrated process for the production of lignocellulosic biomass pyrolysis oils using calcined limestone as a heat carrier with catalytic properties. Fuel 2016;181:430–7. doi:10.1016/j.fuel.2016.05.006.

[46] Veses A, Aznar M, López JM, Callén MS, Murillo R, García T. Production of upgraded bio-oils by biomass catalytic pyrolysis in an auger reactor using low cost materials. Fuel 2015;141:17–22. doi:10.1016/j.fuel.2014.10.044.

[47] Food and Agriculture Organization. Fisheries and Aquaculture Department. Statistics. 2017. www.fao.org/fishery/statistics/en (accessed May 1, 2017).

[48] Murphy JN, Hawboldt K, Kerton F. Enzymatic processing of mussel shells to produce biorenewable calcium carbonate in seawater. Green Chem 2018;20:2913–20. doi:10.1039/c8gc01274a.

[49] Barros MC, Bello PM, Bao M, Torrado JJ. From waste to commodity: transforming shells into high purity calcium carbonate. J Clean Prod 2009;17:400–7. doi:10.1016/j.jclepro.2008.08.013.

[50] Tangboriboon N, Kunanuruksapong R, Sirivat A, Kunanuruksapong R, Sirivat A. Preparation and properties of calcium oxide from eggshells via calcination. Mater Sci Pol 2012;30:313–22. doi:10.2478/s13536-012-0055-7.

[51] Marin F, Luquet G. Les protéines de coquille de mollusque. Comptes Rendus - Palevol 2004;3:469–92. doi:10.1016/j.crpv.2004.07.009.

[52] Lertwattanaruk P, Makul N, Siripattarapravat C. Utilization of ground waste seashells in cement mortars for masonry and plastering. J Environ Manage 2012;111:133–41. doi:10.1016/j.jenvman.2012.06.032.

[53] Cubillas P, Köhler S, Prieto M, Chaïrat C, Oelkers EH. Experimental determination of the dissolution rates of calcite, aragonite, and bivalves. Chem Geol 2005;216:59–77. doi:10.1016/j.chemgeo.2004.11.009.

[54] Nebel H, Neumann M, Mayer C, Epple M. On the structure of amorphous calcium carbonate--a detailed study by solid-state NMR spectroscopy. Inorg Chem 2008;47:7874–9. doi:10.1021/ic8007409.

[55] Weiner S, Addadi L. Design strategies in mineralized biological materials. J Mater Chem 1997;7:689–702. doi:10.1039/a604512j.

[56] Zhang Y, Cui H, Yi W, Song F, Zhao P, Wang L, et al. Highly effective decarboxylation of the carboxylic acids in fast pyrolysis oil of rice husk towards ketones using CaCO3 as a recyclable agent. Biomass and Bioenergy 2017;102:13–22. doi:10.1016/j.biombioe.2017.04.004.

[57] Zhang L, Zhang B, Yang Z, Yan Y. Pyrolysis behavior of biomass with different Ca-based additives. RSC Adv 2014;4:39145–55. doi:10.1039/C4RA04865B.

[58] Han L, Wang Q, Ma Q, Yu C, Luo Z, Cen K. Influence of CaO additives on wheat-straw pyrolysis as determined by TG-FTIR analysis. J Anal Appl Pyrolysis 2010;88:199–206. doi:10.1016/j.jaap.2010.04.007.

[59] Lin Y, Zhang C, Zhang M, Zhang J. Deoxygenation of bio-oil during pyrolysis of biomass in the presence of CaO in a fluidized-bed reactor. Energy & Fuels 2010;24:5686–95. doi:10.1021/ef1009605.

[60] Papari S, Hawboldt K. A review on condensing system for biomass pyrolysis process. Fuel Process Technol 2018;180:1–13. doi:10.1016/j.fuproc.2018.08.001.

[61] Elliott DC, Meier D, Oasmaa A, Van De Beld B, Bridgwater A V., Marklund M. Results of the International Energy Agency Round Robin on Fast Pyrolysis Bio-oil Production. Energy & Fuels 2017;31:5111–9. doi:10.1021/acs.energyfuels.6b03502.

[62] Oasmaa A, Fonts I, Pelaez-Samaniego MR, Garcia-Perez ME, Garcia-Perez M. Pyrolysis Oil Multiphase Behavior and Phase Stability: A Review. Energy and Fuels 2016;30:6179–200. doi:10.1021/acs.energyfuels.6b01287.

[63] Sharma A, Pareek V, Zhang D. Biomass pyrolysis - A review of modelling, process parameters and catalytic studies. Renew Sustain Energy Rev 2015;50:1081–96. doi:10.1016/j.rser.2015.04.193.

[64] Papari S, Hawboldt K, Helleur R. Pyrolysis: A Theoretical and Experimental Study on the Conversion of Softwood Sawmill Residues to Biooil. Ind Eng Chem

Res 2015;54:605–11. doi:10.1021/ie5039456.

[65] Goos P, Jones B. Optimal design of experiments. A case study approach. Chichester, GB: John Wiley & Sons, Ltd.; 2011.

[66] Alsbou E, Helleur R. Accelerated aging of bio-oil from fast pyrolysis of hardwood. Energy & Fuels 2014;28:3224–35. doi:10.1021/ef500399n.

[67] Murphy JN, Kerton FM. Characterization and Utilization of Waste Streams from Mollusc Aquaculture and Fishing Industries. In: Kerton FM, Yan N, editors. Fuels, Chem. Mater. from Ocean Aquat. Sources. First Edit, John Wiley & Sons, Ltd; 2017, p. 189–227.

[68] Bamdad H, Hawboldt K. Comparative study between physicochemical characterization of biochar and metal organic frameworks (MOFs) as gas adsorbents. Can J Chem Eng 2016;94:2114–20. doi:10.1002/cjce.22595.

[69] Olarte M V., Zacher AH, Padmaperuma AB, Burton SD, Job HM, Lemmon TL, et al. Stabilization of Softwood-Derived Pyrolysis Oils for Continuous Bio-oil Hydroprocessing. Top Catal 2016;59:55–64. doi:10.1007/s11244-015-0505-7.

[70] Carpenter D, Westover TL, Czernik S, Jablonski W. Biomass feedstocks for renewable fuel production: a review of the impacts of feedstock and pretreatment on the yield and product distribution of fast pyrolysis bio-oils and vapors. Green Chem 2014;16:384–406. doi:10.1039/C3GC41631C.

[71] Krutof A, Hawboldt K. Blends of pyrolysis oil, petroleum, and other bio-based fuels: A review. Renew Sustain Energy Rev 2016;59:406–19. doi:10.1016/j.rser.2015.12.304.

[72] Oasmaa A, Elliott DC, Korhonen J. Acidity of biomass fast pyrolysis bio-oils. Energy and Fuels 2010;24:6548–54. doi:10.1021/ef100935r.

[73] Rahman S, Helleur R, MacQuarrie S, Papari S, Hawboldt K. Upgrading and isolation of low molecular weight compounds from bark and softwood bio-oils through vacuum distillation. Sep Purif Technol 2018;194:123–9. doi:10.1016/j.seppur.2017.11.033.

[74] Brassard P, Godbout S, Raghavan V. Pyrolysis in auger reactors for biochar and bio-oil production: A review. Biosyst Eng 2017;161:80–92. doi:10.1016/j.biosystemseng.2017.06.020.

[75] Greco G, Videgain M, Di Stasi C, González B, Manyà JJ, Di C, et al. Evolution of the mass-loss rate during atmospheric and pressurized slow pyrolysis of wheat straw in a bench-scale reactor. J Anal Appl Pyrolysis 2018;136:18–26. doi:10.1016/j.jaap.2018.11.007.

[76] Qian Y, Zhang J, Wang J. Pressurized pyrolysis of rice husk in an inert gas sweeping fixed-bed reactor with a focus on bio-oil deoxygenation. Bioresour Technol 2014;174:95–102. doi:10.1016/j.biortech.2014.10.012.

[77] Liu C, Wang H, Karim AM, Sun J, Wang Y. Catalytic fast pyrolysis of

lignocellulosic biomass. Chem Soc Rev 2014;43:ASAP. doi:10.1039/c3cs60414d.

[78] Garcia-Perez M, Adams TT, Goodrum JW, Geller DP, Das KC. Production and Fuel Properties of Pine Chip Bio-oil/Biodiesel Blends. Energy & Fuels 2007;21:2363–72. doi:10.1021/ef060533e.

[79] Vitasari CR, Meindersma GW, De Haan AB. Laboratory scale conceptual process development for the isolation of renewable glycolaldehyde from pyrolysis oil to produce fermentation feedstock. Green Chem 2012;14:321–5. doi:10.1039/c1gc16200d.

[80] Vitasari CR. Extraction of Bio-based Glycolaldehyde from Wood-derived Pyrolysis Oils. Eindhoven University of Technology, 2012. doi:10.6100/IR738958.

[81] Pourzolfaghar H, Abnisa F, Wan Daud WMA, Aroua MK. Atmospheric hydrodeoxygenation of bio-oil oxygenated model compounds: A review. J Anal Appl Pyrolysis 2018;133:117–27. doi:10.1016/j.jaap.2018.04.013.

[82] Mortensen PM, Grunwaldt J-D, Jensen PA, Knudsen KG, Jensen AD. A review of catalytic upgrading of bio-oil to engine fuels. Appl Catal A Gen 2011;407:1–19. doi:10.1016/j.apcata.2011.08.046.

[83] Asmadi M, Kawamoto H, Saka S. Gas- and solid/liquid-phase reactions during pyrolysis of softwood and hardwood lignins. J Anal Appl Pyrolysis 2011;92:417–25. doi:10.1016/j.jaap.2011.08.003.

[84] Nakamura T, Kawamoto H, Saka S. Condensation reactions of some lignin related compounds at relatively low pyrolysis temperature. J Wood Chem Technol 2007;27:121–33. doi:10.1080/02773810701515143.

[85] Hosoya T, Kawamoto H, Saka S. Journal of Analytical and Applied Pyrolysis Secondary reactions of lignin-derived primary tar components 2008;83:78–87. doi:10.1016/j.jaap.2008.06.003.

[86] Chi Z, Zhao X, Daugaard T, Dalluge D, Rover M, Johnston P, et al. Comparison of product distribution, content and fermentability of biomass in a hybrid thermochemical/biological processing platform. Biomass and Bioenergy 2019;120:107–16. doi:10.1016/j.biombioe.2018.11.006.

[87] Lian J, Mckenna R, Rover MR, Nielsen DR, Wen Z, Jarboe LR. Production of biorenewable styrene: utilization of biomass-derived sugars and insights into toxicity. J Ind Microbiol Biotechnol 2016;43:595–604. doi:10.1007/s10295-016-1734-x.

[88] Zhang X, Li J, Yang W, Blasiak W. Formation mechanism of levoglucosan and formaldehyde during cellulose pyrolysis. Energy and Fuels 2011;25:3739–46. doi:10.1021/ef2005139.

[89] Kuzhiyil N, Dalluge D, Bai X, Kim H. Pyrolytic Sugars from Cellulosic Biomass

2012;50011:2228–36. doi:10.1002/cssc.201200341.

[90] Demirbas A. The influence of temperature on the yields of compounds existing in bio-oils obtained from biomass samples via pyrolysis. Fuel Process Technol 2007;88:591–7. doi:10.1016/j.fuproc.2007.01.010.

Chapter 5 Co-pyrolysis of softwood with waste mussel shells: Part 2 char analysis

A modified version of this chapter has been submitted for publication; A. Krutof, H. Bamdad, K. A. Hawboldt, S. MacQuarrie. Co-pyrolysis of softwood with waste mussel shells: Biochar analysis.

Abstract

In this work, fisheries by-product (mussel shells) is co-pyrolyzed with forestry residues in a fast pyrolysis lab scale reactor to determine impact on biochar quality. The pyrolysis temperature, nitrogen flow, and wood-to-mussel shell ratio were varied, and thermal, physical, and chemical properties of the produced biochars were investigated via response surface methodology (RSM). The smaller mussel shell (MS) particles decreased the surface area by filling the pores in the biochar structure. Biochars containing MS showed lower heating values, higher alkaline pH values, and higher ash content (due to formation of CaO from $CaCO_3$). Surface analysis showed higher functionality in co-pyrolyzed biochars, decreased hydrogen and increased nitrogen and oxygen. These surface properties could potentially improve adsorption of hydrophobic molecules (e.g. VOCs), acidic gases, and metal ions in aqueous solution compared to forestry biochar.

Keywords: Biochar; co-pyrolysis; mussel shell; response surface methodology; soil amendment; gas adsorption

5.1 Highlights

- Mussel shell as co-pyrolysis additive improves liquid and char adsorbent properties
- Co-pyrolysis char is suitable for soil amendment with pH increased to 9
- *In-situ* chars not for combustion due to incombustible mussel shell and high ash
- Potential adsorbent for hydrophobic molecules, acidic gases, and metal ions (aq)
- Waste products with similar chemical make-up can replace commercial catalysts

5.2 Introduction

Fast pyrolysis, with its short residence times (0.5-5 s) and fast heating rates (100-1000 °C/min), is used primarily to convert biomass to liquid products for the production of a second-generation liquid biofuel [1,2]. However, fast pyrolysis can convert all of the lignocellulosic material to value-added products, including liquid, non-condensable gas, and biochar [3]. Slow pyrolysis biochar has been studied extensively, as the slow pyrolysis' long residence times (10 min-hours) and low heating rates (< 10°C/min) result in char being the primary pyrolysis product [1,4–6]. In fast pyrolysis, the biochar is a by-product and typically used as a low-grade solid fuel [3,6,7]. However, fast pyrolysis biochar is attracting more attention in higher value applications such as soil amendment, adsorbent, and nanocarbon material, among others [4]. The characteristics of fast pyrolysis biochar from forestry residues are well known, but there is little study of biochar from fast co-pyrolysis of forestry residues and fishery (by-)products. In 2016, 171 million tonnes of fisheries products were harvested globally, with 88% for human consumption, 35-70% of which was waste by-product [8,9]. In previous work, we studied the co-pyrolysis of forestry residues with a mussel processing by-product (mussel shells) with the primary purpose of assessing the potential

impact on the liquid product [10]. In this paper, we investigate the impact on the biochar characteristics (e.g. surface area, surface functional groups, etc.) on potential applications.

Fast pyrolysis bio-oil (FPBO) (50-75 wt%) is the main product of fast pyrolysis with by-products of biochar (yield of 12-20 wt%) and non-condensable gas (NCG) (13-16 wt%) [6,11–13]. In pyrolysis, the vapours can be upgraded prior to condensation (*ex-situ* vapour upgrading), or an additive/catalyst can be in contact with the biomass during *in-situ* upgrading (most commonly referred to as catalytic fast pyrolysis) or co-pyrolysis (combination of different feedstocks) [14].

The bulk of biochar studies from fishery is focussed on slow pyrolysis or gasification, with some fishery waste and co-pyrolysis work [8,15,16]. Fadhil et al. produced pyrolysis oil and activated carbon from de-oiled finfish waste in a fixed-bed laboratory scale slow pyrolysis reactor at 500 °C [17]. Activated carbon was produced through steam activation of the produced biochar [17]. Rowland et al. gasified salmon processing waste and mixtures of pine wood pellets and salmon waste producing bio-syngas [18].

Abeynaike et al. [19] and Currie et al. [20] partially calcined powdered mussel shells via slow pyrolysis at 650-800 °C to produce biochar for phosphate removal from wastewater. Shikhaliyeh et al. studied the transesterification of glycerol and dimethyl carbonate over fishmeal biochar [21]. Ahmad et al. used mussel shell, cow bone, and oak biochar as a soil amendment (5 wt%) to reduce lead toxicity [22,23]. High carbon and nitrogen fish waste (bones, scales, chitin) has been investigated as a feedstock for

the production of new carbon materials [24–27]. Guo et al. produced a porous three-dimensional carbon nano-network for electrocatalysis through two-step slow pyrolysis of protein-rich fish scale waste [24]. Wang et al. studied slow pyrolysis of fish bones at 800 °C producing an N-doped porous carbon material [25]. Raj et al. produced activated carbon as an oxygen and nitrogen enriched supercapacitor from squid gladius chitin [26]. Wallace et al. co-pyrolysed sewage sludge and fish waste at 950 °C, producing biochar with enhanced H_2S adsorption properties [28]. Wang et al. studied the fast pyrolysis of *Enteromorpha clathrate* sea-weed bio-coke with rice husk volatiles (*ex-situ*) in a fixed bed, laboratory scale, tube furnace reactor at 550 °C increasing the adsorption capacity of the bio-coke [29]. Mineral composites such as montmorillonite and iron have been successfully added to biochar to improve its adsorbent capacities for anionic pollutants such as nitrates and phosphate, respectively [30,31].

In this work, we are studying the co-pyrolysis biochar product of forestry residues and mussel shells (MS), which contain high levels of calcium carbonate ($CaCO_3$) [32]. In Canada, 23 kt blue mussels (Figure 2-1) worth 34 million USD were farmed in 2015 [33]. Once the meat is removed, the shells represent 30-50 wt% of the harvested material and are often disposed of in landfills [9,19,32,34].

MS consist of 95-99 wt% mineral phase (mainly $CaCO_3$ >90%) and 1-5 wt% organic matrix composed of β-chitin fibrils in silk fibroin-like proteins that determine crystallization structure and counteract calcite brittleness [19,32,35–37]. Since the anhydrous $CaCO_3$ polymorphs contain little to no water, they would not directly contribute

to the water in FPBO or char [38,39]. At temperatures above 700 °C, $CaCO_3$ forms calcium oxide (lime, CaO) and carbon dioxide (CO_2) [32,40].

There has been limited study of this type of material in pyrolysis, e.g. [41]. In our study, a design of experiment (DoE) approach was used to assess the impact on the biochar when MS (cleaned with enzymes [34]) were co-pyrolyzed with forestry residues. The impact of temperature (400-525 °C), nitrogen flow (50-300 mL/min), amount of MS additive (0-50 wt%), and operational mode (*in-* or *ex-situ*) was studied using response surface methodology (RSM).

5.3 Materials and methods

5.3.1 Statistical methods

Design Expert® software (11.0.6.0) was used to determine the number of experimental runs (D-optimal design, one block, quadratic model with three lack of fit and three repetition points). Based on the analysis of variance (ANOVA) results, the factors temperature (*A*), nitrogen flow (*B*), amount of MS additive (*C*), and operational mode (*D*), as well as their 2 factor interactions (2FI), and quadratic effects were included in the model if the p-value was < 0.05 or between 0.05 and 0.1. To ensure hierarchy of the model factors with p-values > 0.1 were included in the model if their 2FI or quadratic effect were significant. The following three model selection criterions were applied: p-values (significance level < 5% to max. 10% with forward selection direction), Akaike information criterion (AICc, forward selection direction), and adjusted R^2. Significance of each

model is defined as p-value < 0.05, F-value as 'adequately large', adjusted R^2 and predicted R^2 close to 1 with a difference between the two of < 0.2, the adequate precision coefficients as a measure for the signal-to-noise ratio (> 4), and a graphical comparison of predicted and actual values.

5.3.2 Experimental methods

A mixture of Newfoundland pine and spruce softwood shavings supplied by Sexton Lumber Co Sawmill, Bloomfield NL Canada, was ground to < 2 mm in a cutting mill, to be comparable to industrial-scale applications, for use in the tube furnace reactor [10,42]. The MS were treated with enzymes to remove any residual organics to allow for transportation and reduce nitrogen in the liquid FPBO product [10,43]. Shells were then ground to a powder in a ball mixer mill for 8 min with two ¼ in stainless steel balls. After grinding, the wood and MS additive were dried at 75 °C for at least 2 hours, cooled to room temperature, and stored in airtight containers. The feedstock was analyzed for moisture with a Mettler Toledo Compact Halogen Moisture Analyzer HB34-S at 105 °C. Particle size distribution was determined via sieve analysis (RRSB distribution). The feedstock (softwood and MS) and biochars, were analyzed with scanning elector microscopy (SEM), Fourier-transform infrared spectroscopy (FTIR), (Brunauer-Emmett-Teller) BET surface area, elemental C/H/N(O) and thermogravimetric analysis (TGA), high heating value (HHV), pH, and bulk density. Biochar was ground with mortar and pestle in four portions of 1.9 g for 60 sec each to be used for all analyses. BET surface area of the biochars was measured and viewed via SEM as described in [44]. Standard deviation of BET duplicate runs ranged from 0.02 to 1.84 m^2/g. FTIR of the

biochar samples was carried out at the Cape Breton University, as described in [44]. For SEM and FTIR analysis chars were labelled as 'Char <DoE run no.>: <temperature in °C >-<nitrogen flow in mL/min>-<MS additive in wt% of total biomass feed>-<operational mode with 'i' for *in-situ* and 'e' for *ex-situ*>, e.g. char 1 was labelled as 'Char 1: 525-300-50-e'. Calcium content of the MS was determined via inductively coupled plasma mass spectrometry (ICP-MS). Biochar samples were analyzed for carbon, hydrogen, nitrogen, and oxygen (by difference) (C/H/N(O)) at the Ocean Science Centre (Newfoundland, Canada). Samples were weighed using a Mettler Toledo UMT 2 balance into tin capsules (Isomass, Calgary, AB), folded to ensure no loss of sample and placed into a 96 well plate. The plate was stored in a desiccator until the samples could be run on the Perkin Elmer 2400 Series II CHNS/O analyzer. The CHN was calibrated before the run using acetanilide (Isomass, Calgary, AB) and a standard was run after every 10 samples. To determine O_{total} by difference the percentage of inorganic minerals (mostly Ca) in char $Ca_{total} = Ca_{mussel}$ is determine by multiplying the amount of MS in char by the weight % of Ca in MS (35.3 wt%). The amount of MS in the char is calculated as:

$$mussel\ in\ char\ (wt\%) = \frac{m_{mussel}}{y_{char} * m_{wood} + m_{mussel}} \quad (5.1)$$

Where m_{mussel} is the mass of MS in the feed, y_{char} is the char yield as wt% of softwood feed, and m_{wood} is the mass of the softwood feed. Therefore:

$$Ca_{mussel}\ in\ char\ (wt\%) = mussel\ in\ char * 0.353 \quad (5.2)$$

It is assumed H and N content in MS are negligible compared to the softwood. The total oxygen in the char (oxygen in wood char and MS) is calculated by difference:

$$O_{total} = 100 - C_{total} - H_{total} - N_{total} - Ca_{total} \quad (5.3)$$

The differences between duplicate DoE runs 16 and 20, 2 and 11, and 6 and 9 are 0.3-4.3 wt%, 0.3-0.8 wt%, 0.0-0.1 wt%, and 0.1-4.5 wt% for C, H, N, and O. In the TGA analyses (TGA Q500 TA Instruments) a 10-20 mg biochar sample is heated at 15 °C/min to 800 °C under nitrogen (50 mL/min) atmosphere. At 800 °C the carrier gas is switched over to air (50 mL/min) and the temperature is held for 15 min to combust the remaining carbon. The mass loss is recorded as four groups: moisture (< 150 °C), volatile matter (150-600 °C), fixed carbon (and CO_2, 600-800 °C), and ash (including CaO, > 800 °C). One of the samples was analyzed in triplicate to estimate the error as 95% confidence interval. The errors were ± 0.3 wt%, ± 6.4 wt%, ± 6.1 wt%, and ± 0.1 wt% for moisture, volatile matter, fixed carbon, and ash, respectively.

HHV is the energy released per unit mass or per unit volume of fuel after complete combustion [45]. The HHV of the solids was determined in duplicate, analogous to the HHV of the FPBO as outline in previous work. However, the sample size was reduced to 0.13 g, and two drops of water were added into the gelatine capsule to aid complete combustion. HHV was analyzed in duplicate with additional measurements if the results varied more than 1.5 MJ/kg. by triplicate analysis. The pH of the biochars was determined by mixing 1 g of char with 20 g of distilled water in a 50 ml beaker for 30 min using a magnetic stir bar and plate. A calibrated (at pH 7 and 10) VWR SympHony B10P pH meter with 89231-604 electrode was used, and measurements were carried out in duplicate with an estimated error of 0.3. The initial bulk density $\rho_{b(initial)}$ of the biochars was estimated by loosely filling 15 ml of char into a glass vial

and scrapping of the excess, loosely following ASTM 6683 Section 8.6. Compression by tapping the jar on a table 20 times increases bulk density by a factor of 1.26 to 1.52. The error in bulk density measurement was estimated to be ± 6.9 kg/m³ from the 95% confidence interval of a triplicate measurement.

5.4 Results and discussion

Unless otherwise indicated, the response models, and factors discussed below were significant as determined by Design Expert® software (11.0.6.0). Resulting model equations are summarized in Table 5-1 (normalized factors) and *Appendix E.2* (actual factors).

5.4.1 Feedstock properties

The feedstock was first characterized to assess the impact of pyrolysis on solid properties. The moisture of the MS was <0.1 wt% and 0.4-2.0 wt% for the wood. The median particle size was 750 µm for softwood and 70 µm for MS. SEM images of softwoods are well studied [46,47]. SEM images of cleaned MS showing the different $CaCO_3$ polymorphs for the inner (flaky nacreous aragonite) and outer (long string-like prismatic calcite) layer can be found in [43] and (Figure 5-4a and b). Figure 5-1 shows the FTIR spectrum for softwood and Figure 5-2 for MS and laboratory grade $CaCO_3$ and CaO for comparison.

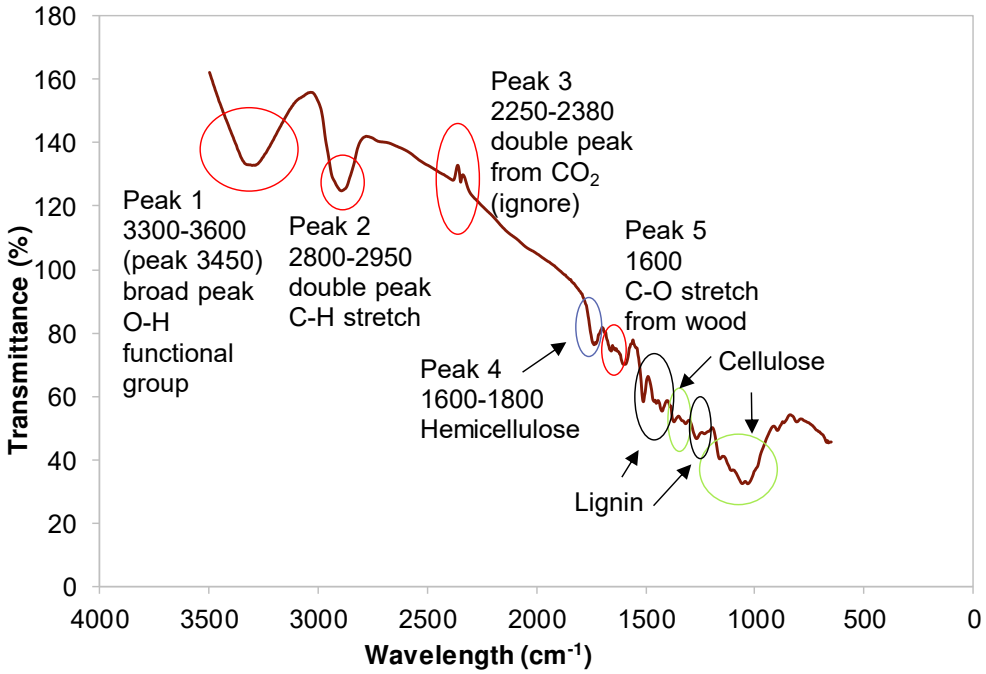

Figure 5-1: FTIR spectra for softwood

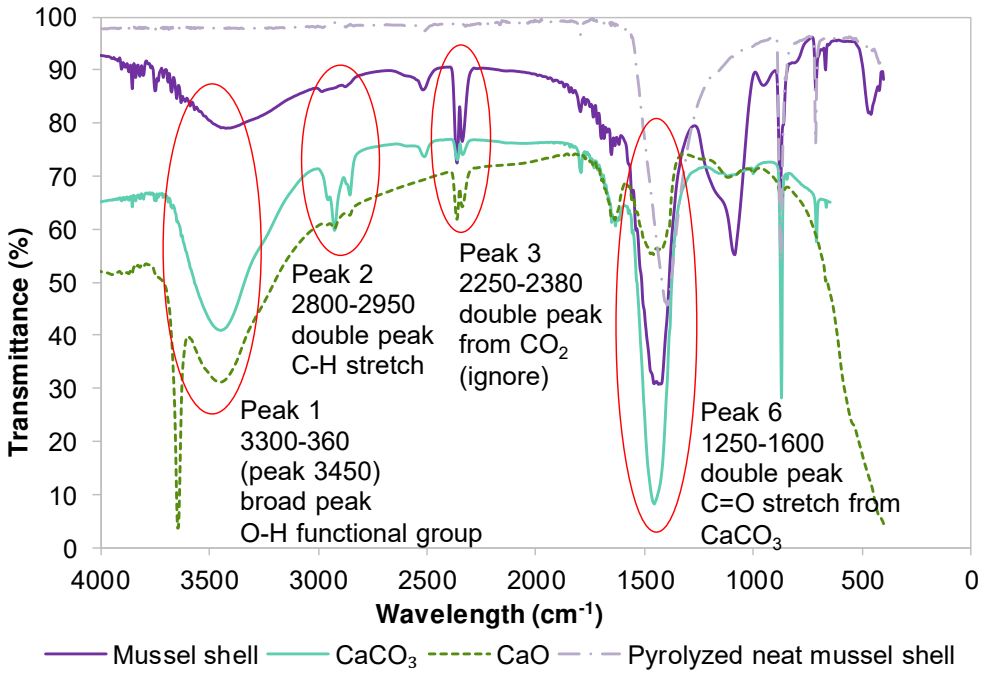

Figure 5-2: FTIR spectra of neat mussel shell, laboratory grade $CaCO_3$ and CaO, and pyrolyzed mussel shell

The three main components of softwood can be seen in Figure 5-1, cellulose (700-1500 cm^{-1}), hemicellulose (1700-2000 cm^{-1}), and lignin (1200-1700 cm^{-1}). The FTIR of softwood was dominated by functional groups from oxygenated organics due to the carbohydrate structure of cellulose and hemicellulose (Figure 5-1) [48]. The C=O stretch from $CaCO_3$ was in the range of 1500 cm^{-1} for all materials with comparable intensities (Figure 5-2). The FTIR of MS, pyrolized at 500 °C with 50 mL/min nitrogen flow rate, resembles the FTIR of $CaCO_3$ more closely compared to the FTIR of MS, potentially due to the loss of organics during pyrolysis. In particular the peak at 1000 cm^{-1} was reduced in pyrolized MS compared to non-pyrolized MS. The MS did not calcinate during pyrolysis at 500 °C, the C=O peak at 1250-1600 cm^{-1} is not reduced compared to non-pyrolyzed MS and $CaCO_3$.

BET surface area of softwood was 5.3 m^2/g and of MS was 8.7 m^2/g. Carbon, hydrogen, nitrogen, and oxygen are 47.7-56.8, 4.7-5.8, 0.0-1.1, and 37.1-46.6 wt% [49,50] for softwood, and 12.9, 0.0, 0.5, and 51.2 wt% for MS. The calcium in the MS was 35.3 wt%. The moisture, volatile matter, fixed carbon/CO_2, and ash were 1.8, 84.8,

12.6, and 0.8 wt% for softwood and 0.4, 3.5, 42.0, and 54.1 wt% for MS, respectively (Figure 5-3).

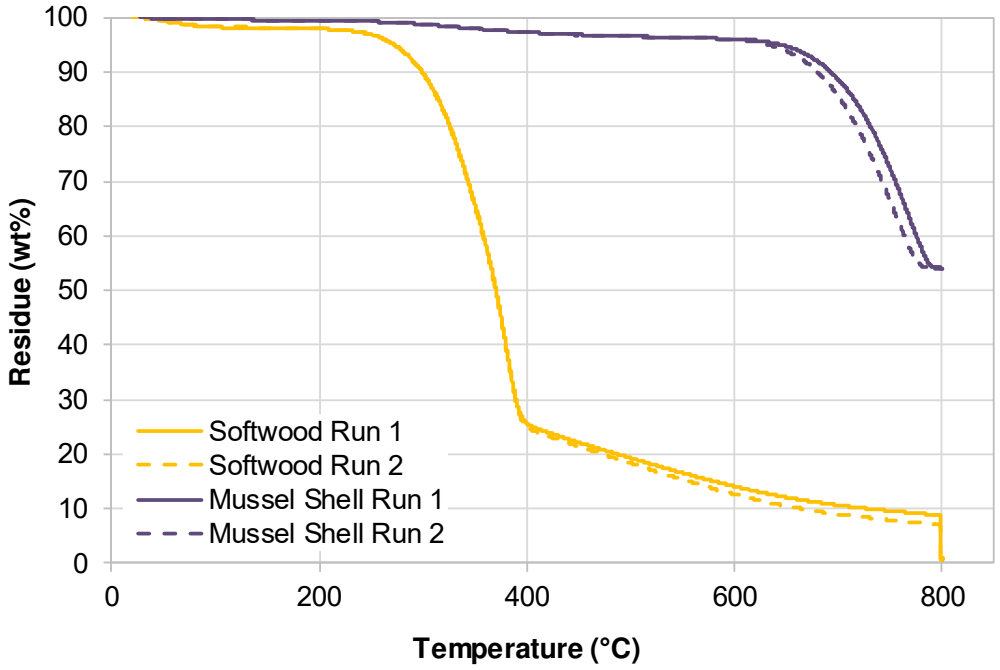

Figure 5-3: TGA of softwood and mussel shell feedstock

Most of the MS weight loss (95 wt%) occurred at temperatures above 600 °C due to the calcination of $CaCO_3$ to CaO and CO_2. The residue at 800 °C (ash) is the remaining CaO and other trace minerals/elements from the source material. The HHV of softwood was 19.51 ± 0.48 MJ/kg (triplicate measurement), MS does not combust. The pH was 4.60 ± 0.08 for softwood and 8.64 ± 0.11 for MS. The bulk density of loose softwood and MS was 132.0 and 925.0 kg/m³, respectively while compressed samples were 171.2 and 1347.1 kg/m³.

5.4.2 Pyrolysis yields

Yields were calculated based on oil and char produced from wood biomass over the initial wood biomass and corrected for MS content to compare *in-situ* and *ex-situ* yields. Gas yields were calculated by difference. The oil, biochar, and gas yield were fit to models (Table 5-1) with factors temperature, nitrogen flow, MS loading, and operational mode by ANOVA.

Both oil and gas yields increased with temperature and were highest at 525 °C with no MS. The oil yield was highest at 50 mL/min (62.9 wt%), while the gas yield was highest at 300 mL/min (26.9 wt%). The amount of MS and operational mode did not impact oil yield. Gas yield follows the same trend over the range of MS loadings as a function of temperature and nitrogen flow. The overall gas yield for 25 wt% and for 50 wt% MS was 2-3 wt% and 5-6 wt% higher compared to no MS likely due to increased vapour residence time (as described below) and/or secondary reactions as a result of the MS. The biochar yield is highest (27-33 wt%) at 400 °C over the range of flow rates and MS loadings studied. The maximum yield of biochar occurred at 20 wt% MS, values below and above 20 wt% produced less biochar at the same temperature. *Ex-situ*, the fixed carbon in the char was minimal at 20-25 wt% MS, while moisture, volatile, and ash increase with MS addition as discussed in *Section 5.4.3.5*. Interestingly, the maximum char yield and minimum acetic acid in oil was at 25 wt% MS, possibly due to the secondary decarboxylation [41] and cracking reactions [42,51]. Acetic acid is reduced to ketones, however, as MS increases secondary cracking reactions dominate producing

more char, water, and NCG. With increasing MS loadings and nitrogen flow the pressure/residence time in the reaction zone likely increased *ex-situ* as the vapours had to pass through the quartz wool plug loaded with MS. *In-situ* the MS was mixed with the wood and the obstruction of the flow due to the quartz wool plug was minimal. Increased pressure/residence times are known to favour secondary reactions such as dehydration and decarboxylation [52,53]. *In-situ*, dehydration, decarboxylation, and reduction of acetic acid to ketones occur through direct contact with the MS $CaCO_3$. The dependence of biochar yield on temperature and MS follows the same trend for *in-situ* and *ex-situ*. However, the *in-situ* biochar yield was slightly higher (2.0 wt %) compared to *ex-situ*. This is potentially due to increased secondary reaction leading to increased *in-situ* biochar formation, water (in oil and char), and NCG formation [42,51].

Table 5-1: Model equations resulting from designed experiment describing char properties in coded factors normalized from -1 to +1, with *A* pyrolysis temperature -1 = 400 °C and +1 = 525 °C, *B* nitrogen flow -1 = 50 and +1 = 300 mL/min, *C* MS -1 = 0 wt% and +1 = 50 wt%, and *D* operational mode *in-situ* (-1) and *ex-situ* (+1)

Response	Unit	Integer	A	B	C	D	AB	AC	AD	BC	BD	CD	A^2	B^2	C^2	D^2
Yield oil	**wt%**	54.360	2.448	-3.636			-2.444									
Yield char	**wt%**	24.110	-4.980		-1.070	-0.998							2.340		-2.170	
Yield gas	**wt%**	21.437	2.348	4.044	2.818		1.886									
BET surface area	**m^2/g**	0.632	3.690	0.106	-0.161	0.551				1.790	2.580	2.130	5.120	4.650		
Carbon	**wt%**	56.080	0.171		-12.140	12.830		-3.200				10.790			6.280	
Hydrogen	**wt%**	1.770	-0.545		-0.770	0.669			-0.217			0.671	0.701			
Nitrogen	**wt%**	0.123	-0.023	0.009	0.050	-0.029		-0.032			0.025					
Oxygen	**wt%**	32.550	0.064		6.140	-5.630		2.370				-4.530			-4.230	
Moisture	**wt%**	3.130	0.654	0.299	-0.441	0.767		-0.459				0.721				
1/Volatiles	**1/wt%**	0.059	0.006	-0.004	0.012	-0.014						-0.016		-0.010		
Fixed carbon	**wt%**	59.930	0.830	-1.550	-7.280	5.680		-3.440				3.170		-5.970	6.270	
ln(Ash)	**ln(wt%)**	2.250	0.080		0.942	-0.669						-0.366	-0.476			
HHV	**MJ/kg**	19.380	0.147	-0.077	-5.830	5.370	1.230					4.140	1.600		1.890	
pH		8.430	0.352		0.732	-0.422									-0.758	
Bulk density	**kg/m^3**	267.680	20.950	-0.444	80.190	-82.950	-10.920	11.490	-12.130	17.040		-76.320				

5.4.3 Biochar properties

The biochars characterized in this work are outlined in Table 5-3 and *Appendix E.2*. Although the *ex-situ* MS experiments should not have impacted the biochar quality directly, there may be indirect effects due to increased pressure/residence time compared to *in-situ*.

5.4.3.1 Scanning electron microscope (SEM) imaging

Particles sizes of the ground biochar varied: smaller and less regular with higher temperature (Figure 5-5c-f) and as large as 1 mm at 400 °C. Char and softwood structures are similar because the char is the wood after release of volatiles. Square channels measuring 5-30 µm across (Figure 5-4a) with small pores of 1-2 µm in diameter between square channel walls were observed (Figure 5-4b) that fill in with small flake like $CaCO_3$ particles if softwood is co-pyrolysed with MS (Figure 5-5e and f). In between square channels, donut shaped pores appeared as eye shaped pores in cross section (Figure 5-5c and d) measuring 1.5-8.5 µm across with 6-17 µm outer and 1-12 µm inner diameter (Figure 5-4e and f).

$CaCO_3$ crystals appeared in two forms (crystallizations): long string-like (1-2 µm across) from the middle and outer prismatic calcite layer of the MS (Figure 5-5a) and small flake like particles (0.5-6.5 µm across) from the inner nacreous aragonite layer of the MS (Figure 5-5b) [19,43,54]. $CaCO_3$ particles were as large as 500 µm across. However, most MS fragments were small (< 10 µm) particularly at higher pyrolysis temperatures when conversion of calcite to aragonite was favoured [55] (Figure 5-5f).

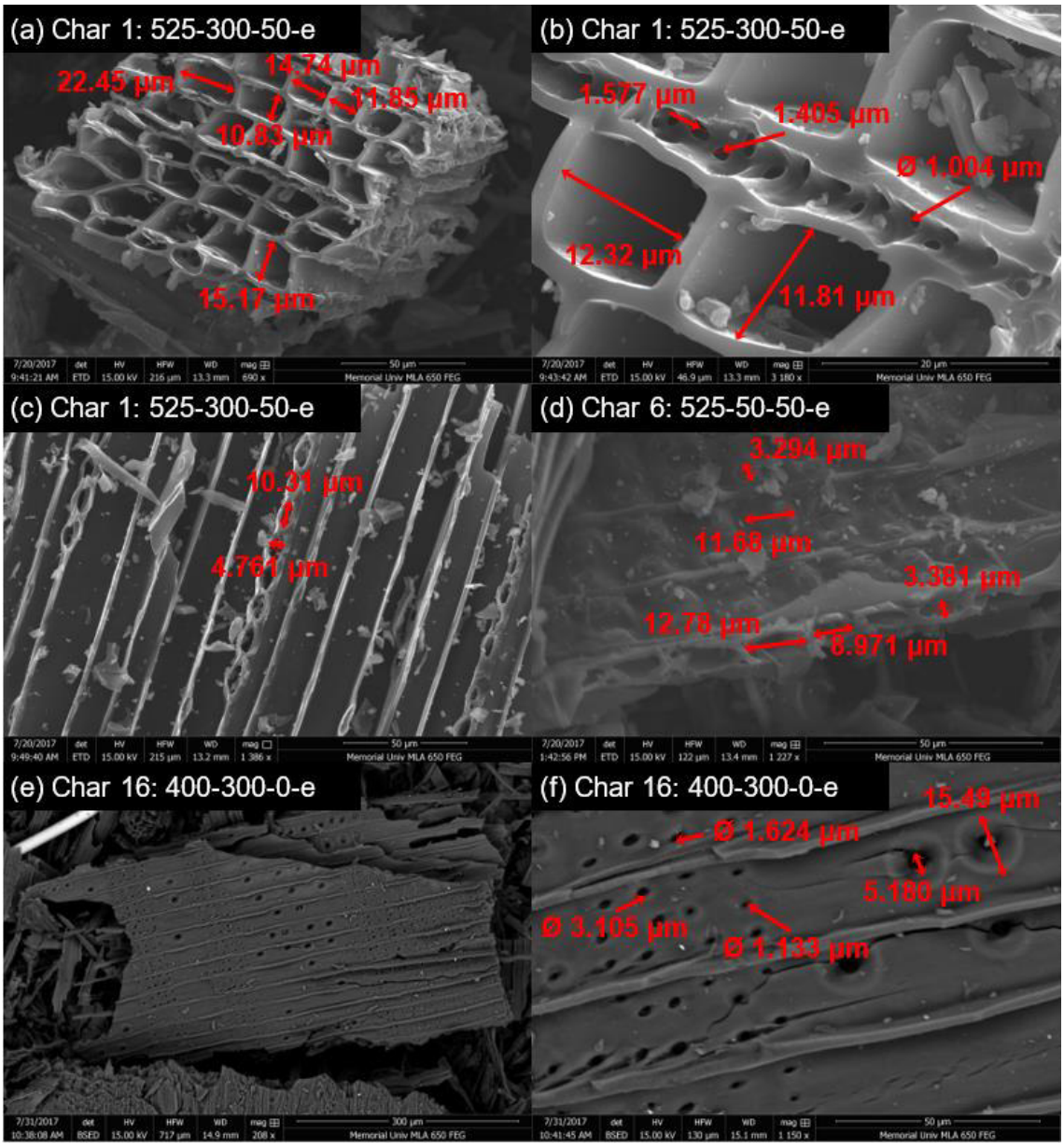

Figure 5-4: (a) Char 1: 525-300-50-e square channels and (b) small pores between square channels; (c) Char 1: 525-300-50-e square lignin channels with donut shaped pores (here eye shaped in cross section) in between square channels; (d) Char 6: 525 - 50-50-e donut shaped pores three dimensional structure; (e and f) Char 16: 400-300-0-e donut shaped pores in various sizes

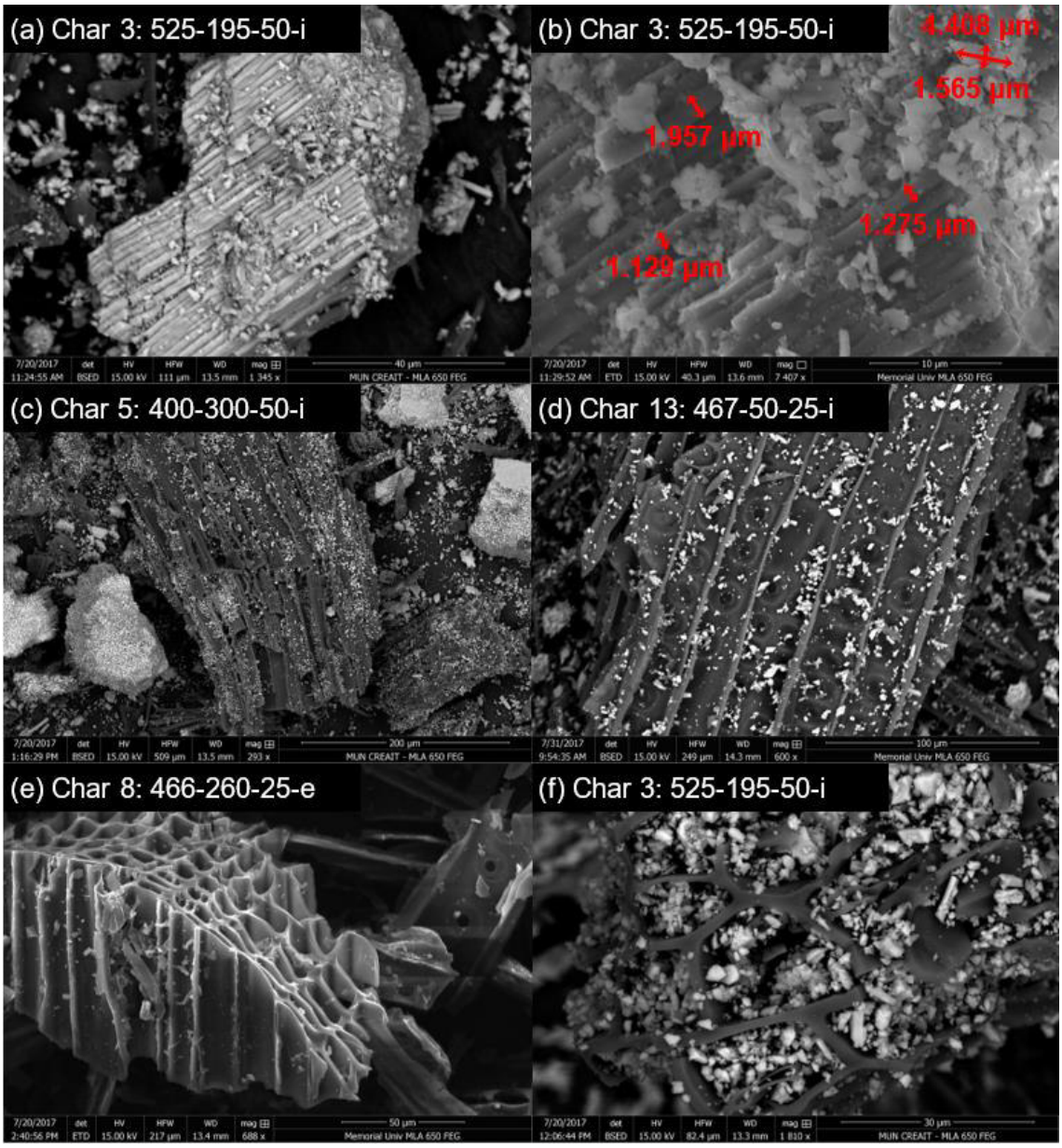

Figure 5-5: Char 3: 525-195-50-i (a) large $CaCO_3$ calcite particle with string like crystal structure and (b) some smaller $CaCO_3$ aragonite particles with flake like crystal structure; (c) Char 5: 400-300-50-i $CaCO_3$ particles (white flakes) on the biochar surface (black structure); (d) Char 13: 467-50-25-i donut shaped pores in lignin structure, $CaCO_3$ (white) spread on structure (right); (e) Char 8: 466-260-25-e lignin structure with channels and no $CaCO_3$ deposits (left), donut shaped pores in structure (right); (f) Char 3: 525-195-50-i square channels filled with $CaCO_3$ aragonite flakes (white)

5.4.3.2 Fourier-transform infrared spectroscopy (FTIR) of biochar

Identified FTIR peaks for biochars produced from the co-pyrolysis of softwood and MS are given in Table 5-2.

Table 5-2: Wavelength (cm^{-1}) and corresponding functional groups of identified FTIR peaks adopted from [48]

Peak no.	Wavelength (cm^{-1})	Functional group
1	3300-3600, broad peak, (3450)	O-H functional group
2	2800-2950, double peak	all sp^3 C-H (alkane C-H), alkyl C-H stretch
3	2250-2380, double peak	CO_2 from air (ignore)
4	1600-1800 (just wood)	-OH plane bending mode, water, carbonyl (C=0) and other common alkane and oxygenated hydrocarbon functional groups
5	1600 (just wood)	C-O
6	1250-1600, two broad peaks	C=O stretching ($CaCO_3$ has strong C=O stretching) - two peaks one at 1400 one at 1600 (1600 overlays with peak no. 5, 1400 overlays with peak no. 7)
7	1030	C-C-O (or C-O-C) asymmetric stretch
8	500-700	O-H out of plane bending modes

Peaks 1-3 of the biochars align with the FTIR peaks identified for softwood Figure 5-1) smaller wavelength peaks are overlaid with peak no. 6 for MS containing biochars. The impact of temperature and MS on the FTIR spectra is outlined in Figure 5-6.

The C-O stretch peak at 1600 cm^{-1} is more pronounced for higher temperatures. For *in-situ* chars (solid lines), the C=O (1250-1600 cm^{-1}), O-H (~3500 cm^{-1}), and C-H (~2800 cm^{-1}) peaks intensify with increasing temperature. For *ex-situ* runs with the same pyrolysis temperature, the C=O (1250-1600 cm^{-1}), O-H (~3500 cm^{-1}), and C-O (1600 cm^{-1}) peaks became slightly more prominent as flow increased. The C=O double

peak at 1250-1600 cm^{-1} appears only for *in-situ* biochars 3, 13, and 15 with MS due to the presence of $CaCO_3$. The C-O stretch peak at 1600 cm^{-1} increases for increasing MS and increasing temperature (Figure 5-6).

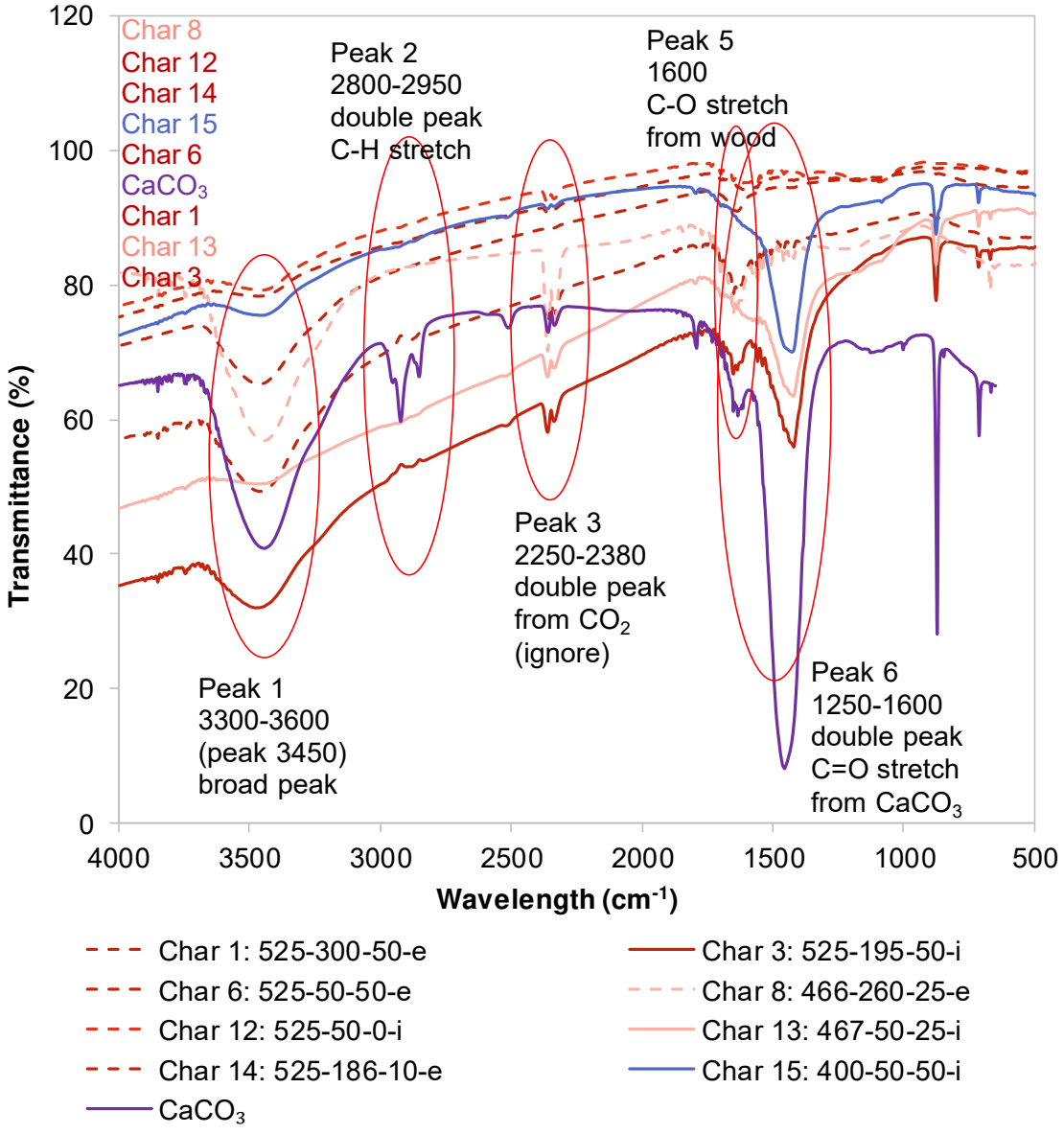

Figure 5-6: FTIR of selected DoE biochars colour coded for reactor temperature (dark blue: 400 °C to dark red: 525 °C), with solid lines for in-situ runs ending in "-i" and dotted lines for ex-situ runs ending in "-e" or in-situ runs without mussel shell additive

5.4.3.3 Brunauer-Emmet-Teller (BET) surface area

Samples were analyzed according to the four BET criteria suggested in [56], results are given in Table 5-3.

Table 5-3: BET surface areas of biochars sorted by temperature, mussel shell content, and operational mode with SW – softwood and MS – mussel shell

Char	Temp	N_2 flow	Mussel	Mode	Char yield	Mussel in char	BET	
							sample mass	surface area
	°C	ml/min	wt%	*in/ex*	wt%	wt%	g	m²/g
SW							0.6	5.3
MS							0.6	8.7
10	400	156	0	*in*	31.6	n/a	0.6	3.1
16	400	300	0	*ex*	28.9	n/a	0.6	3.0
20	400	300	0	*ex*	29.8	n/a	0.2	9.7
2	400	50	25	*ex*	29.8	n/a	0.6	3.0
11	400	50	25	*ex*	30.5	n/a	0.6	3.1
5	400	300	50	*in*	28.8	76.3	0.6	3.7
15	400	50	50	*in*	30.7	75.3	0.2-0.6	6.5
18	428	186	50	*ex*	22.4	n/a	0.2-0.6	5.6
17	439	283	10	*in*	25.5	27.3	0.6	2.9
4	456	50	0	*ex*	22.3	n/a	0.6	3.4
8	466	260	25	*ex*	24.0	n/a	0.6	3.3
13	467	50	25	*in*	24.2	55.3	0.2-0.6	4.9
7	473	300	50	*in*	22.8	80.3	0.6	3.4
12	525	50	0	*in*	21.5	n/a	0.1-0.2	22.4
19	525	300	0	*in*	21.2	n/a	0.2	10.6
14	525	186	10	*ex*	21.9	n/a	0.2	10.9
3	525	195	50	*in*	18.4	83.5	0.6	4.3
1	525	300	50	*ex*	15.5	n/a	0.1	20.1
6	525	50	50	*ex*	17.5	n/a	0.2	10.1
9	525	50	50	*ex*	17.6	n/a	0.1-0.2	14.9

Biochars produced at 525 °C (except biochar 3) did not produce measurable surface area data with 0.6 g of sample as equilibrium vacuum could not be reached due to larger surface areas. Consequently, the first pressure point was reduced (5 points added before

original first point), and sample mass was reduced to 0.1 g to improve initial evacuation time.

Regardless of MS loading, nitrogen flow, and mode, increasing the temperature from 400 °C to approximately 440 °C did not change the surface area. However, as temperature increased from 440 to 525 °C the degree of carbonization and consequently the surface area increased [57] from a low of 0-10 g/m² to 10-21 g/m². At constant temperatures, increasing the MS from 0 to 50 wt% *ex-situ* at 300 mL/min flow increased the surface area by 56-190% from 4.0-13.5 g/m² to 11.5-21 g/m². At lower flowrates the addition of MS did not increase the surface area to the same extent, likely due to the reduced pressure build-up with the loaded quartz wool plug at low flowrates. These effects are less significant *in-situ*. Increasing the MS from 0 to 50 wt% occludes the *in-situ* biochar pores decreasing the BET surface area by 41-75% from 10-20 g/m² to 2-12 g/m² (Figure 5-5f). However, new functional groups are potentially introduced with MS. As the flowrate increased (residence time decreases) any *in-situ* surface area decrease with MS became less pronounced. No change in surface area was observed at 300 mL/min due to shorter residence times. The highest BET surface area occurred at 525 °C, 50 mL/min flow rate no MS for *in-situ* (20.0 m²/g), and at 525 °C, 300 mL/min flow rate, and 50 wt% MS for *ex-situ* (21.0 m²/g). Biochars can be activated to increase surface area; however, the maximum ash in activated carbon of 15 wt% (DIN EN 12903) [3] is exceeded for *in-situ* chars with > 10 wt% MS additive. Though it should be noted that devolatilization (11-14 wt% of *in-situ* biochars) and reaction of $CaCO_3$ to CaO under release of CO_2 (30-40 wt% of *in-situ* char) would occur during activation at

high temperatures (700-1000 °C) increasing the relative ash content compared to untreated biochar.

5.4.3.4 Elemental analysis C/H/N(O)

Regardless of mode, with no MS, an increase in temperature from 400 to 525 °C increased carbon by 10% from 69.1-73.2 wt% to 75.8-79.9 wt%. At 25 wt% MS, there was no change in carbon as temperature increased from 400 to 525 °C. The trend reversed at 50 wt% MS loading where carbon decreased by 20% from 29.6 to 23.6 wt% (*in-situ*) and by 10% 76.9 to 70.8 wt% (*ex-situ*) as temperature increased. Carbon was highest at 525 °C with no MS (75.8-79.9 wt%). A second maximum occurred for *ex-situ* biochar at 400 °C and 50 wt% MS (76.9 wt%) potentially due to increased pressure at high MS loadings *ex-situ* (*Section 5.4.2*). *Ex-situ*, a minimum in carbon (68.3-68.6 wt%) occurred at 20-35 wt% MS corresponding to maximum biochar yield. Carbon in *in-situ* biochar decreased with increasing MS from 69.1-75.8 wt% with no MS to 23.6-29.6 wt% at 50 wt% MS due to the addition of MS (12 wt% carbon in MS).

The hydrogen in the *ex-situ* chars decreases slightly from 3.8 wt% to 2.3 wt% as temperature increased from 400 to 525 °C, while *in-situ* hydrogen was approximately constant. The MS loading had no effect on *ex-situ* char hydrogen. *In-situ* chars hydrogen decreased with increasing MS additive due to the dilution effect of MS (0.0 wt% hydrogen in MS). The highest *in-situ* hydrogen (2.8-3.9 wt%) occurred when there was no MS and decreased as MS was added over the range of temperatures. The lower hydrogen with MS results in biochar with a more hydrophobic surface, potentially more effective for adsorption of hydrophobic molecules [58].

Overall the nitrogen was low (0.0-0.27 wt%). At 50 wt% MS the nitrogen decreased from 0.16-0.27 wt% to 0.05-0.15 wt% as temperature increased from 400 to 525 °C. There was no change with temperature without the MS, outlining the strong interaction effect of temperature and MS. Increased temperatures may cause the volatilization of nitrogen. At 525 °C, no change in nitrogen occurred with MS addition. Adding 50 wt% MS at 400 °C increased the nitrogen from 0.00-0.08 wt% to 0.16-0.27 wt%. Overall, the nitrogen was slightly higher for MS containing *in-situ* biochars compared to the *ex-situ* biochars, due to 0.5 wt% nitrogen in neat MS. However, most of the nitrogen from the MS feedstock ended up in the FPBO as discussed in previous work [10]. Upgrading softwood with MS generates biochar with more nitrogen and subsequently a more basic surface, appropriate for acidic gas adsorption [59].

Regardless of mode, the effect of temperature on the oxygen content was the inverse of carbon. With no MS present, more oxygen was volatilized as temperature increased, decreasing the oxygen from 23-26 wt% to 19-21 wt%. At 25 wt% MS loading no effect of temperature was observed while at 50 wt% MS the oxygen increased with temperature from 42 to 47 wt% (*in-situ*) and from 22 to 27 wt% (*ex-situ*). The effect of the amount of MS on the oxygen in *ex-situ* biochars is non-linear resulting in a maximum of 27 wt% oxygen at 23-37 wt% MS corresponding to a maximum biochar yield and confirming the hypothesis of increased secondary pyrolysis reactions described in *Section 5.4.2*. The *in-situ* oxygen content increases with increasing amount of MS from 21-26 wt% with no MS to 42-47 wt% at 50 wt% MS (48 wt% oxygen in MS). Since the oxygen is calculated by difference, and the mineral content of the *in-situ* biochars is

only estimated (at 35.3 wt% Ca of total MS in biochar), the error for the oxygen (particularly for *in-situ* biochars) is expected to be quite high; however, the observed effects are larger compared to the estimated error of 5 wt%. Mixing softwood with MS increased the oxygen in the biochar, resulting in more oxygen-containing functional groups and enhanced sorption of metal ions in aqueous solution [60].

5.4.3.5 Thermogravimetric analysis (TGA)

Table 5-4 and *Appendix E.2* show the TGA results for biochars produced via the co-pyrolysis of softwood with MS.

Table 5-4: Simplified impact of increase of studied factors temperature, flow rate, MS loading, and mode on TGA char properties

Impact with increase in / **Char property**	**Temperature (°C)**	**Nitrogen flow rate (mL/min)**	**MS loading (wt%)**	**Operational mode (*in/ex-situ*)**
Moisture (wt%)	↑	↑	↓ (*in-situ*)	*in* < *ex*
Volatiles (wt%)	↓↓ (esp. w/o MS)	min. at 150	↓↓ (*in-situ*)	*in* < *ex*
Fixed carbon/CO_2 (wt%)	↑ < 25 wt% MS ↓ > 25 wt% MS	max. at 150	↓↓ (*in-situ*)	*in* < *ex*
Ash (wt%)	max. at 470	ns	↑↑ (*in-situ*)	*ex* < *in*

↑ - increase, ↓ - decrease, ↑↑ - strong increase, ↓↓ - strong decrease, ns – not significant

The highest moisture (4.9-5.0 wt%) was at 525 °C, 300 mL/min nitrogen flow, and no MS. The moisture increased from 2.1-2.7 wt% to 4.3-4.9 wt% with increasing pyrolysis temperature from 400 to 525 °C with no MS. At 50 wt% MS, any impact of temperature was negligible. A slight increase in moisture from 0.7-4.3 wt% to 1.3-4.9 wt% occurred as flow increased from 50 to 300 mL/min at constant temperature and mode. *In-situ*, at

400 °C and constant flow rate, the moisture decreased by 52-66% from 2.1-2.7 wt% with no MS to 0.7-1.3 wt% at 50 wt% MS. At 525 °C moisture decreased by 65-74% from 4.3-4.9 wt% to 1.1-1.7 wt% when MS was increased to 50 wt%. *Ex-situ*, at 400 °C and constant flow rates, moisture increased by 54-68% from 2.2-2.8 wt% with no MS to 3.7-4.3 wt% at 50 wt% MS. At 525 °C there was no change with MS loading. Moisture increased with MS loading *in-situ* due to the dilution effect of the 0.4 wt% moisture MS. The increase in moisture with MS addition *ex-situ* at 400 °C is potentially due to longer residence times and the enhanced impact this could have on secondary or water forming reactions. At 525 °C, the temperature controls secondary reactions more predominantly, and therefore, MS addition has a reduced effect.

An inverse transformation was recommended to improve the model for the volatiles. The volatiles decreased with: increasing temperature for both operational modes; increasing loading of MS *in-situ*; and decreasing loading of MS *ex-situ*. Without MS, the volatiles decreased by 22-33% from 25-39 wt% to 19-26 wt% from 400 to 525 °C at constant flow. At 50 wt% MS, this trend continues *ex-situ*, while there is no change *in-situ*. The non-linear effect of nitrogen flow resulted in a minimum in volatiles at 150 mL/min. Without MS and comparing the same temperatures the volatiles decreased by 13-17% from 19.0-25.0 wt% to 22.0-30.3 wt% as flow increased from 50 to 150 mL/min. Past 150 mL/min the volatiles increased to 26.3-39.1 wt%. With the addition of 50 wt% MS there was no effect of flow rate on volatiles *in-situ*. At 50 wt% MS the volatiles decreased by 51-58% from 19-39 wt% to 10-27 wt% *in-situ* due to the dilution effect of MS. *Ex-situ* at 50 wt% MS, the volatiles increased by 17-40% to

21.1-48.7 wt% compared to no MS particularly at lower temperatures due to the secondary re-polymerization reactions caused by increased residence times and pressures (*Section 5.4.2*).

The fixed carbon/CO_2 increased from 59-72 wt% to 68-80 wt% with increasing temperature without MS. The effect of temperature decreased as MS increased to 25 wt% MS. However, at MS > 25 wt% the carbon decreased with temperature from 45-53 wt% to 40-48 wt% (*in-situ*) and 63-71 wt% to 58-65 wt% (*ex-situ*) over the temperature range studied. This agrees with the C/H/N(O) analyses from *Section 5.4.3.4*. Due to the non-linear effect of flow, the highest amount of fixed carbon was at 525 °C, 160 mL/min, and no MS (75.3-80.4 wt%). The fixed carbon/CO_2 increased by 6-10% as flow increased from 50 to 150 mL/min then dropped by 9-16% at 300 mL/min. The lowest amount of fixed carbon/CO_2 was recorded at 525 °C, 50 and 300 mL/min nitrogen flow rate, and 50 wt% MS for both *in-situ* (40.0-43.8 wt% fixed carbon/CO_2) and *ex-situ* (57.7-60.8 wt%). The effect of MS on the minimum of fixed carbon/CO_2 was larger for *in-situ* compared to *ex-situ*. At 50 wt% MS *in-situ* the fixed carbon decreased by 21-24% (14 wt%) at 400 °C and by 37-41% (28 wt%) at 525 °C. At 400 °C the decrease in fixed carbon/CO_2 with the addition of > 25 wt% MS was negligible. The fixed carbon of the *in-situ* biochar includes the CO_2 emitted due to the conversion of $CaCO_3$ to CaO at 600-800 °C resulting in higher fixed carbon for *in-situ* biochars compared to *ex-situ* biochars. The reduction of relative fixed carbon in the *ex-situ* chars with increased amount of MS is due to the secondary reactions outlined in *Section 5.4.2* and reaches a

maximum at 25 wt% MS: 10-11% decrease compared to no MS at 400 °C and 17-19% decrease at 525 °C.

A natural log transformation was the best fit for the ash content model. The non-linear effect of temperature resulted in a maximum of ash at intermediate temperatures (460-480 °C). At constant MS and mode, increasing the temperature from 400 to 470 °C increased the ash by 74%, increasing the temperature from 470 to 525 °C resulted in a 33% decrease. The lowest ash (1.6-3.3 wt%) was at 400 and 525 °C and no MS. The ash increased with increasing amount of MS; however, the effect was more pronounced *in-situ* (1266% increase) due to the high amount of ash (CaO) from the MS (54.1 wt%) compared to *ex-situ* (216% increase). The highest ash was recorded for 470 °C and 50 wt% MS for *in-situ* (68.2 wt%) and for *ex-situ* (8.6 wt%) char.

5.4.3.6 High heating value (HHV)

Ideally the biochar HHV exceeds the feedstock's if used in energy applications. The HHV is non-linear with temperature resulting in a minimum HHV at 450-475 °C. The highest HHV was recorded for pure softwood biochar at 400 °C and 50 mL/min as well as for 525 °C and 300 mL/min (28.7-31.3 MJ/kg); a 10 MJ/kg increase from the softwood feedstock (19.5 MJ/kg). Increasing pyrolysis temperature from 450-475 to 525 ºC, increased the HHV by 12-61% at 300 mL/min with no change at 50 mL/min. Increased pyrolysis temperatures results in higher concentrations of fixed C and increased HHV due to the increased release of volatile compounds [61]. Adding MS adversely impacted the HHV, particularly of the *in-situ* chars due to the low heating value MS additive. Due

to the HHV reduction and increase in ash (for *in-situ* chars), co-pyrolysis of softwood with MS was not applicable for upgrading the biochar for use as a fuel.

5.4.3.7 pH

The biochar pH increases with increasing temperature and amount of MS (up to 37 wt% MS, maximum calculated through DoE). By increasing the pyrolysis temperature from 400 to 525 °C the pH increases by 10% because more volatile compounds are released, the biochar yield decreases, and the ash content increases. Moreover, as more hydrogen atoms are driven off with increasing temperate, deprotonate hydroxyl groups make the char more alkaline (and the FPBO more acidic) [62–64].

The pH of slow pyrolysis chars, typically used in soil amendment, is generally lower compared to fast pyrolysis chars [65]. The pH for *in-situ* chars is higher by a pH value of 1 compared to *ex-situ* but follows the same trend in relation to temperature and amount of MS. A maximum pH occurred at 37 wt% MS, indicating there is an optimum amount of MS to maximize the pH. The biochar pH values increased from 7.0-7.7 to 8.7-9.4 (*in-situ*) and 6.2-6.9 to 7.8-8.5 (*ex-situ*) by increasing the MS loading from 0 to 37 wt% and plateaued as MS loading increased. The pH increase is likely due to basicity of the MS (pH 8.64 ± 0.11) and the pH decline at > 37 wt% MS additive was potentially due to the dilution effect caused by water and other volatiles in MS or the decreased heat transfer rates due to increased overall mass of feed. Co-pyrolysis of softwood with MS was applicable for upgrading the biochar in terms of pH, especially for uses as soil amendment. Newfoundland soils are known to be very acidic requiring the

use of lime and fertilizers [66]. Therefore, addition of biochar from the co-pyrolysis of softwood and MS would improve pH of Newfoundland soils, locally.

5.4.3.8 Bulk density

The bulk density increased from 165-245 to 435-560 kg/m³ MS from 0 to 50 wt% for *in-situ* biochars due to mixing with high density MS (925 kg/m³). With increasing temperature from 400 to 525 °C, the bulk density increased by 9-43% for most biochars due to increased carbon content. The bulk density of *in-situ* biochars was the highest (560 kg/m³) for 525 °C, 300 mL/min nitrogen flow, and 50 wt% MS and lowest (165 kg/m³) for 400 °C, 50 mL/min nitrogen flow, and no MS. The effect of MS on the bulk density of *ex-situ* biochars was negligible. The bulk density of *ex-situ* biochars ranged from 140-215 kg/m³ comparable to literature values for fast pyrolysis biochar (150-200 kg/m³) [3].

5.5 Conclusions

Liquid analysis has shown that the co-pyrolysis of softwood with MS reduced oxygen in FPBO via decarboxylation and reduction of carboxylic acids to ketones with $CaCO_3$ as well as dehydration. The biochar's physical, chemical, and morphological properties and its application as a fuel, adsorbent, and soil amendment were investigated in this work. MS co-pyrolysis decreased the HHV of the biochar by dilution with non-combustible MS, and therefore, applicability as a fuel is not recommended for *in-situ* biochars. Co-pyrolysis of softwood with MS was applicable for upgrading the biochar in terms of

pH, especially for uses as soil amendment. The pH increased from 7 to 9 with MS addition. Co-pyrolysis (*in-situ*) biochar pores were filled with MS reducing the surface area, and increasing the ash, however new functional groups (N and O containing) were introduced. Increased surface functionality is important for high value applications such as acidic gas adsorption. Post-synthetic modification is costly, *in-situ* modification as demonstrated in this study is a faster more efficient alternative. Compared to the market price of the pyrolysis oil and biochar products, using commercial catalysts in upgrading is not economically feasible at this point. Instead, naturally occurring alternative co-pyrolysis additives such as MS should be considered as a first upgrading step. Additives that pose a disposal task to their respective industries with similar chemical make-up compared to suitable catalysts are favourable.

Bibliography

[1] Staš M, Kubička D, Chudoba J, Pospíšil M. Overview of Analytical Methods Used for Chemical Characterization of Pyrolysis Bio-oil. Energy & Fuels 2014;28:385–402. doi:10.1021/ef402047y.

[2] Wang S, Dai G, Yang H, Luo Z. Lignocellulosic biomass pyrolysis mechanism: A state-of-the-art review. Prog Energy Combust Sci 2017;62:33–86. doi:10.1016/j.pecs.2017.05.004.

[3] Funke A, Niebel A, Richter D, Abbas MM, Müller AK, Radloff S, et al. Fast pyrolysis char - Assessment of alternative uses within the bioliq® concept. Bioresour Technol 2016;200:905–13. doi:10.1016/j.biortech.2015.11.012.

[4] Laird DA, Brown RC, Amonette JE, Lehmann J. Review of the pyrolysis platform for coproducing bio-oil and biochar. Biofuels, Bioprod Biorefining 2009;3:547–62. doi:10.1002/bbb.169.

[5] Qambrani NA, Rahman MM, Won S, Shim S, Ra C. Biochar properties and eco-friendly applications for climate change mitigation, waste management, and wastewater treatment: A review. Renew Sustain Energy Rev 2017;79:255–73. doi:10.1016/j.rser.2017.05.057.

[6] Bridgwater A V. Review of fast pyrolysis of biomass and product upgrading. Biomass and Bioenergy 2012;38:68–94. doi:10.1016/j.biombioe.2011.01.048.

[7] Brewer CE, Schmidt-Rohr K, Satrio JA, Brown RC. Characterization of biochar from fast pyrolysis and gasification systems. Environ Prog Sustain Energy 2009;28:386–96. doi:10.1002/ep.10378.

[8] Wisniewski A, Wosniak L, Scharf DR, Wiggers VR, Meier HF, Simionatto EL. Upgrade of biofuels obtained from waste fish oil pyrolysis by reactive distillation. J Braz Chem Soc 2015;26:224–32. doi:10.5935/0103-5053.20140251.

[9] Food and Agriculture Organization. The State of World Fisheries and Aquaculture. Rome, Italy: 2018.

[10] Krutof A, Hawboldt KA. Co-pyrolysis of softwood with waste mussel shells: Liquid analysis. Fuel 2019;254:115584. doi:10.1016/j.fuel.2019.05.167.

[11] Branca C, Giudicianni P, Di Blasi C. GC/MS characterization of liquids generated from low-temperature pyrolysis of wood. Ind Eng Chem Res 2003;42:3190–202. doi:10.1021/ie030066d.

[12] Zhang L, Liu R, Yin R, Mei Y. Upgrading of bio-oil from biomass fast pyrolysis in China : A review. Renew Sustain Energy Rev 2013;24:66–72. doi:10.1016/j.rser.2013.03.027.

[13] Staš M, Kubička D, Chudoba J, Pospíšil M. Overview of analytical methods used for chemical characterization of pyrolysis bio-oil. Energy and Fuels

2014;28:385–402. doi:10.1021/ef402047y.

[14] Krutof A, Hawboldt KA. Upgrading of biomass sourced pyrolysis oil review: focus on co-pyrolysis and vapour upgrading during pyrolysis. Biomass Convers Biorefinery 2018;8:775–87. doi:10.1007/s13399-018-0326-6.

[15] Wiggers VR, Wisniewski A, Madureira LAS, Chivanga Barros AA, Meier HF. Biofuels from waste fish oil pyrolysis: Continuous production in a pilot plant. Fuel 2009;88:2135–41. doi:10.1016/j.fuel.2009.02.006.

[16] Wisniewski A, Wiggers VR, Simionatto EL, Meier HF, Barros AAC, Madureira LASS, et al. Biofuels from waste fish oil pyrolysis: Chemical composition. Fuel 2010;89:563–8. doi:10.1016/j.fuel.2009.07.017.

[17] Fadhil AB, Ahmed AI, Salih HA. Production of liquid fuels and activated carbons from fish waste. Fuel 2017;187:435–45. doi:10.1016/j.fuel.2016.09.064.

[18] Rowland S, Bower CK, Patil KN, DeWitt CAM. Updraft gasification of salmon processing waste. J Food Sci 2009;74:426–31. doi:10.1111/j.1750-3841.2009.01312.x.

[19] Abeynaike A, Wang L, Jones MI, Patterson DA. Pyrolysed powdered mussel shells for eutrophication control: effect of particle size and powder concentration on the mechanism and extent of phosphate removal. Asia-Pacific J Chem Eng 2011;6:231–43. doi:10.1002/apj.426.

[20] Currie JA, Harrison NR, Wang L, Jones MI, Brookes MS. A preliminary study of processing seafood shells for eutrophication control. Asia-Pacific J Chem Eng 2007:460–7. doi:10.1002/apj.082.

[21] Shikhaliyev K, Okoye PU, Hameed BH. Transesterification of biodiesel byproduct glycerol and dimethyl carbonate over porous biochar derived from pyrolysis of fishery waste. Energy Convers Manag 2018;165:794–800. doi:10.1016/j.enconman.2018.04.001.

[22] Ahmad M, Soo Lee S, Yang JE, Ro HM, Han Lee Y, Sik Ok Y. Effects of soil dilution and amendments (mussel shell, cow bone, and biochar) on Pb availability and phytotoxicity in military shooting range soil. Ecotoxicol Environ Saf 2012;79:225–31. doi:10.1016/j.ecoenv.2012.01.003.

[23] Ahmad M, Lee SESSSE, Lim JE, Lee SESSSE, Cho JS, Moon DH, et al. Speciation and phytoavailability of lead and antimony in a small arms range soil amended with mussel shell, cow bone and biochar: EXAFS spectroscopy and chemical extractions. Chemosphere 2014;95:433–41. doi:10.1016/j.chemosphere.2013.09.077.

[24] Guo C, Hu R, Liao W, Li Z, Sun L, Shi D, et al. Protein-enriched fish “biowaste” converted to three-dimensional porous carbon nano-network for advanced oxygen reduction electrocatalysis. Electrochim Acta 2017;236:228–38. doi:10.1016/j.electacta.2017.03.169.

[25] Wang H, Wang K, Song H, Li H, Ji S, Wang Z, et al. N-doped porous carbon material made from fish-bones and its highly electrocatalytic performance in the oxygen reduction reaction. RSC Adv 2015;5:48965–70. doi:10.1039/C5RA09144F.

[26] Raj CJ, Rajesh M, Manikandan R, Yu KH, Anusha JR, Ahn JH, et al. High electrochemical capacitor performance of oxygen and nitrogen enriched activated carbon derived from the pyrolysis and activation of squid gladius chitin. J Power Sources 2018;386:66–76. doi:10.1016/j.jpowsour.2018.03.038.

[27] Piccirillo C, Moreira IS, Novais RM, Fernandes AJS, Pullar RC, Castro PML. Biphasic apatite-carbon materials derived from pyrolysed fish bones for effective adsorption of persistent pollutants and heavy metals. J Environ Chem Eng 2017;5:4884–94. doi:10.1016/j.jece.2017.09.010.

[28] Wallace R, Seredych M, Zhang P, Bandosz TJ. Municipal waste conversion to hydrogen sulfide adsorbents: Investigation of the synergistic effects of sewage sludge/fish waste mixture. Chem Eng J 2014;237:88–94. doi:10.1016/j.cej.2013.10.005.

[29] Wang S, Jiang D, Cao B, Hu Y, Yuan C, Wang Q, et al. Study on the interaction effect of seaweed bio-coke and rice husk volatiles during co-pyrolysis. J Anal Appl Pyrolysis 2018;132:111–22. doi:10.1016/j.jaap.2018.03.009.

[30] Viglašová E, Galamboš M, Danková Z, Krivosudsky L, Lengauer CL, Hood-Nowotny R, et al. Production , characterization and adsorption studies of bamboo-based biochar / montmorillonite composite for nitrate removal. Waste Manag 2018;79:385–94. doi:10.1016/j.wasman.2018.08.005.

[31] Micháleková-Richveisová B, Fristak V, Pipíska M, Duriska L, Moreno-Jimenez E, Soja G. Iron-impregnated biochars as effective phosphate sorption materials. Environ Sci Pollut Res 2017;24:463–75. doi:10.1007/s11356-016-7820-9.

[32] Barros MC, Bello PM, Bao M, Torrado JJ. From waste to commodity: transforming shells into high purity calcium carbonate. J Clean Prod 2009;17:400–7. doi:10.1016/j.jclepro.2008.08.013.

[33] Food and Agriculture Organization. Fisheries and Aquaculture Department. Statistics. 2017. www.fao.org/fishery/statistics/en (accessed May 1, 2017).

[34] Murphy JN, Hawboldt K, Kerton F. Enzymatic processing of mussel shells to produce biorenewable calcium carbonate in seawater. Green Chem 2018;20:2913–20. doi:10.1039/c8gc01274a.

[35] Marin F, Luquet G. Les protéines de coquille de mollusque. Comptes Rendus - Palevol 2004;3:469–92. doi:10.1016/j.crpv.2004.07.009.

[36] Lertwattanaruk P, Makul N, Siripattarapravat C. Utilization of ground waste seashells in cement mortars for masonry and plastering. J Environ Manage 2012;111:133–41. doi:10.1016/j.jenvman.2012.06.032.

[37] Cubillas P, Köhler S, Prieto M, Chaïrat C, Oelkers EH. Experimental determination of the dissolution rates of calcite, aragonite, and bivalves. Chem Geol 2005;216:59–77. doi:10.1016/j.chemgeo.2004.11.009.

[38] Nebel H, Neumann M, Mayer C, Epple M. On the structure of amorphous calcium carbonate--a detailed study by solid-state NMR spectroscopy. Inorg Chem 2008;47:7874–9. doi:10.1021/ic8007409.

[39] Weiner S, Addadi L. Design strategies in mineralized biological materials. J Mater Chem 1997;7:689–702. doi:10.1039/a604512j.

[40] Tangboriboon N, Kunanuruksapong R, Sirivat A, Kunanuruksapong R, Sirivat A. Preparation and properties of calcium oxide from eggshells via calcination. Mater Sci Pol 2012;30:313–22. doi:10.2478/s13536-012-0055-7.

[41] Zhang Y, Cui H, Yi W, Song F, Zhao P, Wang L, et al. Highly effective decarboxylation of the carboxylic acids in fast pyrolysis oil of rice husk towards ketones using CaCO3 as a recyclable agent. Biomass and Bioenergy 2017;102:13–22. doi:10.1016/j.biombioe.2017.04.004.

[42] Papari S, Hawboldt K, Helleur R. Pyrolysis: A Theoretical and Experimental Study on the Conversion of Softwood Sawmill Residues to Biooil. Ind Eng Chem Res 2015;54:605–11. doi:10.1021/ie5039456.

[43] Murphy JN, Kerton FM. Characterization and Utilization of Waste Streams from Mollusc Aquaculture and Fishing Industries. In: Kerton FM, Yan N, editors. Fuels, Chem. Mater. from Ocean Aquat. Sources. First Edit, John Wiley & Sons, Ltd; 2017, p. 189–227.

[44] Bamdad H, Hawboldt K. Comparative study between physicochemical characterization of biochar and metal organic frameworks (MOFs) as gas adsorbents. Can J Chem Eng 2016;94:2114–20. doi:10.1002/cjce.22595.

[45] Yang X, Wang H, Strong PJ, Xu S, Liu S, Lu K, et al. Thermal properties of biochars derived from Waste biomass generated by agricultural and forestry sectors. Energies 2017;10:1–12. doi:10.3390/en10040469.

[46] Exley RR, Butterfield BG, Meylan BA. Preparation of wood specimens for the scanning electron microscope. J Microsc 1974;101:21–30. doi:10.1111/j.1365-2818.1974.tb03865.x.

[47] Olsson T, Megnis M, Varna J, Lindberg H. Study of the transverse liquid flow paths in pine and spruce using scanning electron microscopy. J Wood Sci 2001;47:282–8. doi:10.1007/BF00766714.

[48] Karim Ghani WAWA. Sawdust-derived Biochar: Characterization and CO2 Adsorption/desorption Study. J Appl Sci 2014;14:1450–4. doi:10.3923/jas.2014.1450.1454.

[49] Olarte M V., Zacher AH, Padmaperuma AB, Burton SD, Job HM, Lemmon TL, et al. Stabilization of Softwood-Derived Pyrolysis Oils for Continuous Bio-oil

Hydroprocessing. Top Catal 2016;59:55–64. doi:10.1007/s11244-015-0505-7.

[50] Carpenter D, Westover TL, Czernik S, Jablonski W. Biomass feedstocks for renewable fuel production: a review of the impacts of feedstock and pretreatment on the yield and product distribution of fast pyrolysis bio-oils and vapors. Green Chem 2014;16:384–406. doi:10.1039/C3GC41631C.

[51] Brassard P, Godbout S, Raghavan V. Pyrolysis in auger reactors for biochar and bio-oil production: A review. Biosyst Eng 2017;161:80–92. doi:10.1016/j.biosystemseng.2017.06.020.

[52] Qian Y, Zhang J, Wang J. Pressurized pyrolysis of rice husk in an inert gas sweeping fixed-bed reactor with a focus on bio-oil deoxygenation. Bioresour Technol 2014;174:95–102. doi:10.1016/j.biortech.2014.10.012.

[53] Greco G, Videgain M, Di Stasi C, González B, Manyà JJ, Di C, et al. Evolution of the mass-loss rate during atmospheric and pressurized slow pyrolysis of wheat straw in a bench-scale reactor. J Anal Appl Pyrolysis 2018;136:18–26. doi:10.1016/j.jaap.2018.11.007.

[54] Murphy JN. Adding value to waste from the mussel aquaculture industry using clean technologies. 2015.

[55] Xiong J, Qin Y, Islam E, Yue M, Wang W. Phosphate removal from solution using powdered freshwater mussel shells. Desalination 2011;276:317–21. doi:10.1016/j.desal.2011.03.066.

[56] Rouquerol F, Rouquerol J, Sing KSW, Llewellyn P, Maurin G. Adsorption by Powders and Porous Solids: Principles, Methodology and Applications. 2nd editio. Elsevier; 2013.

[57] Xue Y, Zhou S, Brown RC, Kelkar A, Bai X. Fast pyrolysis of biomass and waste plastic in a fluidized bed reactor. Fuel 2015;156:40–6. doi:10.1016/j.fuel.2015.04.033.

[58] Zhang X, Gao B, Zheng Y, Hu X, Creamer AE, Annable MD, et al. Biochar for volatile organic compound (VOC) removal: Sorption performance and governing mechanisms. Bioresour Technol 2017;245:606–14. doi:10.1016/j.biortech.2017.09.025.

[59] Bamdad H, Hawboldt K, MacQuarrie S. Nitrogen Functionalized Biochar as a Renewable Adsorbent for Efficient CO2 Removal. Energy & Fuels 2018;32:11742–8. doi:10.1021/acs.energyfuels.8b03056.

[60] Uchimiya M, Chang S, Klasson KT. Screening biochars for heavy metal retention in soil: Role of oxygen functional groups. J Hazard Mater 2011;190:432–41. doi:10.1016/j.jhazmat.2011.03.063.

[61] Crombie K, Mašek O. Pyrolysis biochar systems, balance between bioenergy and carbon sequestration. GCB Bioenergy 2015;7:349–61. doi:10.1111/gcbb.12137.

[62] Xu Y, Deng F, Pang Q, He S, Xu Y, Luo G, et al. Development of waste-derived

sorbents from biomass and brominated flame retarded plastic for elemental mercury removal from coal-fired flue gas. Chem Eng J 2018;350:911–9. doi:10.1016/j.cej.2018.06.055.

[63] Dooley KL. Slow pyrolysis biochar from forestry residue and municipal and farm wastes: Characterization and their use in greenhouses as a soil amendment By. Memorial University of Newfoundland, 2015.

[64] Yuan JH, Xu RK, Zhang H. The forms of alkalis in the biochar produced from crop residues at different temperatures. Bioresour Technol 2011;102:3488–97. doi:10.1016/j.biortech.2010.11.018.

[65] Bruun EW, Ambus P, Egsgaard H, Hauggaard-Nielsen H. Effects of slow and fast pyrolysis biochar on soil C and N turnover dynamics. Soil Biol Biochem 2012;46:73–9. doi:10.1016/j.soilbio.2011.11.019.

[66] Newfoundland and Labrador Fisheries and Land Resources. Soil Survey. For Agrifoods 2018. https://www.faa.gov.nl.ca/agrifoods/land/soils/soilsurvey.html (accessed August 31, 2018).

Chapter 6 Thermodynamic model of fast pyrolysis bio-oil advanced distillation curves

This chapter has been submitted for publication; A. Krutof, K. A. Hawboldt. Thermodynamic model of fast pyrolysis bio-oil advanced distillation curves.

Abstract

Fast pyrolysis bio-oil (FPBO) is a complex organic liquid with over 1000 organic compounds. Therefore, little research exists on the prediction and modelling of liquid physicochemical properties and vapour-liquid phase behaviour. A thermodynamic model of the FPBO vapour-liquid equilibrium (VLE) in distillation will improve the understanding of bulk and FPBO fraction properties, and therefore, aid in the enhancement of FPBO for desired applications, such as condensation of pyrolysis vapours, fractionation, and evaporation during combustion. FPBO produced at 450 °C from softwood sawmill residues at a feed rate of 4 kg/h (~ 20 s residence time) in a pilot-scale auger reactor was distilled in an advanced distillation curve (ADC) apparatus at atmospheric pressure and at a vacuum of 5 kPa (abs). The ADC equipment allows for the data collection of true thermodynamic state points, including vapour phase composition data. UNIQUAC was the selected equation of states (EoS) to model FPBO distillation VLEs in a 20-flash series in VMGSim™. A surrogate mixture of water, 3,4,4'-biphenoltriol (pyrolytic lignin), inert solids, and multiple organic components was used to model and predict the VLE and consequently bulk physicochemical properties. It was found that GC-FID composition data (in area%), water content (Karl Fisher titration), distillation residue, and solid content were sufficient to inform the model (surrogate composition). This work improved the understanding of FPBO phase behaviour, composition, and bulk properties. The method allows for the identification of target components and fractions to enhance FPBO quality for desired applications.

Keywords: Fast pyrolysis bio-oil; advanced distillation curve (ADC); vacuum distillation; thermodynamic model; UNIQUAC; oil upgrading

6.1 Highlights

- Advance distillation curve (ADC) method applied to FPBO including composition data
- Distillation at 1 atm and vacuum (5 kPa) yields true thermodynamic state points
- Simulation of FPBO distillation curves in VMGSim™ using UNIQUAC EoS
- Vacuum distillation of 72 vol% at 345 °C before distillation residue solidified
- Distillation in six distinct steps for value-added chemical recovery proposed

6.2 Introduction

Fast pyrolysis bio-oil (FPBO) from wood residues is a proven renewable fuel for heat and power generation in boilers. FPBO is a complex organic liquid and is challenging to characterize compositionally using traditional crude oil characterization methods. However, this type of characterization is necessary to assess fuel blending applications. Standards such as ASTM D7544 have been developed for FPBO [1–10]. However, assessing FPBO volatility and flammability using methods such as flash point is difficult due to the high water content [8]. In this work, we use the advanced distillation curve (ADC) method to assess fuel properties such as composition [11]. Distillation curves are a common characterization tool in the petroleum industry (e.g. ASTM D86 and D2892) but have not been established as an analysis for FPBO. In fact, FPBO has been considered non-distillable due to thermal instability and polymerization at elevated temperatures [12–14]. Vacuum and atmospheric distillation of FPBO have been carried out with the goal to separate water and other low boiling point (BP) compounds to improve residual oil fuel quality or for bio-oil fractionation for analytics [15]. However, polymerization, increased solid content, and water removal lead to a highly viscous residue with limited applications [16]. Untreated pyrolysis oil yields up to 50 vol% solid residue in

vacuum distillation [14], and therefore fractionation of high BP components is not feasible.

In addition to identifying key fractions and compounds, advanced distillation analyses generate the data required for thermodynamic models. A complete assessment of complex mixtures, such as FPBO, vapour-liquid equilibrium (volatility) can only be done by distillation measurement [17]. In the petroleum industry, the ASTM D86 distillation curve procedure is used for quality control and oversight applications in petroleum fuel volatility assessment [18,19]. Data is recorded as vapour temperature over distilled volume fraction (DVF). However, there are drawbacks of this method such as large uncertainties in temperature measurements, little theoretical significance because the true thermodynamic state points are not measured (vapour, not liquid temperatures are correlated to DVF), hazard of an open flame with liquid fuels, overheating particularly without stirring, splashing of the distillate hindering accurate volume measurements, and instrument dependent results [19]. ASTM D2892, a vacuum distillation method, is used for petroleum fuels to address some of these drawbacks, but requires large samples sizes and increased time, and shows uncertainties in measuring and maintaining the vacuum [20]. Other reduced pressure distillation methods are ASTM D1160 (0.13-6.7 kPa) with similar drawbacks compared to ASTM D86 (see above); and ASTM D5236 and D2892 that focus on separations, not volatility [17].

Bruno et al. developed the ADC method to address the challenges of conventional distillation curves and to allow for modelling of vapour-liquid equilibrium (VLE) data, with an equation of state (EoS) [11]. Advantages of ADC compared to other distillation

curves are: (1) quantified and identified composition data of each DVF (2) temperature, volume, and pressure data as true thermodynamic state points allow for modelling with EoS, (3) consistency with historical data such as ASTM D86, (4) density and enthalpy calculation for each DVF, (5) trace chemical analysis/DVF, (6) corrosivity/sulfur assessment/DVF [20–22]. With the obtained thermodynamic state points, and an accurate EoS, equilibrium and transport properties can be calculated at any temperature and pressure, mixture behaviour can be predicted, and surrogates can be developed for fuel testing for engine design, optimization, and mitigation of pollutants (e.g. particulates) [19,22]. Atmospheric pressure distillation with fuels with low volatility (BP of 350-450 °C) can lead to thermal degradation, cracking, or polymerization. Windom and Bruno improved the ADC by proposing a reduced pressure alternative (V-ADC) [17,23].

The ADC method has been used to characterize a variety of fuels: n-alkanes, azeotropes, crude petroleum oil, bio- and petroleum diesel, gasoline, jet fuel, rocket fuel, and pyrolysis oils (from swine, dairy, pine, and polypropylene feedstocks) [11,18,20,24,25]. V-ADC was used to characterize fuels that degrade with temperature such as soy and algae-based biodiesel [26,27], virgin and waste oil [28], and swine manure pyrolysis oil [11]. ADC of single-phase wood-based FPBO has not been done. Starkey Ott et al. distilled polar, high viscosity, swine manure slurry pyrolysis oil produced by Zhang et al. [29] at 275-350 °C under reducing 0.34-2.76 MPa CO atmosphere [20]. A low boiling region yielding clear, colourless distillate was observed < 150 °C while the distillate in the high boiling region was dark brown at temperatures > 300 °C. A maximum of

65 vol% distilled was observed at 500 °C; the remaining oil was lost to char formation due to polymerization reactions at temperatures > 310 °C (ASTM D2892) [20]. Hsieh and Bruno distilled the same swine manure pyrolysis oil produced by Zhang et al. at 3.5 kPa up to 300 °C when accelerated thermal cracking was observed while collecting composition data [11]. A steep increase in temperature is observed after the removal of water resulting in a sigmoid shaped ADC common for complex fuels [11,20,22]. At low DVF (water removal) atmospheric distillation occurred at higher temperatures compared to V-ADC, while at higher vol% distilled the influence of pressure was negligible on the ADC [11,20].

Harries et al. compared the atmospheric ADC of two pyrolysis oils produced by Kunwar et al. in an auger pyrolysis reactor at 500 °C using polypropylene (PP) corrugated advertisement plastics as a feedstock [18,30]. The hot pyrolysis vapours were condensed in a two-stage condensation system resulting in 35-185 °C BP PP gasoline and 185-350 °C BP PP diesel fuel [18,30]. The authors calculated the bulk net enthalpy of combustion $-\Delta H_c$ (lower heating value) [18].

Harries et al. developed an ADC-offset method for non-homogenous fluids with ponderosa pine shaving and dairy manure pyrolysis oils [24]. Pyrolyzed in a 20 kg/h auger reactor at 450-500 °C both feedstocks resulted in a two-phase pyrolysis oil (aqueous top phase and an organic bottom phase) [24]. The offset method allowed for the comparison of distillation curves of fluids with different water content. The DVF just after the distillation of the water was used as a starting point for the offset distillation curves [24].

Molecular distillation has been used to fractionate FPBO prior to GC-MS analysis [31–33].

ADC phase equilibrium data can be used to model the FPBO phase behaviour. Due to the complex nature of FPBO, modelling is generally done with surrogate compounds to represent all or parts of the oil [34–37]. Zhang et al. developed a surrogate mixture to model the evaporation of FPBO and its mixtures with petroleum diesel, biodiesel, and ethanol at 800 K [38]. Elkasabi et al. modelled the stepwise distillation (six temperature steps) of switchgrass, horse manure, and eucalyptus based tail-gas recycled pyrolysis oil (TGRP) via Pro-II's solution equilibrium activity model and TBP distillation curve feature with Margules and non-random two-liquid (NRTL) activity model [39]. Ille et al. used distillation curve data to predict activity coefficients of water in FPBO to feed their condenser models [40].

In this work, we use V-ADC data to assess the volatility of FPBO and select surrogates to model the distillation curve in a 20-flash series in VMGSim™. For each fraction recovered, a sample is taken for GC analysis. Bulk fuel properties such as enthalpy (heating value, heat capacity, flash point), flow properties (viscosity, density), and average molecular weight are predicted with the VMGSim™ model and compared to experimental data.

6.3 Materials and methods

6.3.1 Fast pyrolysis bio-oil production and characterization

A mixture of Newfoundland pine and spruce softwood shavings supplied by Sexton Lumber Co Sawmill, Bloomfield NL Canada, was ground to < 2 mm in a cutting mill and dried at 75 °C overnight. The resulting median particle size determined via sieve analysis was 750 µm, and moisture content was 0.4-2.0 wt% (Mettler Toledo Compact Halogen Moisture Analyzer HB34-S at 105 °C). The higher heating value (HHV) of softwood was 19.51 ± 0.48 MJ/kg. The auger reactor was operated at 4 kg/h (feed), 450 °C reactor temperature, and 20-25 °C condenser cooling water temperature. The reactor and its operating parameters are described by Papari et al. [41]. The physicochemical FPBO properties investigated were water content, HHV, total acid number (TAN), density (at 20 and 40 °C), dynamic viscosity (at 20 and 40 °C), solid content, elemental composition (C/H/N(O)), thermogravimetric analysis (TGA), and GC-MS/FID as described in [42,43].

6.3.2 Advanced distillation curve apparatus

Advanced distillation curves (ADC) were first introduced by Thomas Bruno (NIST) [19]. Improvements compared to ASTM D86 and ASTM D2892 are noted above. The ADC apparatus is improved in that heating is provided by a two-part aluminum heating jacket with 3 cartridge heaters which are programmed to a heating profile with a Glas-Col Ramptrol LLC 104A PL912T temperature controller (Figure 6-1). The heating profiles were chosen to ensure constant distillate mass flow rate (*Appendix F*). This heater

set-up allows for magnetic stirring of the 200 mL sample in a 500 mL round bottom flask reducing hot spots in the liquid. The temperature is measured via two J-type (atmospheric) or K-type (vacuum) thermocouples: one measuring the distillation head/vapour temperature (T_h) allowing for comparison with historical data (e.g. ASTM D86) and one in the kettle/liquid (T_k). A forced air-cooled condenser allows for flexibility in condenser temperature. A sampling adapter (hammock adapter) is located just before the volumetric receiving flask to ensure uniform sample temperature and avoid vapour lock in the syringe needle. The distillate drops in into a calibrated receiving flask with two communicating tubes to allow for stabilized volume measurements [19]. A vacuum sampling adapter was modified from [26]. The housing was aluminum instead of PTFE, increasing durability, with an additional outside thread and cap with septum for the plunger reducing air leakage into the sampling adapter and V-ADC apparatus. The sampling adapter was connected to a separate vacuum pump with slightly lower pressures of 2.0 kPa compared to 5.0 kPa in the V-ADC apparatus to assist with pulling samples. Composition data is collected via the hammock adapter and chromatographic syringe/vacuum sampling adapter. At 10 DVF intervals, 20 µL distillate samples are taken and dissolved in 250 µL 2-propanol. These samples are analyzed using a GC-FID (as described in *Section 2.1*) and provide temperature/DVF/composition data points. All experiments at vacuum conditions were carried out at 5.0 kPa, slightly above the vapour pressure of water at room temperature. The vacuum was supplied to the apparatus via a Welch DuoSeal™ 1400B-01 rotary vane vacuum pump and controlled by an Alicat PCD-series™ PCD-15PSIA-D-PCA13.PCA13 pressure controller with two stainless steal PCA13 valves calibrated from 0-15 psia. A Welch Self-Cleaning Dry Vacuum

System™ 202701 vacuum pump applied vacuum to the sampling syringe. During V-ADC, for kettle temperatures up to 200 °C, the hammock adapter was cooled with the condenser cooling air outlet to avoid re-evaporation of the distillate. Starting at 250 °C kettle temperature, sampling from the hammock adapter was difficult due to the high viscosity of the sample, cooling air to the condenser was shut off, and the condenser and hammock adapter were heated with a heat gun. Uncertainties were: ± 1.0 °C thermocouples, ± 0.03 kPa apparatus pressure, ± 0.3 mL DVF. "Last drop" samples were taken when T_k measurement decreased because the thermocouple lifted out of the fluid [19].

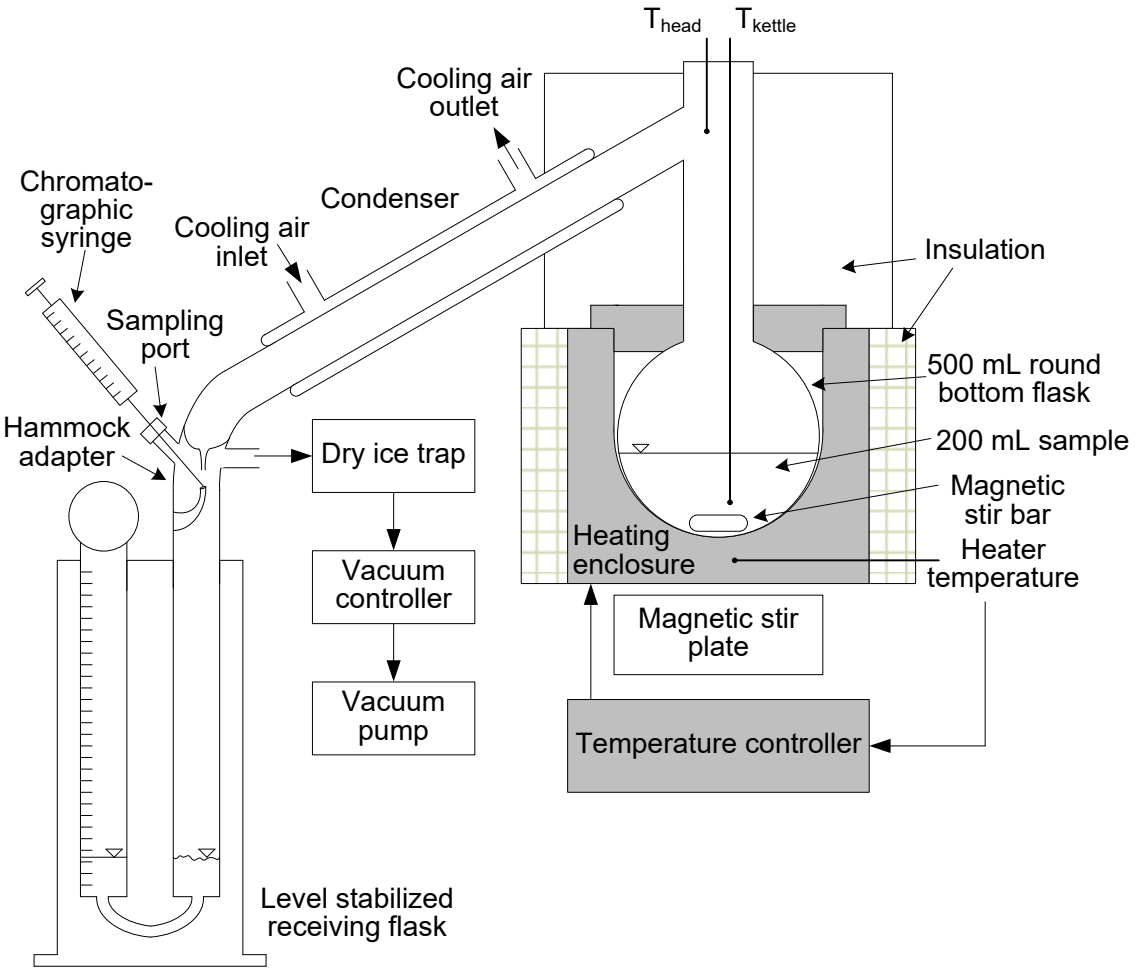

Figure 6-1: Schematic drawing of the (vacuum) advanced distillation curve set-up

6.3.2.1 Validation

The apparatus was validated with two mixtures of n-decane and tetradecane and compared to literature values by Bruno et al. [19]. Mixtures 1 and 2 were a 50:50 and 75:25 mol/mol mixture of n-decane (CAS 124-18-5) and tetradecane (CAS 629-59-4) from Sigma Aldrich at ≥ 99% purity. BPs of the pure compounds at 1 atm are 174.1 °C and 253.5 °C for n-decane ($C_{10}H_{22}$) and n-tetradecane ($C_{14}H_{30}$), respectively [44]. Validation was carried out in triplicate with mixture 1 and duplicate with mixture 2. Composition data was collected for 1 run at atmospheric pressure and 2 runs at vacuum conditions (5.0 kPa) for each validation mixture. Composition samples in n-hexane solvent were analyzed via GC-FID equipped with an Equity™ -5 Capillary 30 m column, 0.25 mm outside diameter coated with 25 µm, at temperature profile heating from 90 to 250 °C at 8 °C/min. The auto sampler injection into split injector is set at 30 mL/min. Calibration by external standard mixtures of 0:100, 20:80, 40:60, 60:40, 80:20, 100:0 mol/mol of decane and tetradecane was carried out. ADC curves were simulated via a 20-flash series with Advanced Peng Robinson fluid package in VMGSim™ Version 10.0.

6.3.3 Thermodynamic model

A 20-flash series (5 vol% distilled per flash via heat exchangers between flashes) was developed in VMGSim™ Version 10.0. The universal quasi-chemical activity coefficients (UNIQUAC) EoS was used for the liquid phase and ideal gas for the vapour. Each 5 vol% step is compared to the experimental data. Gas phase association due to acetic acid and other association compounds was not considered due to the lack of improvement in predictions and long computational times required (seconds compared to

> 10 minutes). Equation 2.1 was used to compute the bubble temperature for a defined liquid composition and pressure.

$$y_i P = x_i \gamma_i P_{vi} \quad (6.1)$$

No complex model is necessary to predict fuel properties, such as enthalpy, (cold) flow properties, mixing behaviour, stability and acidity. The simulated feed temperature (20 °C), and pressure (1 atm and 5 kPa_a) was set according to experimental conditions. Preliminary experiments indicate FPBO distillation shows a sigmoid-shaped curve, indicating the data could potentially be modelled with a few selected surrogate compounds. The surrogate compounds were selected to represent the wide range of functional groups and BP components present in the liquid (Table 6-1).

Table 6-1: Surrogates and quantities in FPBO model with boiling points and functional groups

	Surrogate compound	**Amount in simulation feed wt%**	**BP[a] @ 1 atm °C** [44]	**MW[b] g/mol**	**Functional groups**
1	Water	23.7	100.0	18	
2	Methanol	0.8	64.6 ± 0.3	32	Alcohol
3	Glycolaldehyde (2-hydroxy-acetaldehyde)	3.9	131.3 ± 23	60	Aldehyde, hydroxyl
4	Acetic acid	4.9	117.1 ± 3.0	60	Acid
5	1-Hydroxy-2-propanoate (acetol)	5.4	145.5 ± 0.0	74	Aldehyde, ketone
6	Furfural	0.2	161.8 ± 0.0	96	Aldehyde
7	Furfurylalcohol	1.4	170.0 ± 0.0	98	Alcohol
8	Guaiacol	3.5	205.0 ± 0.0	124	MePh[c]
9	2-Methoxy-4-methylphenol (creosol)	4.7	220.0 ± 0.0	138	MePh, methyl
10	5-Ethyl-guaiacol (modelled in FPBO: 4-ethyl-guaiacol)	1.9	246.5 ± 20	152	MePh, ethyl
11	4-Allyl-2-methoxyphenol (eugenol)	2.8	255.0 ± 0.0	164	MePh
12	4-Propylguaiacol	2.1	263.6 ± 20	166	MePh
13	Syringol	4.6	264.5 ± 0.0	154	MePh
14	Vanillin	1.3	282.6 ± 20	152	MePh, aldehyde
15	Levoglucosan	3.8	383.8 ± 42	152	Anhydrosugar
16	3,4,4'-Biphenoltriol	31.3	416.5 ± 35	202	Pyrolytic lignin
17	Solid[d]	3.8	na		

a - boiling point (BP), b - molecular weight (MW), c - methoxyphenol (MePh)
d - no vapour pressure

The chemical classification is somewhat ambiguous because several compounds have multiple functional groups (Table 6-1). The water content (23.7 wt%) was determined by Karl Fischer titration. The distillation residue is typically 28-32 vol% and consists of solids and polymerized/solidified pyrolytic lignin (acetone, methanol, water-insolubles)

which do not contribute significantly to vapour pressure but do influence activity of volatiles in liquid through dilution and associations [40]. Solids were assigned a vapour pressure of zero, and for simplicity, the binary interaction parameters for binaries containing solids were assumed to be zero. The solid content was 3.75 ± 0.09 wt%, and the remaining distillation residue was pyrolytic lignin. In this work 3,4,4'-biphenyltriol (BP 416 ±30 °C) with 13 molecules, two aromatic rings, and a variety of typical lignin bonds was used as a surrogate component for pyrolytic lignin [40]. The fraction of the remaining surrogates (2-15) was determined using area% from GC-FID.

6.4 Results and discussion

The ADC system was first validated using a simple fluid, and then a series of FPBO experiments were carried out to develop a model that could satisfactorily predict phase behaviour.

6.4.1 Validation results

Atmospheric validation ADC and composition results (Figure 6-2 and Figure 6-3) are summarized in Table 6-2 and Table 6-3. V-ADC validation at 5.0 kPa and composition results (Figure 6-4 to Figure 6-6) are summarized in Table 6-4 and Table 6-5 Bruno et al. found that T_h is instrument (and insulation) depended, therefore T_k was used for comparison of validation experiments to literature and simulated data [19].

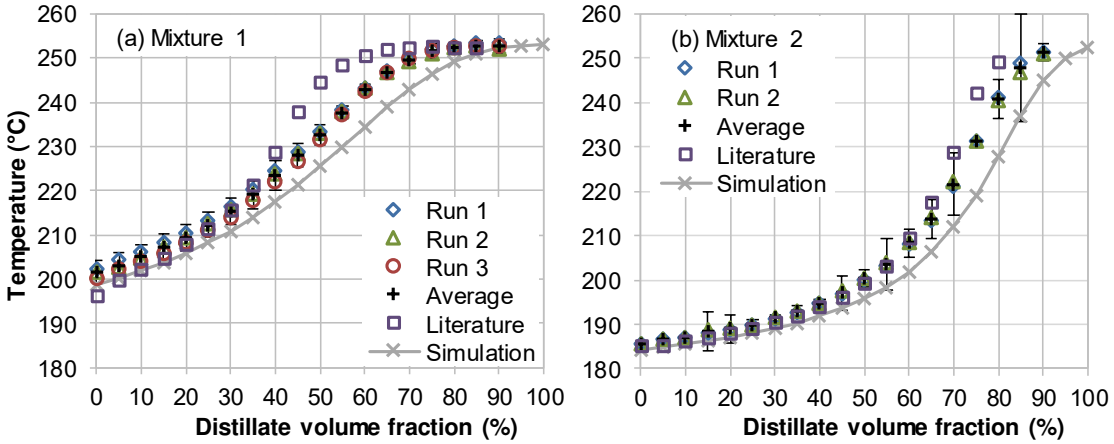

Figure 6-2: Advanced distillation curve recorded at 100.4 kPa with 95% confidence interval and comparison to literature [19] and simulated values for (a) validation mixture 1 50:50 v/v decane tetradecane and (b) validation mixture 2 75:25 v/v decane tetradecane

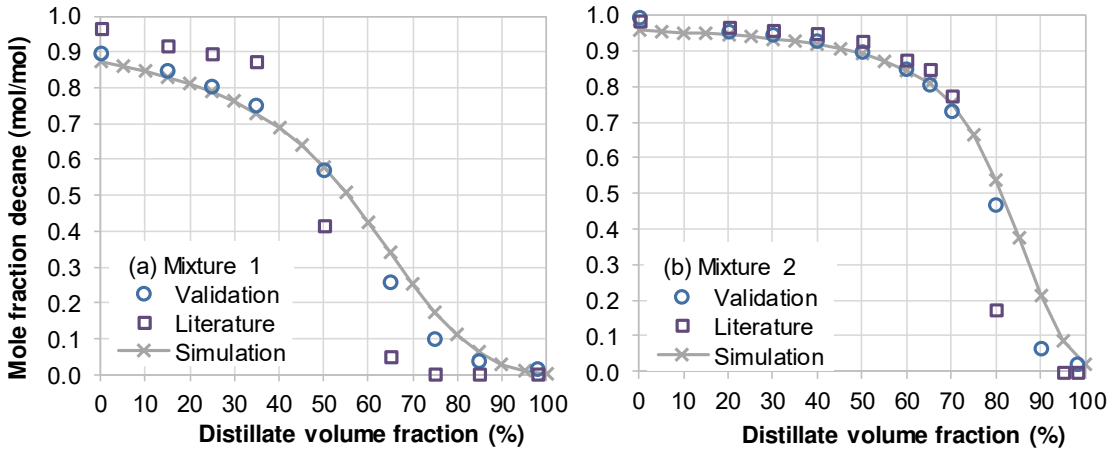

Figure 6-3: Advanced distillation curve composition data recorded at 100.4 kPa with comparison to literature [1] and simulated values for (a) validation mixture 1 50:50 v/v decane:tetradecane and (b) validation mixture 2 75:25 v/v decane:tetradecane

The ADC data showed a good correlation to experimental literature values and simulated data. The difference to literature values could be due to differences in ambient pressure, that is pressures below 1 atm (high altitude) converted to 1 atm via Sydney-Young equation [19]. Differences to the simulated data are due to a small reflux of condensed vapours in the distillation flask head, and the delay between temperature and volume fraction measurements caused by equipment hold-up. Bruno et al. noted that hold-up in the apparatus caused a loss of 2-4 vol% of total liquid [19].

Over three separate runs, the 50:50 mol:mol decane-to-tetradecane mix showed an average standard deviation of 0.6 °C and an average error (95%) of ± 1.6 °C and the average difference compared to literature was -1.6 ± 2.4 °C (-0.6 ± 1.0%) [19] and 5.4 °C ± 1.1 °C (2.4 ± 0.5%) to simulation data. The composition data average difference was 1.7 ± 9.0 mol% to literature and -1.1 ± 3.2 mol% to simulation. The 75:25 mol:mol decane-to-tetradecane mixture ADC showed an average standard deviation of

0.3 °C for two runs with an average difference of -1.3 ± 1.9 °C (-0.5 ± 0.8%) to literature values [19] and 4.9 ± 1.8 °C (2.4 ± 0.8%) to simulation data. The composition data average difference was 1.8 ± 6.5 mol% to literature and -1.5 ± 3.4 mol% to simulation. Bruno et al. noticed the initial boiling temperature for validation mixture 1 and 2 to be below other standards by an average 9.4 °C [19].

Table 6-2: Advanced distillation curve data of validation mix 1 50:50 v/v decane:tetradecane recorded at 101.4 kPa with a 95% confidence interval and comparison with literature [1] and simulated values

	Validation							Literature		Simulated		
Volume distilled	**T_k Run 1**	**T_k Run 2**	**T_k Run 3**	**T_k Average**	**T_k Standard deviation**	**T_k 95% error**	**x, C10**	**T_k**	**x, C10**	**Volume distilled**	**T_k**	**x, C10**
vol%	**°C**	**°C**	**°C**	**°C**	**°C**	**°C**	**mol/mol**	**°C**	**mol/mol**	**vol%**	**°C**	**mol/mol**
0	202.4	201.7	200.3	201.5	1.07	2.66	0.897	196.5	0.966	0	198.7	0.871
5	204.4	202.7	202.2	203.1	1.15	2.86		200.0		5	200.2	0.860
10	206.2	204.9	204.1	205.1	1.06	2.63		202.2		10	201.8	0.846
15	208.4	207.1	205.9	207.1	1.25	3.11	0.847	205.0	0.918	15	203.7	0.831
20	210.6	209.4	208.2	209.4	1.20	2.98		208.0		20	205.8	0.812
25	213.3	212.5	211.1	212.3	1.11	2.77	0.803	211.7	0.896	25	208.2	0.789
30	216.4	215.7	214.0	215.4	1.23	3.07		215.7		30	210.9	0.762
35	220.3	219.3	217.8	219.1	1.26	3.13	0.748	221.3	0.875	35	213.9	0.729
40	224.4	223.9	221.9	223.4	1.32	3.29		228.8		40	217.4	0.688
45	228.7	228.5	226.8	228.0	1.04	2.59		237.8		45	221.2	0.638
50	233.4	233.1	231.7	232.7	0.91	2.25	0.570	244.6	0.416	50	225.4	0.577
55	238.2	237.9	237.1	237.7	0.57	1.41		248.6		55	229.9	0.506
60	243.3	243.2	242.4	243.0	0.49	1.23		250.8		60	234.5	0.426
65	247.0	246.6	246.7	246.8	0.21	0.52	0.257	252.0	0.049	65	239.0	0.339
70	250.0	249.2	249.8	249.7	0.42	1.03		252.5		70	243.0	0.253
75	252.1	250.8	251.6	251.5	0.66	1.63	0.099	252.6	0.000	75	246.4	0.175
80	252.7	252.3	252.4	252.5	0.21	0.52		252.4		80	249.1	0.109
85	253.3	252.6	252.6	252.8	0.40	1.00	0.037	252.4	0.000	85	251.0	0.061
90	253.5	252.2	252.7	252.8	0.66	1.63		253.3[a]		90	252.2	0.029
95								258.6[a]		95	252.9	0.011
98							0.013		0.000	100	253.2	0.002
Onset[b]	164.5	164.1	168.0	165.5	2.15	164.5		191.8				
Sustained[b]	201.8	201.0	198.0	200.3	2.00	201.8		193.6				
Vapour rise[c]	202.1	201.2	200.2	201.2	0.95	202.1		196.5				
First drop	202.4	201.6	200.2	201.4	1.11	202.4						

a - temperature recorded after lift-out of thermocouple, b - bubbling onset and sustained bubbling could not be observed due to dark, opaque nature of fast pyrolysis bio-oil, c - initial boiling point

Table 6-3: Advanced distillation curve data of validation mix 2 75:25 v/v decane:tetradecane recorded at 101.4 kPa with a 95% confidence interval and comparison with literature [1] and simulated values

	Validation						Literature		Simulated		
Volume distilled	**T_k Run 1**	**T_k Run 2**	**T_k Average**	**T_k Standard deviation**	**T_k 95% error**	**x, C10**	**T_k**	**x, C10**	**Volume distilled**	**T_k**	**x, C10**
vol%	**°C**	**°C**	**°C**	**°C**	**°C**	**mol/mol**	**°C**	**mol/mol**	**vol%**	**°C**	**mol/mol**
0	185.6	185.6	185.6	0.00	0.00	0.996	185.4	0.986	0	184.3	0.958
5	186.5	186.5	186.5	0.00	0.00		185.4		5	184.9	0.955
10	187.1	187.1	187.1	0.00	0.00		186.2		10	185.5	0.952
15	188.0	188.7	188.4	0.49	4.45		186.9		15	186.2	0.949
20	188.8	189.3	189.1	0.35	3.18	0.954	188.0	0.969	20	187.0	0.944
25	189.8	190.0	189.9	0.14	1.27		189.1		25	188.0	0.940
30	191.4	191.5	191.5	0.07	0.64	0.945	190.5	0.958	30	189.0	0.934
35	192.8	193.0	192.9	0.14	1.27		191.9		35	190.3	0.927
40	194.8	194.9	194.9	0.07	0.64	0.927	194.2	0.949	40	191.8	0.918
45	196.8	197.4	197.1	0.42	3.81		196.3		45	193.6	0.907
50	200.1	200.4	200.3	0.21	1.91	0.899	199.5	0.929	50	195.7	0.892
55	203.1	204.0	203.6	0.64	5.72		203.1		55	198.4	0.873
60	208.1	208.6	208.4	0.35	3.18	0.848	209.4	0.875	60	201.9	0.846
65	213.4	214.1	213.8	0.49	4.45	0.804	217.7	0.848	65	206.2	0.808
70	221.0	222.1	221.6	0.78	6.99	0.731	228.7	0.773	70	211.9	0.751
75	231.3	231.3	231.3	0.00	0.00		242.1		75	219.2	0.665
80	241.1	240.4	240.8	0.49	4.45	0.469	249.3	0.173	80	227.9	0.540
85	248.8	246.9	247.9	1.34	12.07		256.7[a]		85	237.0	0.377
90	251.4	251.1	251.3	0.21	1.91	0.064	265.1[a]		90	244.9	0.211
95								0.000	95	250.0	0.086
98						0.019		0.000	100	252.5	0.020
Onset[b]	180.4	158.8	169.6	15.27	137.2		182.0				
Sustained[b]	185.6	185.6	185.6	0.00	0.00		183.3				
Vapour rise[c]	185.6	185.6	185.6	0.00	0.00		184.6				
First drop	185.6	185.6	185.6	0.00	0.00						

a - temperature recorded after lift-out of thermocouple, b - bubbling onset and sustained bubbling could not be observed due to dark, opaque nature of fast pyrolysis bio-oil, c - initial boiling point

The apparatus was also validated at vacuum pressure.

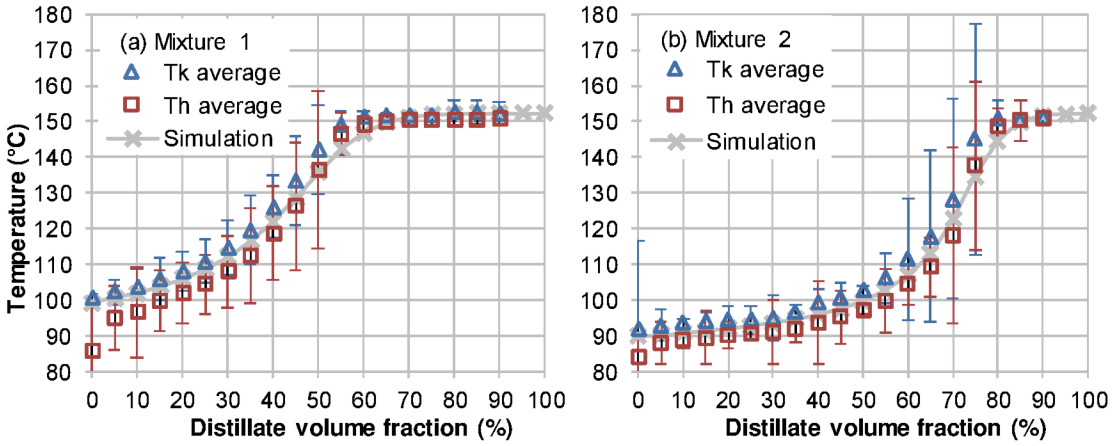

Figure 6-4: Vacuum advanced distillation curve validation recorded at 5.0 kPa comparing kettle (T_{kettle}) and head (T_{head}) temperatures with simulated kettle temperatures for (a) mixture 1 50:50 v/v decane:tetradecane and (b) mixture 2 75:25 v/v decane:tetradecane

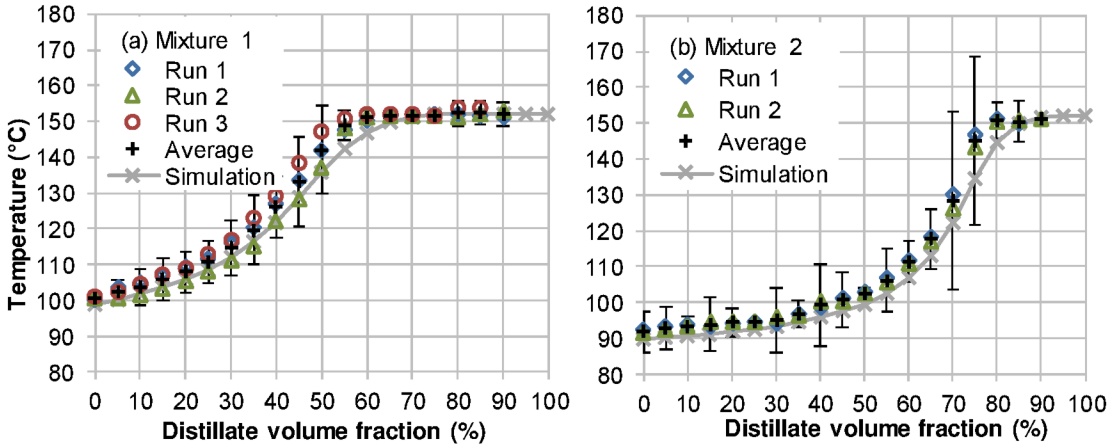

Figure 6-5: Vacuum advanced distillation curve validation recorded at 5.0 kPa with 95% confidence interval and comparison to simulated values for (a) mixture 1 50:50 v/v decane tetradecane and (b) mixture 2 75:25 v/v decane tetradecane

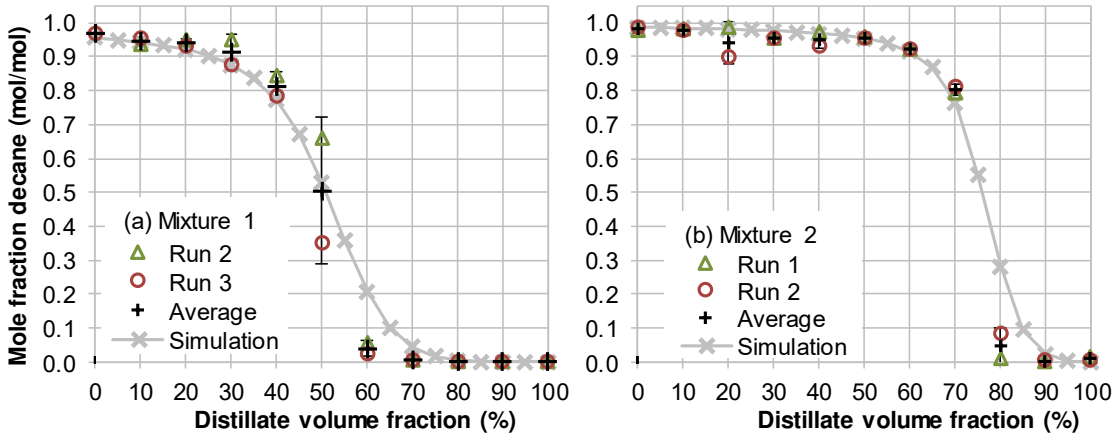

Figure 6-6: Vacuum advanced distillation curve composition data recorded at 5.0 kPa with standard deviation and comparison to simulated values for (a) validation mixture 1 50:50 v/v decane tetradecane and (b) validation mixture 2 75:25 v/v decane tetradecane

The distillation curves for both mixtures reached the boiling point of pure tetradecane (253.6 °C) at lower DVF compared to the simulation. This left-shift of the experimental distillation curves is due to hold-up in the apparatus and reflux to the distillation flask. Even though reflux was limited as much as possible through short distances and insulation of the distillation flask, it was not eliminated 100%. The measured V-ADC data showed a good correlation to simulated data. Differences to the simulated data are due to a small reflux of condensed vapours in the distillation flask head, and the delay between temperature and volume fraction measurements caused by equipment hold-up (<5 vol%). The 50:50 mol:mol decane-to-tetradecane mix (three runs) had an average standard deviation of 2.0 °C and an average error (95%) of ± 5.1 °C. Average difference to simulation data was 2.4 ± 1.0 °C (2.0 ± 0.7%). The composition data average difference to simulation was -1.1 ± 3.8 mol%. The 75:25 mol:mol decane-to-tetradecane mixture ADC (two runs) had an average standard deviation of 0.9 °C for two runs. The average

difference to simulation data was 3.3 ± 1.1 °C (3.1 ± 0.8%), and the composition data average difference to simulation was -2.9 ± 5.3 mol%.

Table 6-4: Vacuum advanced distillation curve data of validation mix 1 50:50 v/v decane:tetradecane recorded at 5.0 kPa with a 95% confidence interval and comparison with simulated values

Validation								Simulation		
Volume distilled	**T_k Run 1**	**T_k Run 2**	**T_k Run 3**	**T_k Average**	**T_k Standard deviation**	**T_k 95% error**	**x, C10 Average**	**Volume distilled**	**T_k**	**x, C10**
vol%	**°C**	**°C**	**°C**	**°C**	**°C**	**°C**	**mol/mol**	**vol%**	**°C**	**mol/mol**
0	100.2	100.6	101.0	100.6	0.40	0.99	0.970	0	99.1	0.956
5	103.5	100.6	102.3	102.1	1.46	3.62		5	100.3	0.950
10	105.1	101.4	104.4	103.6	1.97	4.88	0.947	10	101.9	0.943
15	107.3	103.2	107.4	106.0	2.40	5.95		15	103.7	0.933
20	109.2	105.3	109.1	107.9	2.22	5.52	0.940	20	105.9	0.921
25	111.7	108.1	112.7	110.8	2.42	6.01		25	108.7	0.903
30	115.8	111.2	116.9	114.6	3.02	7.51	0.913	30	112.1	0.876
35	120.5	115.3	122.9	119.6	3.89	9.65		35	116.4	0.836
40	126.9	122.2	129.0	126.0	3.48	8.65	0.814	40	121.9	0.772
45	133.4	128.2	138.3	133.3	5.05	12.55		45	128.5	0.673
50	141.7	137.3	147.3	142.1	5.01	12.45	0.505	50	135.7	0.528
55	147.8	148.1	150.8	148.9	1.65	4.10		55	142.2	0.359
60	150.4	151.0	151.9	151.1	0.75	1.88	0.040	60	146.9	0.207
65	151.6	151.4	152.1	151.7	0.36	0.90		65	149.7	0.102
70	151.9	151.5	152.0	151.8	0.26	0.66	0.007	70	151.2	0.044
75	152.1	151.5	151.6	151.7	0.32	0.80		75	151.8	0.017
80	151.9	151.3	154.0	152.4	1.42	3.52	0.001	80	152.1	0.006
85	151.4	152.2	154.0	152.5	1.33	3.31		85	152.2	0.002
90	151.2	153.0		152.1	1.27	3.16	0.000	90	152.2	0.000
								95	152.2	0.000
								100.0	152.2	0.000
Onset[a]	96.7	93.2		95.0						
Sustained[a]	96.9	96.6		96.8						
Vapour rise[b]	100.1	98.9		99.5						
First drop	100.2	100.6	101.0	99.5	0.85	0.89				

a - bubbling onset and sustained bubbling could not be observed due to dark, opaque nature of fast pyrolysis bio-oil, b - initial boiling point

Table 6-5: Vacuum advanced distillation curve data of validation mix 2 75:25 v/v decane:tetradecane recorded at 5.0 kPa with a 95% confidence interval and comparison with simulated values

	Validation						Simulated		
Volume distilled	**T_k Run 1**	**T_k Run 2**	**T_k Average**	**T_k Standard deviation**	**T_k 95% error**	**x, C10**	**Volume distilled**	**T_k**	**x, C10**
vol%	**°C**	**°C**	**°C**	**°C**	**°C**	**mol/mol**	**vol%**	**°C**	**mol/mol**
0	92.4	91.5	92.0	0.64	5.72	0.996	0	89.8	0.987
5	93.3	92.4	92.9	0.64	5.72		5	90.2	0.986
10	93.6	93.2	93.4	0.28	2.54		10	90.7	0.985
15	93.3	94.5	93.9	0.85	7.62		15	91.2	0.983
20	94.1	94.7	94.4	0.42	3.81	0.954	20	91.9	0.981
25	94.4	94.4	94.4	0.00	0.00		25	92.6	0.979
30	94.3	95.7	95.0	0.99	8.89	0.945	30	93.5	0.977
35	97.0	96.4	96.7	0.42	3.81		35	94.5	0.973
40	98.4	100.2	99.3	1.27	11.44	0.927	40	95.8	0.969
45	101.3	100.1	100.7	0.85	7.62		45	97.5	0.963
50	102.8	102.6	102.7	0.14	1.27	0.899	50	99.6	0.954
55	106.9	105.5	106.2	0.99	8.89		55	102.5	0.940
60	111.8	110.9	111.4	0.64	5.72	0.848	60	106.7	0.915
65	118.4	117.1	117.8	0.92	8.26	0.804	65	113.0	0.868
70	130.2	126.3	128.3	2.76	24.78	0.731	70	122.4	0.766
75	146.9	143.2	145.1	2.62	23.51		75	134.6	0.554
80	151.1	150.3	150.7	0.57	5.08	0.469	80	144.7	0.281
85	150.0	150.9	150.5	0.64	5.72		85	149.9	0.096
90		151.2	151.2			0.064	90	151.7	0.023
95							95	152.2	0.004
98						0.019	100	152.2	0.000
Onset[a]									
Sustained[a]		90.0	90.0						
Vapour rise[b]		90.6	90.6						
First drop	92.4	91.5	92.0	0.64	2.74				

a - bubbling onset and sustained bubbling could not be observed due to dark, opaque nature of fast pyrolysis bio-oil, b - initial boiling point

6.4.2 Pyrolysis yields and oil properties

Yields based on wet biomass (0.4-2.0 wt% moisture) were: 48.1 wt% oil, 16.8 wt% char, and 35.1 wt% gas. The gas yield was determined by difference. Properties of the oil are outlined in Table 6-6. VMGSim™ simulation results are discussed in *Section 6.4.5*.

Table 6-6: Properties of FPBO used in this work and comparison to ASTM 7544 and typical FPBO

Property	**Average**[a]		**95% conf. interval**	**VMGSim prediction**	**ASTM 7544 min/max**	**ASTM 7544 Grade G**	**ASTM 7544 Grade D**	**Typical FPBO** [6,10,45–47]
Oil yield, wt%	48.1							50-75
Char yield, wt%	16.8							12-22
Gas yield, wt%	35.1							13-23
Gross heat of combustion, HHV, MJ/kg	18.2	±	0.08	21.1	min	15	15	13-18
Water content, wt%	23.7	±	0.26		max	30	30	20-40
Solid content, wt%	3.75	±	0.09		max	2.5	0.25	0.01-3
Kinematic viscosity (20 °C), cSt = mm²/s	48.2	±	na	2.62				6-140
Kinematic viscosity (40 °C), cSt = mm²/s	18.1	±	na	1.62	max	125	125	< 35
Density (20 °C), g/mL	1.204	±	0.001	1.124	report	1.1-1.3	1.1-1.3	1.05-1.25
TAN, mgNaOH/gOil	47.6	±	3.44					36-93
TAN, mgKOH/gOil	66.7	±	na					50-130
pH						report	report	2-3
Flash point[b], °C				22.9	min	45	45	40-110
Pour point, °C					max	-9	-9	-9 to -36
$C_{dry,}$ wt%	57.9	±	1.76					56-62
$H_{dry,}$ wt%	6.2	±	0.40					6-8
$N_{dry,}$ wt%	<0.2	±	Na					<0.3
O_{dry} (by difference), wt%	35.9	±	1.70					30-60[c]
$S_{dry,}$ wt%	0.0	±	0.00		max	0.05	0.05	0-0.05
Highly volatiles <200 °C, wt%	63.4	±	6.85					
Medium volatiles 200-600 °C, wt%	24.4	±	1.44					
Combustibles 600-700 °C, wt%	11.8	±	5.52					
Ash > 700 °C, wt%	0.42	±	0.09		max	0.25	0.15	0.01-0.7

a - without filtering, b - now Sustained Combustion Test [8], c - wet and dry oil

6.4.3 Atmospheric pressure advanced distillation curves

A pressure correction to 1 atm was not necessary as the ADC was performed at sea level. The average room temperature was 23.8 °C. ADC results are given in Figure 6-7 and Table 6-7.

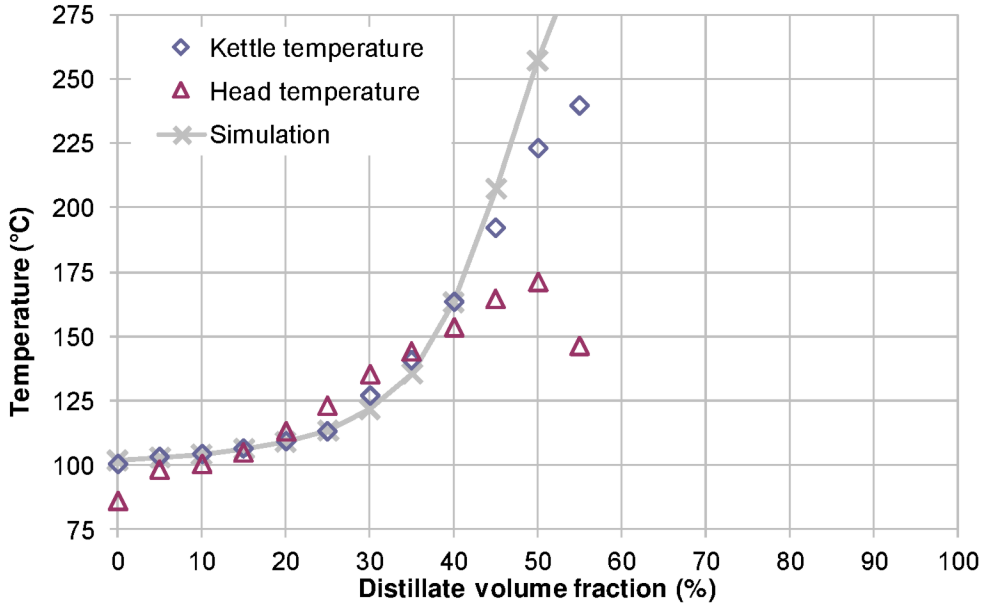

Figure 6-7: Advanced distillation curve recorded at 100.4 kPa for fast pyrolysis bio-oil comparing kettle (◊) and head (Δ) temperatures with simulated liquid (×) temperatures

Table 6-7: Advanced distillation curve kettle and head temperatures (in °C) of fast pyrolysis bio-oil recorded at 100.4 kPa and simulated kettle temperatures

	Experimental		Simulated
Volume fraction (vol%)	**T_{kettle} (°C)**	**T_{head} (°C)**	**T_{kettle} (°C)**
0	100.2	86.2	101.6
5	103.0	98.4	102.6
10	104.1	100.4	104.0
15	106.2	104.7	106.0
20	109.3	113.1	109.0
25	113.0	122.8	113.6
30	127.0	135.2	121.4
35	140.8	143.8	135.7
40	163.6	153.3	163.0
45	192.3	164.3	207.5
50	223.4	171.0	257.2
55	239.8	146.3	299.2
60			333.4
65			362.7
70			386.8
75			402.2
80			409.8
85			413.8
90			419.5
95			1,209.9
Onset[a]	-		
Sustained[a]	<96.4		
Vapour rise[b]	76.1		
First drop	100.2		

a - bubbling onset and sustained bubbling could not be observed due to dark, opaque nature of fast pyrolysis bio-oil, b - initial boiling point

Up to 55 vol% could be distilled before the distillation residue turned into solid residue (highly viscous at distillation temperature, friable, coke-like solid after cooling) due to polymerization reactions [20]. The average difference of experimental kettle temperature to simulated values was 1.1 ± 1.9 °C (0.9 ± 1.5%) up to 40 vol% distilled (comparable to validation experiments) and increased to -8.2 ± 12.4 °C (-2.7 ± 4.6%) for 40-55 vol% due to polymerization reactions. Due to the high water and low volatile content FPBO does not meet either of the ASTM D4814 spark-ignition engine fuel volatility requirements: (1) T_h (measured ASTM D86) does not exceed 70 °C at 10 vol% distilled, (2) T_h does not exceed 121 °C at 50 vol% distilled [18]. The decrease in T_h above 50 DVF (atmospheric pressure) and 65 DVF (5 kPa) is due to temperature loss through the insulation of the distillation head at high temperatures and a reduced vapour mass flow. Results are comparable to pyrolysis oil advanced distillation curves recorded by Harries et al. after correction for water content (offset method) [24].

6.4.4 Vacuum advanced distillation curves

V-ADC results for 3 runs are shown in Table 6-8, Figure 6-8, and Figure 6-9. Composition data GC-FID chromatograms are given for run 3 in Figure 6-10 and Table 6-9.

Table 6-8: Vacuum advanced distillation curve kettle temperatures (in °C) of fast pyrolysis bio-oil recorded at 5.0 kPa and 95% confidence interval calculations

	Experimental T_{kettle} (°C)						Simulated
Volume fraction (vol%)	**Run 1**	**Run 2**	**Run 3**	**Average**	**Standard deviation**	**95% error**	**T_{kettle} (°C)**
0	33.4	33.4	33.4	33.4	0.00	0.00	33.5
5	34.6	34.4	34.8	34.6	0.20	0.50	34.3
10	35.5	35.5	35.7	35.6	0.12	0.29	35.3
15	37.8	38.8	37.9	38.2	0.55	1.37	36.5
20	41.1	44.5	41.8	42.5	1.80	4.46	38.3
25	48.7	56.4	49.7	51.6	4.19	10.40	41.0
30	63.3	79.9	65.9	69.7	8.93	22.18	45.5
35	87.3	105.0	91.0	94.4	9.34	23.19	53.8
40	108.7	121.0	112.5	114.1	6.30	15.64	72.4
45	123.5	138.3	127.0	129.6	7.73	19.21	111.8
50	146.7	165.1	147.1	153.0	10.51	26.11	155.9
55	167.5	197.0	174.5	179.7	15.41	38.29	187.7
60	190.5	236.8	205.4	210.9	23.63	58.71	213.3
65	234.2	284.7	260.9	259.9	25.26	62.76	238.6
66	270.4	288.1	265.8	274.8	11.81	29.33	243.3
68		295.0	275.5	285.2	13.80		252.7
70			285.2	285.2			262.1
71			298.8	298.8			264.9
72			345.7	345.7			267.7
75							276.0
80							282.2
85							286.7
90							295.4
95							664.1
Onset[a]	-	-	-	-	-	-	
Sustained[a]	-	-	-	-	-	-	
Vapour rise[b]	33.1	33.2	32.7	33.0	0.26	0.66	
First drop	33.4	33.4	33.4	33.4	0.00	0.00	

a - bubbling onset and sustained bubbling could not be observed due to dark, opaque nature of fast pyrolysis bio-oil, b - initial boiling point

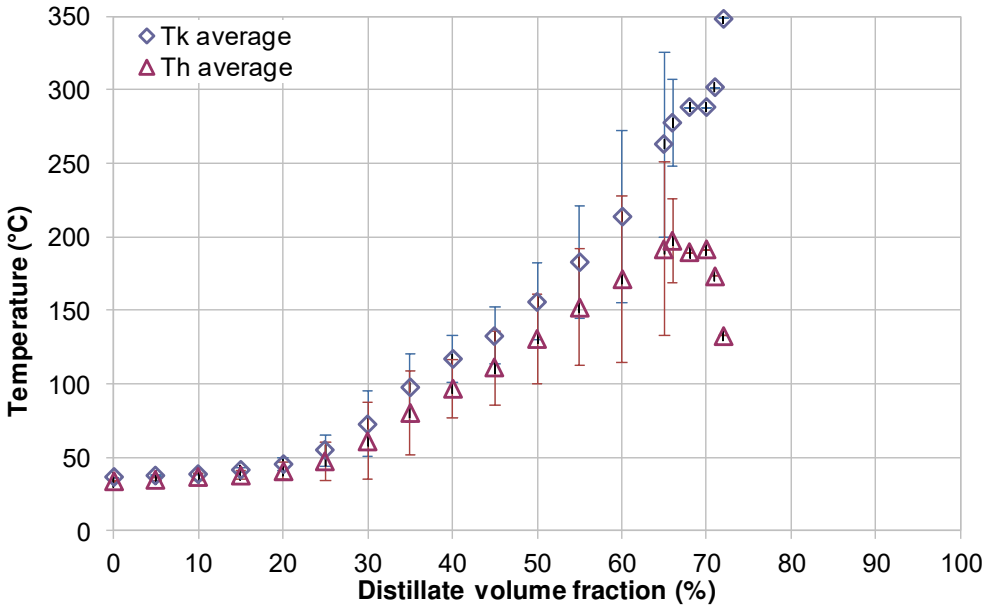

Figure 6-8: Vacuum advanced distillation curves of fast pyrolysis bio-oil recorded at 5.0 kPa comparing average kettle (◊) and average head (Δ) temperatures with 95% confidence intervals

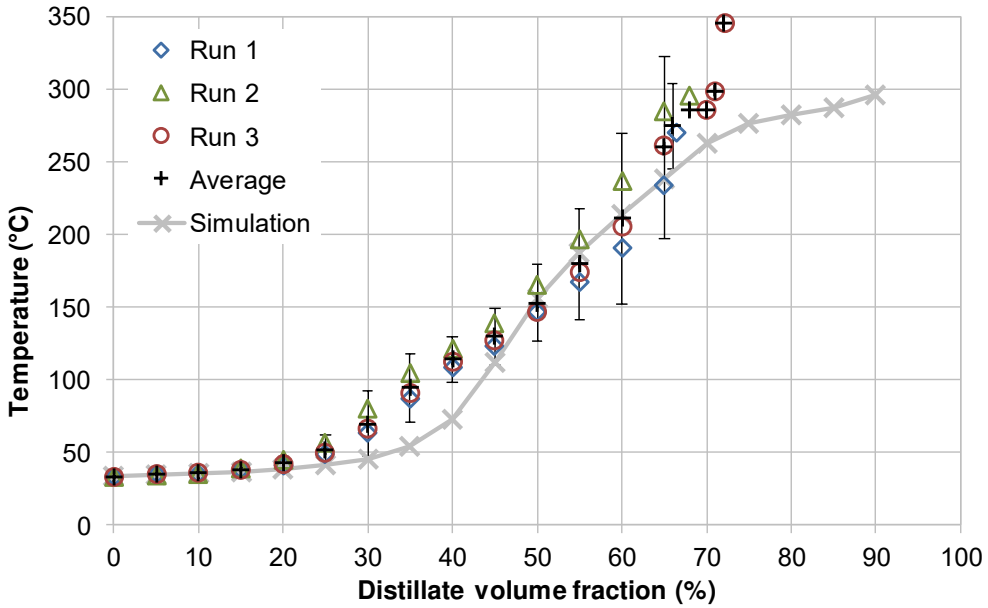

Figure 6-9: Vacuum advanced distillation curves (kettle temperatures) of fast pyrolysis bio-oil recorded at 5.0 kPa comparison of 3 runs (◊, Δ, and ○) with average (+) and 95% confidence interval compared to simulated kettle temperature (×)

The distillable volume fraction increased to 72 vol% under vacuum. The average standard deviation was 8.7 °C with an average error (95%) of ± 20.8 °C for three runs. The absolute average difference between the experimental average and the simulated values increased compared to atmospheric distillation 18.3 ± 10.4 °C (17.0 ± 10.7%). 3,4,4'-biphenyltriol as pyrolytic lignin surrogate suggested by Ille et al. was a good fit [40].

The composition samples were analyzed using a GC-MS/FID (Figure 6-10 and Table 6-9). Five distinct distillation steps were identified that could potentially allow for the separation of high-value chemicals. (1) At 5 and 10 vol% distilled, methanol was the dominant compound along with water. (2) At 20 and 30 vol% distilled, the methanol content decreased and acetic acid and acetol dominated, particularly at 30 vol%, after the removal of water (23.7 wt% of total FPBO). (3) At 40 vol% distilled, acetic acid and acetol were still present, as well as glycolaldehyde and light phenols, such as guaiacol. (4) At 50 vol% distilled, only phenols were identified and at 60 vol% distilled a shift to high BP phenols occurred. (5) Large amounts of anhydrosugars, such as levoglucosan, were present in the 65 vol% distilled sample along with very high BP phenols and vanillin. Glycolaldehyde, acetic acid, acetol, guaiacol, and levoglucosan have been identified as high-value chemicals for a variety of applications including food, pharmaceutical, pesticide, surfactant and polymer production [43,48–54]. Applications for the distillation residue have been studied by Elkasabi et al. [55]. Small traces of methanol, acetic acid, and furfural have been identified in high DVF samples while glycolaldehyde was only found in the 30 and 40 vol% samples. This is potentially due to the polymerization and thermal cracking of FPBO compounds at higher distillation temperatures yielding

small MW compounds such as methanol, acetic acid, and furfural. Moreover, these components show more associating effects with other FPBO compounds, decreasing their separation selectivity.

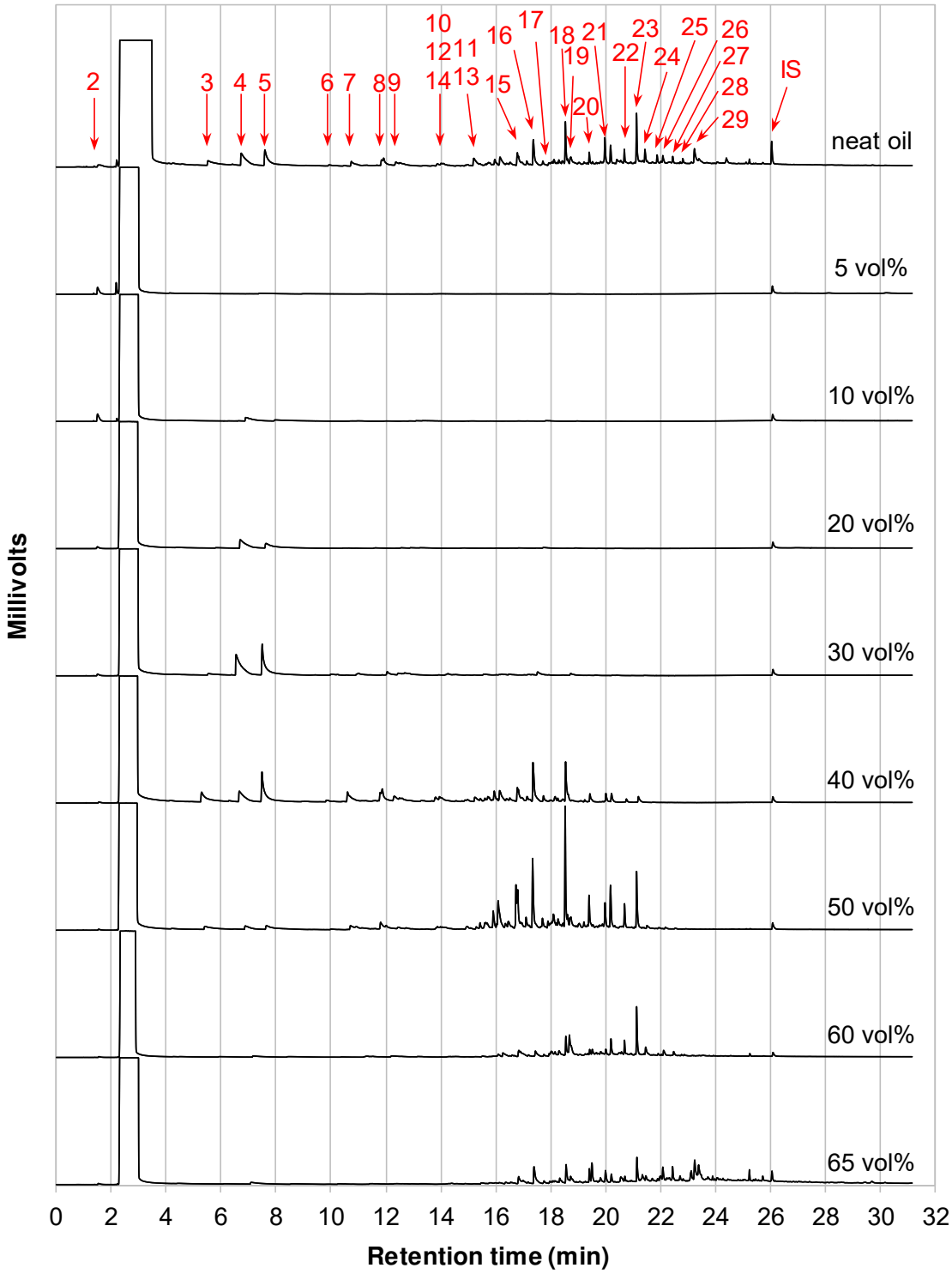

Figure 6-10: Vacuum advanced distillation curve of fast pyrolysis bio-oil composition data GC-FID results (run 3) component names and area% in Table 6-9

Table 6-9: GC-FID peaks with retention time (RT) and area% for each volume fraction and the whole oil

Peak No.	Surrogate No.	RT	Component	5%	10%	20%	30%	40%	50%	60%	65%	whole oil
		1.1	Unknown 0	0.0	0.0	0.0	0.0	0.0	0.0	0.0	0.0	0.0
		1.4	Unknown 1	2.0	0.6	0.0	0.0	0.0	0.0	0.0	0.0	0.1
2	2	1.5	**Methanol**	41.1	25.1	4.0	1.1	0.3	0.2	0.4	0.6	1.1
		2.2	Unknown 3	26.6	3.1	0.2	0.1	0.0	0.0	0.1	0.1	0.7
		4.2	Unknown 4	2.8	0.8	1.3	0.4	0.2	0.2	0.0	0.0	0.6
3	3	5.5	**Glycolaldehyde**	0.0	0.0	0.0	3.2	7.1	0.0	0.0	0.0	5.8
		6.5	Unknown 5	0.0	0.0	0.0	0.2	0.7	0.3	0.0	0.0	0.6
4	4	6.9	**Acetic acid**	0.0	38.3	48.6	30.7	7.2	1.9	2.0	3.2	7.0
5	5	7.7	**Acetol**	0.0	16.7	36.5	31.0	12.6	3.3	0.0	0.0	7.9
6	6	10.2	**Furfural**	0.0	0.0	0.0	1.4	0.7	0.2	0.0	0.6	0.4
7	7	11.0	**2-Furfurylalcohol**	0.0	0.0	0.0	2.9	5.1	2.2	1.5	0.3	2.0
8		12.1	2,3-Butanedione	0.0	0.0	0.0	3.3	6.7	3.6	1.0	0.0	3.6
9		12.7	2-Acetylfuran	0.0	0.0	0.0	7.8	6.5	1.7	0.5	0.0	3.0
10, 12, 14		14.3	3-Methyl-2,5-furandione	0.0	0.0	0.0	4.5	12.7	10.8	3.6	2.8	6.4
11, 13		15.4	5-Methyl-2-furaldehyde	0.0	0.0	0.0	3.6	4.9	3.6	2.6	1.8	4.8
15		16.9	(5H)-Furan-2-one	0.0	0.0	0.0	1.1	5.5	11.3	6.6	4.9	3.8
16	8	17.5	**Guaiacol**	0.0	0.0	0.0	3.1	9.1	9.0	3.6	7.2	5.0
17		18.2	3-Hydroxymethyfurfural	0.0	0.0	0.0	0.3	2.2	5.7	4.0	3.0	2.0
18	9	18.6	**4-Methyl-guaiacol**	0.0	0.0	0.0	1.7	8.1	12.5	6.0	5.9	6.2
19	10	18.8	**4-Ethyl-guaiacol**	0.0	0.0	0.0	0.0	1.0	3.8	14.3	3.8	2.9
20		19.5	4-Vinylguaiacol	0.0	0.0	0.0	0.3	2.1	4.8	3.3	8.3	2.3
21	11	20.0	**Eugenol**	0.0	0.0	0.0	0.5	2.0	5.6	3.3	3.2	3.7
22	12	20.2	**4-Propyl-guaiacol**	0.0	0.0	0.0	0.0	1.8	5.9	8.0	2.3	3.1
		20.7	Unknown 6	0.0	0.0	0.0	0.0	0.9	3.8	5.2	4.5	2.1
23	13	21.2	**Syringol**	0.0	0.0	0.0	0.1	1.5	5.9	13.7	5.7	6.7
24		21.5	4-Methyl-syringol	0.0	0.0	0.0	0.0	0.1	1.1	6.5	3.6	3.4
		21.9	Unknown 7	0.0	0.0	0.0	0.0	0.0	0.6	1.8	1.8	1.3
25	14	22.1	**Vanillin**	0.0	0.0	0.0	0.0	0.0	0.4	4.0	7.1	1.9
26		22.5	4-Ethylsyringol	0.0	0.0	0.0	0.0	0.0	0.4	2.7	4.3	1.9
27		22.9	4-Allylsyringol	0.0	0.0	0.0	0.0	0.0	0.2	1.1	1.9	1.4
28		23.1	Syringaldehyde	0.0	0.0	0.0	0.0	0.0	0.0	0.8	4.0	0.0
29	15	23.2	**Levoglucosan**	0.0	0.0	0.0	0.0	0.0	0.1	1.9	16.4	5.5
		26.1	IS Fluoranthene	27.4	15.5	9.3	2.7	1.2	1.0	1.5	2.7	2.8

6.4.5 Bulk fuel property prediction

Table 6-6 compares the bulk fuel properties: heating value, heat capacity, flash point, viscosity, and density predicted with the VMGSim™. The average molecular weight was predicted to be 52.7 g/mol, and the heat capacity (c_p) was 111.0 kJ/kmolK.

The MW is potentially underestimated due to the selection of the pyrolytic lignin surrogate (3,4,4'-biphenyltriol). Elliott et al. determine the average MW of pyrolytic lignin (water-insolubles, 3-29 wt% of FPBO on wet basis) to be 1000-2500 g/mol [10] compared to 200 g/mol for 3,4,4'-biphenyltriol. However, MW could not be determined experimentally. Density (by 7%) and viscosity (by 90%) were underestimated potentially due to the lower complexity, MW, and density of the pyrolytic lignin surrogate. HHV was overestimated by 16% due to the reduced oxygen content of the surrogate mixture.

6.5 Conclusions

ADC of our FPBO compares well with Harries ADC after correction for water content (offset procedure). V-ADC improved distillable fraction to 72 vol% compared to 55 vol% at atmospheric conditions by limiting polymerization reactions at high temperatures. The selected surrogates (Table 6-1) behave well in prediction of ADC and V-ADC. The presented thermodynamic model can be used to identify the role of specific components on the overall FPBO volatility and other fuel properties such as HHV, viscosity and density). These results can then be applied to FPBO upgrading work (e.g. in condenser design, co-processing, and blending) to increase or decrease the composition of selected target components. The distillation curve relates to several operational parameters, including engine starting ability, vehicle drivability, fuel system icing, vapour lock, fuel injection schedule, and autoignition [19].

6.6 Bibliography

[1] McKinley JW, Overend RP, Elliott DC. The ultimate analysis of biomass liquefaction products: The results of the IEA round robin #1. Estes Park, Colorado, USA: 1994.

[2] Meier D. Round robin testing. In: Bridgwater A V., Czernik S, Leech J, Meier D, Oasmaa A, Piskorz J, editors. IEA Bioenergy Pyrolysis Act. Final Rep., 1998.

[3] Oasmaa A, Meier D. Fast pyrolysis bio-oil analyses - The results of IEA-EU Round Robin. In: Bridgwater A V., editor. Fast pyrolysis biomass A Handb. (Volume 2), Newbury: CPL Press; 2002, p. 424.

[4] Oasmaa A, Meier D. Norms and standards for fast pyrolysis liquids: 1. Round robin test. J Anal Appl Pyrolysis 2005;73:323–34. doi:10.1016/j.jaap.2005.03.003.

[5] Oasmaa A, Elliott DC, Müller S. Quality Control in Fast Pyrolysis Bio-Oil Production and Use. Environ Prog Sustain Energy 2009;28:404–409. doi:10.1002/ep.

[6] Elliott DC, Oasmaa A, Preto F, Meier D, Bridgwater A V. Results of the IEA Round Robin on Viscosity and Stability of Fast Pyrolysis Bio-Oils. Energy & Fuels 2012;26:3769–76. doi:10.1021/ef300384t.

[7] Elliott DC, Oasmaa A, Meier D, Preto F, Bridgwater A V. Results of the IEA Round Robin on Viscosity and Aging of Fast Pyrolysis Bio-oils: Long-Term Tests and Repeatability. Energy & Fuels 2012;26:7362–6. doi:10.1021/ef301607v.

[8] Oasmaa A, Källi A, Lindfors C, Elliott DC, Springer D, Peacocke C, et al. Guidelines for transportation, handling, and use of fast pyrolysis bio-oil. 1. flammability and toxicity. Energy & Fuels 2012;26:3864–73. doi:10.1021/ef300418d.

[9] Oasmaa A, van de Beld B, Saari P, Elliott DC, Solantausta Y. Norms, Standards, and Legislation for Fast Pyrolysis Bio-oils from Lignocellulosic Biomass. Energy & Fuels 2015;29:2471–84. doi:10.1021/acs.energyfuels.5b00026.

[10] Elliott DC, Meier D, Oasmaa A, Van De Beld B, Bridgwater A V., Marklund M. Results of the International Energy Agency Round Robin on Fast Pyrolysis Bio-oil Production. Energy & Fuels 2017;31:5111–9. doi:10.1021/acs.energyfuels.6b03502.

[11] Hsieh PY, Bruno TJ. Pressure-controlled advanced distillation curve analysis and rotational viscometry of swine manure pyrolysis oil. Fuel 2014;132:1–6. doi:10.1016/j.fuel.2014.04.039.

[12] Alsbou E, Helleur R. Accelerated aging of bio-oil from fast pyrolysis of hardwood. Energy & Fuels 2014;28:3224–35. doi:10.1021/ef500399n.

[13] Chiaramonti D, Oasmaa A, Solantausta Y. Power generation using fast pyrolysis liquids from biomass. Renew Sustain Energy Rev 2007;11:1056–86. doi:10.1016/j.rser.2005.07.008.

[14] Bridgwater A V. Review of fast pyrolysis of biomass and product upgrading. Biomass and Bioenergy 2012;38:68–94. doi:10.1016/j.biombioe.2011.01.048.

[15] Rahman S, Helleur R, MacQuarrie S, Papari S, Hawboldt K. Upgrading and isolation of low molecular weight compounds from bark and softwood bio-oils through vacuum distillation. Sep Purif Technol 2018;194:123–9. doi:10.1016/j.seppur.2017.11.033.

[16] Bridgwater A V. Challenges and Opportunities in Fast Pyrolysis of Biomass : Part I. Johnson Mathhey Technol Rev 2018;62:118–30. doi:10.1595/205651318X696693.

[17] Windom BC, Bruno TJ. Improvements in the Measurement of Distillation Curves. 5. Reduced Pressure Advanced Distillation Curve Method. Ind Eng Chem Res 2011;50:1115–26. doi:10.1021/ie101784g.

[18] Harries ME, Kunwar B, Sharma BK, Bruno TJ. Application of the Advanced Distillation Curve Method to Characterize Two Alternative Transportation Fuels Prepared from the Pyrolysis of Waste Plastic. Energy and Fuels 2016;30:9671–8. doi:10.1021/acs.energyfuels.6b02068.

[19] Bruno TJ. Improvements in the Measurement of Distillation Curves. 1. A Composition-Explicit Approach. Ind Eng Chem Res 2006;45:4371–80. doi:10.1021/ie051393j.

[20] Starkey Ott L, Smith BL, Bruno TJ. Advanced distillation curve measurement: Application to a bio-derived crude oil prepared from swine manure. Fuel 2008;87:3379–87. doi:10.1016/j.fuel.2008.04.038.

[21] Starkey Ott L, Bruno TJ. Modifications to the copper strip corrosion test for the measurement of sulfur-related corrosion. J Sulfur Chem 2007;28:493–504. doi:10.1080/17415990701516432.

[22] Starkey Ott L, Smith BL, Bruno TJ. Composition-explicit distillation curves of mixtures of diesel fuel with biomass-derived glycol ester oxygenates: A fuel design tool for decreased particulate emissions. Energy and Fuels 2008;22:2518–26. doi:10.1021/ef800238m.

[23] Windom BC, Bruno TJ. Novel reduced pressure-balance syringe for chromatographic analysis. J Chromatogr A 2010;1217:7434–9. doi:10.1016/j.chroma.2010.09.045.

[24] Harries ME, McDonald AG, Bruno TJ. Measuring the distillation curves of non-homogeneous fluids: Method and case study of two pyrolysis oils. Fuel 2017;204:23–7. doi:10.1016/j.fuel.2017.04.066.

[25] Hsieh PY, Abel KR, Bruno TJ. Analysis of Marine Diesel Fuel with the

Advanced Distillation Curve Method. Energy & Fuels 2013;27:804–10. doi:10.1021/ef3020525.

[26] Windom BC, Bruno TJ. Pressure-controlled advanced distillation curve analysis of biodiesel fuels: Assessment of thermal decomposition. Energy and Fuels 2012;26:2407–15. doi:10.1021/ef3000642.

[27] Hsieh PY, Widegren JA, Fortin TJ, Bruno TJ. Chemical and Thermophysical Characterization of an Algae-Based Hydrotreated Renewable Diesel Fuel. Energy & Fuels 2014;28:3192–205. doi:10.1021/ef500237t.

[28] Windom BC, Bruno TJ. Application of Pressure-Controlled Advanced Distillation Curve Analysis: Virgin and Waste Oils. Ind Eng Chem Res 2013;52:327–37. doi:10.1021/ie302399v.

[29] He BJ, Zhang Y, Funk TL, Riskowski GL, Yin Y. Thermochemical Conversion of Swine Manure: An Alternative Process for Waste Treatment and Renewable Energy Production. Trans ASAE 2000;43:1827–33.

[30] Conversion PT, Kunwar B, Chandrasekaran SR, Moser BR, Deluhery J, Kim P, et al. Catalytic Thermal Cracking of Postconsumer Waste Plastics to Fuels. 2. Pilot-Scale Thermochemical Conversion. Energy & Fuels 2017;31:2705–15. doi:10.1021/acs.energyfuels.6b02996.

[31] Staš M, Kubička D, Chudoba J, Pospíšil M. Overview of analytical methods used for chemical characterization of pyrolysis bio-oil. Energy and Fuels 2014;28:385–402. doi:10.1021/ef402047y.

[32] Wang S, Gu Y, Liu Q, Yao Y, Guo Z, Luo Z, et al. Separation of bio-oil by molecular distillation. Fuel Process Technol 2009;90:738–45. doi:10.1016/j.fuproc.2009.02.005.

[33] Guo X, Wang S, Guo Z, Liu Q, Luo Z, Cen K. Pyrolysis characteristics of bio-oil fractions separated by molecular distillation. Appl Energy 2010;87:2892–8. doi:10.1016/j.apenergy.2009.10.004.

[34] Sharma A, Pareek V, Zhang D. Biomass pyrolysis - A review of modelling, process parameters and catalytic studies. Renew Sustain Energy Rev 2015;50:1081–96. doi:10.1016/j.rser.2015.04.193.

[35] Papari S, Hawboldt K. A review on the pyrolysis of woody biomass to bio-oil: Focus on kinetic models. Renew Sustain Energy Rev 2015;52:1580–95. doi:10.1016/j.rser.2015.07.191.

[36] Hallett WLH, Clark NA. A model for the evaporation of biomass pyrolysis oil droplets. Fuel 2006;85:532–44. doi:10.1016/j.fuel.2005.08.006.

[37] Hallett WLH, Beauchamp-Kiss S. Evaporation of single droplets of ethanol-fuel oil mixtures. Fuel 2010;89:2496–504. doi:10.1016/j.fuel.2010.03.007.

[38] Zhang L, Kong SC. Multicomponent vaporization modelling of bio-oil and its mixtures with other fuels. Fuel 2012;95:471–80. doi:10.1016/j.fuel.2011.12.009.

[39] Elkasabi Y, Mullen CA, Boateng AA. Distillation and isolation of commodity chemicals from bio-oil made by tail-gas reactive pyrolysis. ACS Sustain Chem Eng 2014;2:2042–52. doi:10.1021/sc5002879.

[40] Ille Y, Kröhl F, Velez A, Funke A, Pereda S, Schaber K, et al. Activity of water in pyrolysis oil—Experiments and modelling. J Anal Appl Pyrolysis 2018;135:260–70. doi:10.1016/j.jaap.2018.08.027.

[41] Papari S, Hawboldt K. Development and Validation of a Process Model to Describe Pyrolysis of Forestry Residues in an Auger Reactor. Energy and Fuels 2017;31:10833–41. doi:10.1021/acs.energyfuels.7b01263.

[42] Alsbou E. Pyrolysis Bio-oil as a Renewable Fuel and Source of Chemicals: Its Production, Characterization and Stability. Memorial University of Newfoundland, 2014.

[43] Krutof A, Hawboldt KA. Co-pyrolysis of softwood with waste mussel shells: Liquid analysis. Fuel 2019;254. doi:10.1016/j.fuel.2019.05.167.

[44] National Institute of Standards and Technology. NIST Webbook. 2017.

[45] Fermoso J, Pizarro P, Coronado JM, Serrano DP. Advanced biofuels production by upgrading of pyrolysis bio-oil. Wiley Interdiscip Rev Energy Environ 2017;6. doi:10.1002/wene.245.

[46] Abnisa F, Wan Daud WMA. A review on co-pyrolysis of biomass: An optional technique to obtain a high-grade pyrolysis oil. Energy Convers Manag 2014;87:71–85. doi:10.1016/j.enconman.2014.07.007.

[47] Basu P. Biomass gasification and pyrolysis: Practical design and theory. Oxford UK: Elsevier Inc.; 2010.

[48] Vitasari CR, Meindersma GW, De Haan AB. Laboratory scale conceptual process development for the isolation of renewable glycolaldehyde from pyrolysis oil to produce fermentation feedstock. Green Chem 2012;14:321–5. doi:10.1039/c1gc16200d.

[49] Vitasari CR. Extraction of Bio-based Glycolaldehyde from Wood-derived Pyrolysis Oils. Eindhoven University of Technology, 2012. doi:10.6100/IR738958.

[50] Pourzolfaghar H, Abnisa F, Wan Daud WMA, Aroua MK. Atmospheric hydrodeoxygenation of bio-oil oxygenated model compounds: A review. J Anal Appl Pyrolysis 2018;133:117–27. doi:10.1016/j.jaap.2018.04.013.

[51] Mortensen PM, Grunwaldt J-D, Jensen PA, Knudsen KG, Jensen AD. A review of catalytic upgrading of bio-oil to engine fuels. Appl Catal A Gen 2011;407:1–19. doi:10.1016/j.apcata.2011.08.046.

[52] Asmadi M, Kawamoto H, Saka S. Gas- and solid/liquid-phase reactions during pyrolysis of softwood and hardwood lignins. J Anal Appl Pyrolysis 2011;92:417–25. doi:10.1016/j.jaap.2011.08.003.

[53] Zhang X, Li J, Yang W, Blasiak W. Formation mechanism of levoglucosan and formaldehyde during cellulose pyrolysis. Energy and Fuels 2011;25:3739–46. doi:10.1021/ef2005139.

[54] Elkasabi Y, Mullen CA, Boateng AA. Distillation and isolation of commodity chemicals from bio-oil made by tail-gas reactive pyrolysis. ACS Sustain Chem Eng 2014;2:2042–52. doi:10.1021/sc5002879.

[55] Elkasabi Y, Mullen CA, Jackson MA, Boateng AA. Characterization of fast-pyrolysis bio-oil distillation residues and their potential applications. J Anal Appl Pyrolysis 2015;114:179–86. doi:10.1016/j.jaap.2015.05.018.

Chapter 7 Conclusions and recommendations for future work

7.1 Conclusions

Enhancing FPBO quality and stability while recovering high-value chemicals is desirable to expand FPBO applications from heating to transport fuel. The most fundamental upgrading need is deoxygenation, preferably through decarboxylation or dehydration. Decarbonylation should be avoided to increase the carbon and hydrogen (energy) yield.

In this work a review of methods to enhance FPBO was done. In general, upgrading requires a balance of mass and energy yields, FPBO oxygen content, carbon loss, and hydrogen demand, as well as feed/production and product cost. Catalysts required for catalytic pyrolysis and liquid upgrading and the operation of catalytic reactions are often expensive (high temperature and pressure). To improve the economics of the pyrolysis process and enhance the oil and biochar quality the co-processing of the biomass with additives in the form of by-products from the fisheries and/or mining industry to enhance oil and char quality was studied in a screening analysis of co-pyrolysis with shrimp residues, mussel shells, and red mud both *in-situ* and *ex-situ*. Preliminary experiments indicate that red mud is not a viable additive for fuel applications due to cracking of high molecular weight compounds leading to high water content. Oil produced with shrimp shell additive showed nitrogenous compounds that would cause issues in refining and blending application of the pyrolysis oil. Mussel shells (95 wt% $CaCO_3$) as a co-pyrolysis additive showed the most promising results.

Co-pyrolysis of softwood with MS reduced oxygen in FPBO via decarboxylation and reduction of carboxylic acids to ketones with $CaCO_3$ as well as dehydration. Optimal conditions minimizing the acetic acid content while maximizing the yield of oil were at

500-525 °C with low sweep gas flow rate (50 mL/min) and 25 wt% MS loading (*in-situ*). At 525 °C with 50 wt% MS loading, TAN was reduced from 67 to 48-56 mgNaOH/gOil and oxygen from 38 wt% to 30 wt% compared to no MS addition. The MS increased the water content, decreasing the overall HHV while still producing a one phase oil. However, a small increase in the HHV of the water free oil, as well as a reduced TAN and oxygen content confirm MS favouring deoxygenation reactions through dehydration and decarboxylation in both operational modes. A maximum of nitrogen in the dry oil was reached at 525 °C and 50 wt% MS. The nitrogen originates from the organics (5 wt%) in the MS and can limit fuel applications due to nitrous oxide emissions.

In-situ biochars are not suitable as a solid fuel due to dilution with non-combustible MS reducing the HHV and resulting in high ash content. The pH increased from 7 to 9 with 50 wt% MS loading making it suitable as a soil amendment for acetic soils. Higher value applications such as acidic gas adsorption could be investigated due to the introduction of new N and O containing functional groups. Post-synthetic modification of FPBO and biochar is costly, *in-situ* modification, as demonstrated in this thesis, is a faster, more efficient alternative. Compared to the market price of the pyrolysis oil and biochar products, using commercial catalysts in upgrading is econcomically challenging. Instead, naturally occurring alternative co-pyrolysis additives such as MS should be considered. Additives that pose a disposal task to their respective industries with similar chemical make-up compared to suitable catalysts are favourable. If co-pyrolysis additives enhance pyrolysis oil as well as char quality, and if the additives are incorporated

within the char, an additional separation step is not necessary decreasing operational cost further compared to catalytic upgrading processes.

Understanding FPBO volatility further improves oil upgrading. A thermodynamic model was developed requiring little input data (water and solid content and GC analysis of the bulk oil, and vol% distillation residue). Surrogates were selected representative to the boiling point range and functional groups of FPBO. More complex models could potentially give more detailed and flexible results, but it would be difficult to obtain data required to run the model (e.g. interaction parameters). Vacuum advanced distillation curve (V-ADC) experiments improved distillable fraction to 72 vol% compared to 55 vol% at atmospheric conditions by limiting polymerization reactions at high temperatures. The presented thermodynamic model can be used to identify the role of specific components on the overall FPBO volatility (and other fuel properties such as enthalpy (heating value, heat capacity, flash point), flow properties (viscosity, density), and average molecular weight). These results can then be applied to FPBO upgrading work (e.g. in condenser design, co-processing, and blending) to increase or decrease the composition of selected target components. Moreover, it was found that FPBO can be distilled in 6 fractions to recover value-added chemicals: (1) methanol and water; (2) acetic acid, acetol, and remaining water; (3) glycolaldehyde and light phenols; (4) phenols; (5) anhydrosugars; and (6) distillation residue (mostly carbon).

Biomass use for renewable fuels should be limited to rural areas where no renewable alternatives exist and applications with high GHG/CO_2 mitigation potential. Co-pyrolysis of forestry or sawmill with waste mussel shell for FPBO and biochar production is a

good opportunity for rural Newfoundland. However, incentives are needed to grow a market for pyrolysis products.

7.2 Recommendations for future work

More work is required investigating reaction mechanisms, particularly identifying possible catalytic reactions when mussel shells are used as a co-pyrolysis additive to enhance liquid and char properties. A comprehensive comparison to synthetic catalysts, investigation of the nitrogen-containing components in the FPBO produced from co-pyrolysis of wood and MS, and a techno-economic feasibility study are needed. The MS additive should be compared to other additives such as reagent grade $CaCO_3$, CaOH, or NaOH.

The co-pyrolysis process investigated here could be scaled up to the auger reactor. However, mussel particle residue in the steel shot heat carrier and possible build-up in the reactor should be considered for possible scale-up applications.

For V-ADC experiments, the vacuum should be increased slightly (e.g. to 15 kPa) for future experiments because the vapour pressure of methanol is 12.8 kPa at 20 °C and 16.96 kPa at 25 °C [1]. At 5 kPa most of the methanol is lost, and sampling of the first drop was difficult at ambient temperatures due to evaporation of the sample in the syringe. Moreover, Ortiz et al. introduce a factor to account for equipment hold-up and time delay in their simulations that could be applied to future simulations, improving the agreement of experimental and simulated values [2]. The ADC model could be replaced with a more complex model that could potentially give more detailed and flexible results, but it would be more difficult to obtain data required to run the model (e.g. interaction parameters). Trajectory optimization could be used to improve the model

(surrogate mixture composition) [2,3]. The model could possibly be improved by measuring boiling point elevations to determine binary interaction parameters for binaries containing solids. Here they were assumed to be zero. Finally, the surrogate mixture could also be used for other modelling work, such as corrosion models.

V-ADC with the addition of mussel shells could be considered to upgrade (dehydration, deoxygenation, decarboxylation) the oil during distillation [4]. Three fractions could be selected: low boiling point aqueous phase, upgraded pyrolysis oil, and distillation residue (including mussel shell). Possible applications could be chemicals or fuel for fuel cells; heating fuel; and soil amendment or adsorbent, respectively.

7.3 Bibliography

[1] National Institute of Standards and Technology. NIST Webbook. 2017.

[2] Ortiz DP, Satyro MA, Yarranton HW. Thermodynamics and fluid characterization using trajectory optimization. Fluid Phase Equilib 2013;351:34–42. doi:10.1016/j.fluid.2012.09.006.

[3] Satyro MA, Yarranton HW. Oil characterization from simulation of experimental distillation data. Energy & Fuels 2009;23:3960–70. doi:10.1021/ef9000242.

[4] Zheng JL, Wei Q. Improving the quality of fast pyrolysis bio-oil by reduced pressure distillation. Biomass and Bioenergy 2011;35:1804–10. doi:10.1016/j.biombioe.2011.01.006.